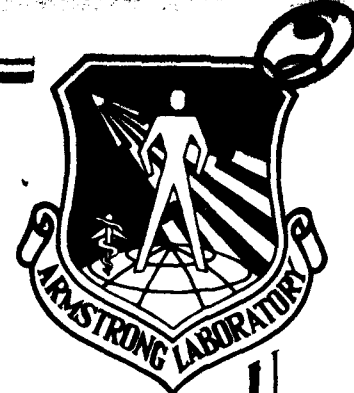


AL-TR-1991-0089

AD-A278 768



ARMSTRONG

LABORATORY

APPLICATION OF SURFACE-RELIEF DIFFRACTIVE OPTICS TO HELMET-MOUNTED DISPLAYS

C. T. Cotton
D. Faklis
J. P. Bowen
G. M. Morris

ROCHESTER PHOTONICS CORPORATION
80 O'CONNOR ROAD
FAIRPORT, NY

JULY 1991

DTIC
ELECTE
MAY 02 1994
S G D

FINAL REPORT FOR PERIOD 24 September 1990 to 22 March 1991

DTIC QUALITY INSPECTED 3

Approved for public release; distribution is unlimited.

04 4 29 024

AIR FORCE SYSTEMS COMMAND
WRIGHT-PATTERSON AIR FORCE BASE, OHIO 45433-6573

94-13119



12448

NOTICES

When US Government drawings, specifications, or other data are used for any purpose other than a definitely related Government procurement operation, the Government thereby incurs no responsibility nor any obligation whatsoever, and the fact that the Government may have formulated, furnished, or in any way supplied the said drawings, specifications, or other data, is not to be regarded by implication or otherwise, as in any manner licensing the holder or any other person or corporation, or conveying any rights or permission to manufacture, use, or sell any patented invention that may in any way be related thereto.

Please do not request copies of this report from the Armstrong Aerospace Medical Research Laboratory. Additional copies may be purchased from:

National Technical Information Service
5285 Royal Road
Springfield, Virginia 22161

Federal Government agencies and their contractors registered with the Defense Technical Information Center should direct requests for copies of this report to:

Defense Technical Information Center
Cameron Station
Alexandria, Virginia 22314

TECHNICAL REVIEW AND APPROVAL

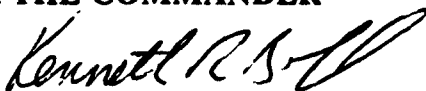
AL-TR-1991-0089

This report has been reviewed by the Office of Public Affairs (PA) and is releasable to the National Technical Information Service (NTIS). At NTIS, it will be available to the general public, including foreign nations.

The voluntary informed consent of the subjects used in this research was obtained as required by Air Force Regulation 169-3.

This technical report has been reviewed and is approved for publication.

FOR THE COMMANDER



KENNETH R. BOFF
Acting Division Chief
Human Engineering Division
Armstrong Laboratory

REPORT DOCUMENTATION PAGE			Form Approved OMB No. 0704-0188	
Public reporting burden for this collection of information is estimated to average 1 hour per response, including the time for reviewing instructions, searching existing data sources, gathering and maintaining the data needed, and completing and reviewing the collection of information. Send comments regarding this burden estimate or any other aspect of this collection of information, including suggestions for reducing this burden, to Washington Headquarters Services, Directorate for Information Operations and Reports, 1215 Jefferson Davis Highway, Suite 1204, Arlington, VA 22202-4302, and to the Office of Management and Budget, Paperwork Reduction Project (0704-0188), Washington, DC 20503.				
1. AGENCY USE ONLY (Leave blank)	2. REPORT DATE July 1991	3. REPORT TYPE AND DATES COVERED Final (24 Sep 90 - 22 Mar 91)		
4. TITLE AND SUBTITLE Application of surface-relief diffractive optics to helmet-mounted displays		5. FUNDING NUMBERS C - F41622-90-C-1013 PR - 7184 TA - 11 WU - 57		
6. AUTHOR(S) C.T. Cotton, D. Faklis, J.P. Bowen and G.M. Morris				
7. PERFORMING ORGANIZATION NAME(S) AND ADDRESS(ES) Rochester Photonics Corporation 80 O'Connor Road Fairport NY 14450		8. PERFORMING ORGANIZATION REPORT NUMBER 2-CWS-91-10		
9. SPONSORING / MONITORING AGENCY NAME(S) AND ADDRESS(ES) AL/CFHV Wright-Patterson AFB OH 45433-6573		10. SPONSORING / MONITORING AGENCY REPORT NUMBER AL-TR-1991-0089		
11. SUPPLEMENTARY NOTES				
12a. DISTRIBUTION / AVAILABILITY STATEMENT Approved for public release; distribution is unlimited.		12b. DISTRIBUTION CODE		
13. ABSTRACT (Maximum 200 words) Recent advances in diffractive optics technology suggest that diffractive optics may provide a revolutionary solution to the problem of developing lightweight optical assemblies for helmet-mounted displays. Surface-relief diffractive optics provide the optical designer with additional degrees of freedom to correct for chromatic and geometric aberrations. Fabrication techniques exist to blaze the phase profile of each zone; this provides a diffractive lens that exhibits high diffraction efficiency, that is nearly all of the incident light goes to the principal focus. The objective of the R&D is to demonstrate the feasibility of utilizing diffractive optics technology to answer head-borne weight and center of gravity constraints in helmet-mounted display systems. Both monochromatic and polychromatic conditions for on-axis and off-axis systems are addressed. A significant portion of the effort is concerned with the chromatic correction of the optical assembly. The effect of diffraction efficiency on image quality is also investigated. Fabrication of the refractive and diffractive components is studied for further development in Phase II. DTIC QUALITY INSPECTED 3				
14. SUBJECT TERMS Helmet- mounted displays, diffractive optics, binary optics		15. NUMBER OF PAGES 113		
		16. PRICE CODE		
17. SECURITY CLASSIFICATION OF REPORT Unclassified	18. SECURITY CLASSIFICATION OF THIS PAGE Unclassified	19. SECURITY CLASSIFICATION OF ABSTRACT Unclassified	20. LIMITATION OF ABSTRACT Unclassified	

PREFACE

This report was prepared under the direction and sponsorship of the Armstrong Laboratory, Paul M. Fitts Human Engineering Division, Visual Display Systems Branch of the United States Air Force as part of Project 71841157. Mr Dean F. Kocian was the workunit and program technical monitor. The impetus for this work arose from the continuing efforts of the Laboratory to exploit optical technology that can lead to helmet-mounted display systems providing desirable field-of-view, exit pupil, and aberration-correction performance while minimizing head-borne weight. The work described in this report was performed by Rochester Photonics Corporation under contract number F41622-90-C-1013 as part of the Small Business Innovation Research (SBIR) Program.

Accession For	
NTIS	CRA&I <input checked="checked" type="checkbox"/>
DTIC	TAB <input checked="checked" type="checkbox"/>
Unannounced	<input type="checkbox"/>
Justification	
By	
Distribution /	
Availability Codes	
Dist	Avail and / or Special
A-1	

Table of Contents

Table of Contents.....	iv
List of Figures.....	vi
List of Tables	ix
1.0 Introduction.....	1
1.1 Purpose.....	1
1.2 Background	1
1.3 Objective	4
1.4 Scope	4
1.5 Executive Summary	5
1.6 Format	7
2.0 Diffractive Helmet-Mounted Display Systems.....	8
2.1 General.....	8
2.2 Optical System Parameters	9
2.3 Design Methodology	9
2.3.1 Review of Diffractive Optics.....	9
2.3.2 Scope of Work	21
3.0 Helmet-Mounted Display Design Using Diffractive Optics.....	22
3.1 Introduction.....	22
3.2 All-diffractive HMD Design.....	22
3.3 On-axis Aspheric Hybrid Refractive/Diffractive HMD Design	44
3.4 On-axis Refractive/Diffractive Relay Lens: Throughput Analysis.....	57
3.5 Off-axis Aspheric Hybrid Refractive/Diffractive HMD Design.....	59
3.6 On-axis Refractive/Diffractive Relay Lens: Tolerance Analysis	66
3.7 Hardware Requirements for HMD System	71
3.8 Summary	72
4.0 Fabrication of Diffractive Optical Elements.....	74
4.1 Introduction.....	74
4.2 Photolithographic Techniques	74
4.2.1 Fabrication Using Microelectronics Technology	75
4.3 Single-Point Diamond Turning.....	79
4.4 Element Replication	81

Table of Contents (continued)

5.0 Characterization and Testing of the Diffractive Components of the HMD	82
5.1 Introduction.....	82
5.2 Diffraction Efficiency.....	83
5.2.1 Theory.....	83
5.3 Stray Light Analysis for Diffractive Optics	92
5.4 Summary.....	95
6.0 Future Research.....	96
Appendix A	99
Appendix B	102
Appendix C	105
Appendix D	108
Appendix E	111

List of Figures

Fig. 2-1	Refractive and diffractive lenses.	11
Fig. 2-2	Paraxial diffractive lens illustrating the radii of the first four zones.....	12
Fig. 2-3	TACH for a hybrid doublet over the visible region.....	17
Fig. 2-4	TACH for an F/5 apochromatic system with $e\text{fl}=10$ mm that utilizes hybrid refractive/diffractive elements	19
Fig. 3-1	Baseline configuration of the optical train for a HMD using an on-axis combiner and relay system.....	24
Fig. 3-2	Head-mounted, on-axis combiner/visor system.....	25
Fig. 3-3	Binocular FOV of on-axis combiner.....	26
Fig. 3-4	Unfolded system diagram for system A.....	28
Fig. 3-5	Unfolded system diagram for system B.....	29
Fig. 3-6	Monochromatic performance for system A with a 5 mm eye pupil in the straight-ahead viewing configuration.....	31
Fig. 3-7	Monochromatic performance for system A with a 5 mm eye pupil in the on-axis viewing configuration.....	32
Fig. 3-8	Monochromatic performance for system B with a 5 mm eye pupil in the straight-ahead viewing configuration.....	33
Fig. 3-9	Monochromatic performance for system B with a 5 mm eye pupil in the on-axis viewing configuration.....	34
Fig. 3-10	Eye rotation for viewer looking straight ahead.	35
Fig. 3-11	Eye rotation for a viewer looking along the optical axis of the system	35
Fig. 3-12	Polychromatic performance for system A with a spectral bandwidth of 0.5 nm	37
Fig. 3-13	Polychromatic performance for system A with a spectral bandwidth of 1.0 nm	38
Fig. 3-14	Polychromatic performance for system A with a spectral bandwidth of 1.5 nm	39
Fig. 3-15	Polychromatic performance for system B with a spectral bandwidth of 0.5 nm	40
Fig. 3-16	Polychromatic performance for system B with a spectral bandwidth of 1.0 nm	41

Fig. 3-17	Polychromatic performance for system B with a spectral bandwidth of 1.5 nm.	42
Fig. 3-18	Effect of the spectral bandwidth of the illumination source on polychromatic MTF.....	43
Fig. 3-19	The spectral energy distribution for P53 phosphor.....	45
Fig. 3-20	Unfolded system diagram for system C.....	47
Fig. 3-21	Unfolded system diagram for system D.....	48
Fig. 3-22	Chromatic ray error plot exhibiting spherochromatism.....	49
Fig. 3-23	Effect of spherochromatism, for a 5 mm pupil decentered from the axis by 7 mm.....	50
Fig. 3-24	Polychromatic performance for system C with a 5 mm eye pupil in the straight-ahead viewing configuration.	52
Fig. 3-25	Polychromatic performance for system C with a 5 mm eye pupil in the on-axis viewing configuration.	53
Fig. 3-26	Polychromatic performance for system D with a 5 mm eye pupil in the straight-ahead viewing configuration.	54
Fig. 3-27	Polychromatic performance for system D with a 5 mm eye pupil in the on-axis viewing configuration.	55
Fig. 3-28	Off-axis HMD configuration using an off-axis ellipsoidal combiner, 30° FOV, 15 mm EPD and a 19 mm CRT.	61
Fig. 3-29	Plot showing the transverse chromatic aberration (lateral color) across the field of the system.	62
Fig. 3-30	Polychromatic MTF of the off-axis HMD system with the viewer looking straight ahead for three field points as shown in Fig. 3-31.	63
Fig. 3-31	Configuration for evaluation of system performance for off-axis HMD system.....	64
Fig. 3-32	Distortion mapping required on the CRT face for keystone distortion correction.	65
Fig. 3-33	Engineering Drawing.....	68
Fig. 3-34	Engineering Drawing.....	69
Fig. 3-35	Engineering Drawing.....	70
Fig. 4-1	Describing the fabrication process for a binary phase grating.	76

Fig. 4-2	Implementation of an additional lithographic mask for the fabrication of a multi-level phase grating.	78
Fig. 4-3	Electron micrographs of a replica from a diamond-turned diffractive master.	80
Fig. 5-1	The optical transfer function (OTF) for a 100%-efficient diffraction-limited imaging system vs. the OTF of the same system with an integrated efficiency equal to η , where η is less than 100%.	89
Fig. 5-2	Sawtooth blaze profile, where α is the maximum phase deviation produced by the grating.	89
Fig. 5-3a	The relative efficiency for the $m=1$ order. The efficiency peaks at the design wavelength, and falls off to either side.	91
Fig. 5-3b	The relative amounts of power diffracted into the $m=0$ and $m=2$ orders.	91
Fig. 5-4	Images formed in a system with diffractive optics, at infinity (a), near viewer (b), and beyond infinity (c).	94

List of Tables

Table 2-1	Design parameters for the HMD optical system design.....	9
Table 3-1	Design parameters associated with systems A and B.....	44
Table 3-2	Generation of the spectral weighting function.....	56
Table 3-3	The relative throughput for the relay lens, using typical values for glass filters (top) and a diffractive element without any filters (bottom).	58
Table 3-4	Tolerance budget for an on-axis HMD.	67
Table 3-5	Summary of CRT data appropriate for HMDs.....	71
Table 5-1	The grating efficiencies for the primary wavelengths of the P53 phosphor. .	92



1.0 Introduction

1.1 Purpose

The purpose of this document is to satisfy the requirements for a Federal SBIR Phase I final report in accordance with the U.S. Air Force Armstrong Laboratory (Human Systems Division) contract no. F41622-90-C-1013, dated 24 SEP 1990.

1.2 Background

A helmet-mounted display (HMD) provides the pilot with a dedicated visually-coupled interface that offers increased vision as well as improved target acquisition and weapons delivery. The HMD presents the wearer with avionics symbology superimposed on sensor imagery or a natural scene. The flight scene may consist of a sunlit terrain or it may consist of the output of a night vision sensor or FLIR. Two recent conferences have examined the latest applications of HMD optical systems in tactical aircraft, rotorcraft, simulators, and land vehicles.^{1,2}

Current HMD systems have advanced to the point where reducing the head-borne weight and maintaining a reasonable center of gravity is technically difficult.³ Concentrating on the helmet optical system, it remains possible to achieve weight reductions through the use of optical glasses of lower density and by reducing the overall number of optical elements. Such modifications usually give rise to inferior system performance⁴ whether it be decreased field-of-view, reduced unvignetted exit pupil

¹ J. T. Carollo, *Helmet-mounted displays*, SPIE 1116 (1989).

² R. J. Lewandowski, *Helmet-mounted displays II*, SPIE 1290 (1990).

³ See, for example, D. F. Kocian, "Design considerations for virtual panoramic display (VPD) helmet systems," *Man-Machine Interface in Tactical Aircraft Design and Combat Automation*, AGARD Conference Proceedings No. 425 22-1,32 (1988).

⁴ M. J. Wells, M. Venturino, and R. K. Osgood, "The effect of field-of-view size on performance at a simple simulated air-to-air mission," *Proc. SPIE 1116*, 126 (1989); *Electro-optical displays*, *Opt. Eng.*, 29, Aug. 1990; R. A. Buchroeder, "Helmet-mounted displays," *SPIE-OE/LASE*, Los Angeles, CA T72 (1989); J. E. Melzer and E. W. Larkin, "An integrated approach to helmet display system design," *SPIE 778*, 83 (1987); M. Shenker, "Optical design criteria for binocular helmet-mounted displays," *SPIE 778*, 70 (1987).

diameter or increased chromatic aberration. It is evident at this point in HMD optical system evolution that advanced optical materials and devices are required to make significant improvements in performance and weight reduction in the next generation HMD systems.

Recent innovations in diffractive (or binary) optics technology reveal that diffractive optical elements offer the potential to reduce significantly the size, weight, and cost of a variety of optical systems, which currently utilize refractive and/or reflective components. Unlike a conventional lens, a diffractive lens is an optical device that utilizes interference and diffraction in an image forming capability. Familiar diffractive optical elements are holographic optical elements (both optically recorded and computer generated), surface-relief optical elements (kinoforms) and zone plates.

Volume holographic lenses are known to have certain severe limitations. These elements are typically recorded in dichromated gelatin or other photopolymers to provide high-efficiency Bragg diffraction into a particular diffracted order. Although these elements can have high diffraction efficiencies, they are usually plagued by poor optical performance over the field-of-view.⁵ However, there are specific, non-imaging applications in high-energy laser optics that benefit greatly from volume diffractive structures in dichromated gelatin. Also, volume (Bragg) structures are used for spectral filtering applications. In general, as a result of poor wide-field imaging characteristics, holographic lenses (both optically recorded and computer generated) have found little use in sophisticated imaging systems.

The kinoform is a diffractive structure in which the phase modulation is introduced by a surface-relief profile.^{6,7} In most kinoforms, the maximum relief depth is chosen such that, at the design wavelength, the maximum phase modulation introduced by the kinoform is 2π . Similar to other types of diffractive optics, it is possible to use kinoforms as lenses. Kinoform lenses have the advantage of being thin zone-plate-type structures with very high diffraction efficiencies. In contrast with holographic lenses, it has been shown that kinoforms can produce high quality wavefronts over wide fields-of-view.

5 There are many associated references. See, for example, Ivan Cindrich, Editor, *Holographic Optics: Design and Applications*, Proc. SPIE 883, (1988).

6 J. A. Jordan, P. M. Hirsch, L. B. Lesem, and D. L. Van Rooy, "Kinoform lenses," *Appl. Opt.* 9, 1883 (1970).

7 L. B. Lesem, P. M. Hirsch, and J. A. Jordan, Jr., "The kinoform: a new wavefront reconstruction device," *IBM J. Res. Dev.* 13, 150 (1969).

Recent advances^{8,9} in surface-relief diffractive optics (e.g. kinoform optics) provide the optical designer with additional degrees of freedom to help reduce both chromatic and monochromatic aberrations. It has been shown for a number of applications that a single diffractive lens can perform better than conventional lens systems consisting of several conventional air-spaced glass elements. Fabrication techniques exist to "blaze" or tailor the phase profile of each zone; this provides a diffractive lens that exhibits high diffraction efficiency (i.e. nearly all of the incident light goes to the principal focus). The required profile can be realized in a wide variety of materials using photolithographic techniques common in fabrication of electronic integrated circuits,¹⁰ or by using diamond turning methods¹¹ to generate the desired surface-relief profile. Depending on the particular optical requirements, the savings in weight, alignment complexity and manufacturing cost can be substantial.

Based on prior experience with wide-field diffractive singlets, it appears possible to design lightweight optical relay assemblies for HMDs using surface-relief diffractive optical elements. Since the blazed diffractive elements are very thin (the comparable index of refraction is essentially infinite), the overall system weight may be decreased significantly. Using current replication technologies, stable (thermally and mechanically) components can be manufactured to minimize component cost while assuring repeatable performance.

At Rochester Photonics Corporation (RPC), researchers have designed and analyzed a series of HMD optical systems that combine surface-relief diffractive optics with conventional refractive optics. The integration of diffractive and refractive lenses offers the potential for the realization of compact and lightweight HMD optical relay assemblies that operate with illumination of reduced temporal coherence.

8 D. A. Buralli, G. M. Morris, and J. R. Rogers, "Optical performance of holographic kinoforms," *Appl. Opt.* **28**, 979 (1989).

9 D. A. Buralli and G. M. Morris, "Design of a wide field diffractive landscape lens," *Appl. Opt.* **28**, 3950 (1989).

10 G. J. Swanson, "Binary optics technology: The theory and design of multi-level diffractive optical elements," MIT Lincoln Laboratory Tech. Rep. 854, (1989); G. J. Swanson and W. B. Veldkamp, "Infrared applications of diffractive optical elements," *Proc. SPIE* **883**, 155 (1988).

11 See, for example, C. Londono and P. P. Clark, "The design of achromatized hybrid diffractive lens systems," *Int'l. Lens Design Conf.*, June 1990.

1.3 Objective

The primary objective of this research and development effort is to investigate the feasibility of high-performance optical relay assemblies for HMDs that utilize diffractive optical elements. An important constraint in the development of the HMD is to minimize the overall size and weight of the optics module while maintaining strict performance levels as defined by the AL mission.

Throughout the investigation, particular emphasis is placed on the color correction of the optics. Because it is theoretically impossible to design a system that consists solely of diffractive lenses that produces an achromatic real image,¹² our approach is to design the optical assembly using a combination of diffractive and refractive optical elements. The inclusion of the surface-relief diffractive elements allows the additional degree of freedom in the system design to correct for chromatic (as well as geometric) aberration. It is our intention to properly design the relay system such that the need for a notch filter (present in current designs to limit the CRT phosphor's bandwidth) is eliminated. Both on-axis and off-axis HMD designs are investigated.

For narrowband HMD systems, with particular application to future laser-based systems, an all-diffractive HMD is designed and analyzed. The operational wavelength band for a specified level of performance shall be identified.

Toward further implementation of the diffractive optics HMD in a specific mission scenario, imaging performance of the HMD design over wide fields-of-view and diffraction efficiency considerations of the diffractive components are investigated. Our objective is to identify a successful methodology for diffractive HMD advanced development under the Federal SBIR Phase II program.

1.4 Scope

This report fulfills the objectives within the scope of the statement of work as presented in RPC's original SBIR Phase I proposal dated 27 DEC 1989.

¹² D. A. Buralli and J. R. Rogers, "The use of Gaussian brackets in holographic optical design," J. Opt. Soc. Am. A 4, P17 (1987); D. A. Buralli and J. R. Rogers, "Some fundamental limitations of achromatic holographic systems," J. Opt. Soc. Am. A 6 1863 (1989).

1.5 Executive Summary

During the SBIR Phase I research and development effort, several diffractive HMD system designs have been analyzed. Size and weight characteristics of the HMD optical system were given high priority in the design. It was found that through the use of surface-relief diffractive optics technology lightweight HMD systems that operate over wide fields-of-view are feasible and can be implemented with current fabrication technologies.

Surface-relief diffractive optics have a number of features that are important to HMD systems. These features include: (1) Arbitrary phase functions can be encoded to help achieve optimum optical performance; (2) Wavelength dispersion is opposite in sign to that of conventional optical elements and the dispersion is quite large. This fact permits the correction of chromatic aberrations using diffractive/refractive hybrid elements; (3) Diffractive lenses do not contribute to Petzval curvature and can provide for flat field imaging; (4) Diffractive elements can be fabricated on thin substrates to help reduce system size and weight; (5) Diffractive optics can also be fabricated directly on the surface of conventional optical elements for aberration control thereby eliminating the need for the addition of extra optical components.

Several HMD geometries were investigated with special emphasis given to the correction of chromatic aberration. We have considered the design of an all-diffractive relay lens for use with an on-axis combiner system to investigate the feasibility of the class of on-axis, all-diffractive HMDs. Results indicate that, while an all-diffractive system can be extremely lightweight, there are severe limitations on the spectral bandwidth of the illumination source [see Fig. 3-18]. The all-diffractive relay lenses may be useful for future systems that utilize laser sources. We have also investigated the use of combinations of refractive and diffractive elements in the relay lens to provide color correction. The feasibility of color-corrected HMD systems using hybrid refractive/diffractive systems was investigated by considering the design of color-corrected hybrid relay lenses for on-axis and off-axis combiner configurations. The spectral band used for color correction was obtained from the emission curve for P53 phosphor. For the case of the on-axis combiner geometry [see Figs. 3-1 and 3-2], an acceptable hybrid, color-corrected relay weighs less than two ounces. The chromatic aberration was corrected for the spectrum of P53 and not just for the green spectral peak of P53. The preliminary design for the off-axis geometry

also indicates that diffractive optics can play an important role in extending the operational bandwidth and in reducing the weight of HMD systems.

Techniques for the fabrication of the diffractive components were reviewed. In all of our designs, we have included fabrication constraints and applied design-for-manufacture procedures. Methods based on photolithographic techniques and single-point diamond turning can be used to fabricate the diffractive elements. Diamond turning methods provide excellent performance for rotationally-symmetric optical elements. We have also determined that replication schemes using stable materials that meet military specifications exist for the potential production phase.

We have also reported on some inherent characteristics of systems that employ diffractive optical elements. Diffraction efficiency is clearly a critical parameter in the design and implementation of diffractive optical systems. It was shown that the undiffracted background has the effect of reducing the contrast, particularly at low spatial frequencies. This background noise will ultimately limit the operational bandwidth of the HMD system. Unfortunately, the amount of undiffracted light that a human observer can tolerate from an HMD over extended periods of time is a unknown.

The technical advances to date regarding kinoform fabrication, replication and testing strongly suggest that diffractive optics technology can provide unique solutions in the development of several military and commercial applications both with bulk optics and waveguide optics. The Federal Government, and particularly the Department of Defense, considers diffractive optics technology *critical* to the United States. Currently RPC, in a collaborative effort with a larger company, is developing an internal capability to fabricate diffractive optics for military and commercial systems. It is our intention to use our internal research and development partnership to develop fabrication methods and to use the SBIR program to develop applications of diffractive optics. The marriage of the two programs will enhance significantly the commercial opportunities, which is exactly in line with the charter of the SBIR program. We have already identified several commercial application areas that include bioengineering, optical data storage, optical testing, and materials processing that will benefit from the research herein. Our goal is to be a leader in the fabrication and testing of systems based on diffractive optics by way of our industrial partnerships and the SBIR program.

1.6 Format

The report format is structured according to the following:

- 1. Section 2.0 Diffractive Helmet-Mounted Display Systems**
- 2. Section 3.0 Helmet-Mounted Display Design Using Diffractive Optics**
- 3. Section 4.0 Fabrication of Diffractive Optical Elements**
- 4. Section 5.0 Characterization and Testing of the Diffractive Components of the HMD**
- 5. Section 6.0 Future Research**

These sections include a critique of the major components in the RPC diffractive optics HMD system design, a description of these components and fabrication and test methods. The report concludes with some recommendations for future R&D and SBIR Phase II development.

2.0 Diffractive Helmet-Mounted Display Systems

2.1 General

For the Federal SBIR Phase I effort, we have analyzed several HMD designs that utilize diffractive optics to reduce system weight and to increase optical performance. Our primary goal is to investigate the feasibility of color-corrected diffractive designs using CRT phosphor P53. Better utilization of the available illumination is an important consideration for flyable systems. Also, the development of color-corrected designs may provide some additional insight into full three-color systems. The use of spectral information will provide the pilot with another sensory dimension. A secondary goal is to study an all-diffractive HMD design for future applications that may use miniature laser scanners.

During this investigation, we modelled the performance of both on-axis and off-axis HMD geometries. The system parameters that guided the feasibility study are discussed in Section 2.2. A discussion of the design methodology is presented in Section 2.3 along with a brief review of the properties of diffractive optical elements.

2.2 Optical System Parameters

The parameters that were used for the optical system design are summarized in Table 2-1. A description of the HMD optical system design is located in Section 3.0.

System	Configuration	Color Correction	Monocular FOV	Binocular FOV	EPD	Eye Relief	CRT Size
A	On-axis	None	50°H x 37.5°V	80°H x 37.5°V	19 mm	125 mm	19 mm
B	On-axis	None	50°H x 37.5°V	80°H x 37.5°V	19 mm	125 mm	23 mm
C	On-axis	490 nm - 590nm	50°H x 37.5°V	80°H x 37.5°V	19 mm	125 mm	19 mm
D	On-axis	490 nm - 590 nm	50°H x 37.5°V	80°H x 37.5°V	19 mm	125 mm	23 mm
E	Off-axis	490 nm - 590 nm	30°H x 22.5°V	30°H x 22.5°V	15 mm	100 mm	19 mm

Table 2-1. Design parameters for the HMD optical system design.

2.3 Design Methodology

Surface-relief diffractive optics can play a role in the improvement of the optical properties of helmet optical systems and the reduction of HMD head-borne weight. Our approach to the HMD design problem is to employ diffractive elements for color and wavefront correction. In Section 2.3.1, a brief review of the important properties of diffractive optics is presented. An outline of the computer simulations is presented in Section 2.3.2.

2.3.1 Review of Diffractive Optics

Optical elements interact with wavefronts using the processes of refraction, reflection and diffraction. Diffractive optical elements, as employed in this development effort, rely on diffraction to alter the *phase* of the incident wavefront. (Depending on the particular method of implementation, diffractive optics can also produce transformations in

the wave amplitude). The primary physical characteristic of a diffractive element is a diffraction-grating-like structure. For example, in the case of a diffractive cylindrical lens, the element consists of a chirped (variable period) linear grating. The phase of the incident field is modified by the grating structure; therefore, the corresponding ray paths are also modified. In general, the desired wavefront transformation is encoded in the grating structure, specifically in the grating spacing. Unlike a uniform-period linear diffraction grating that simply changes the angle of propagation of an incident beam, the general diffractive optic grating spacing is a function of the spatial location on the optic. The potentially complicated grating structure, which may represent an off-axis aspheric transformation, is typically calculated and optimized using commercial optical design software. Like diffraction gratings, diffractive optical elements can be "blazed" to concentrate energy in a given diffracted order.

Practically speaking, the prescription for a diffractive element results directly from the desired phase transformation relating the input and output wavefronts. The phase transformation can be implemented by a number of techniques including optically recorded and computer-generated holographic optical elements and surface-relief (kinoform) optical elements. Since HMD systems require rather complicated computer-generated diffractive correction, we limit our discussion to the (manufacturable) case where the phase transformation is encoded in a high-efficiency surface-relief profile.

A conventional refractive lens produces a phase transformation using the properties of polished, curved optical substrates [see Fig. 2-1]. For the generation of surface-relief diffractive lenses, a modulo 2π operation is performed on the optical phase transformation to determine the zone structure (fringe spacing) of the diffractive element. This reduced expression for the phase transformation describes the wavefront characteristics of the diffractive element. For many important cases, the phase transformation occurs across the clear aperture over a thin region of thickness approximately equal to $2\lambda_0$, where λ_0 is the design wavelength.

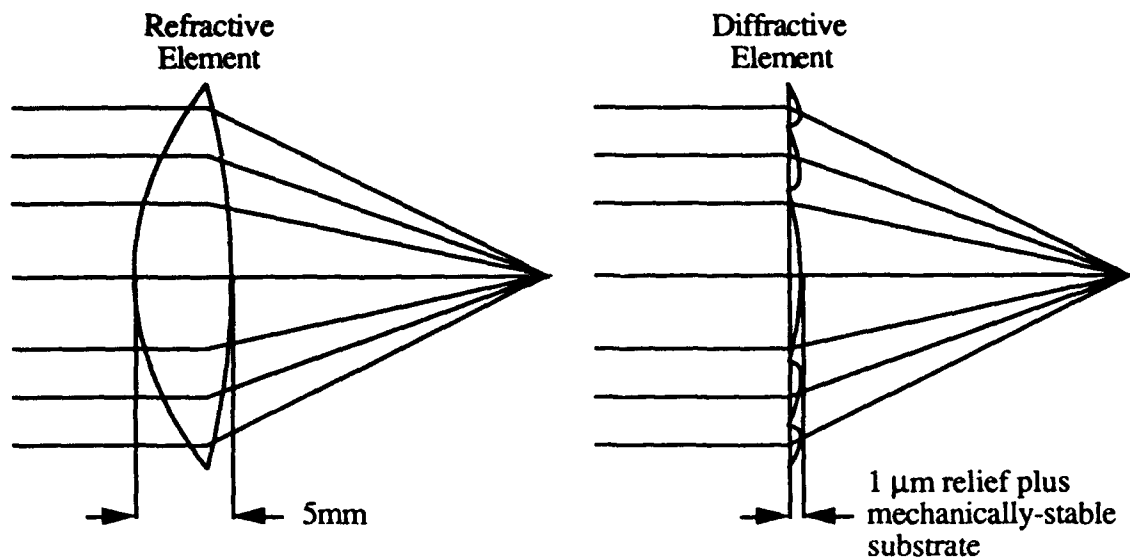


Fig. 2-1. Refractive and diffractive lenses. The diffractive lens can be many times lighter than the refractive element because it derives optical power from a surface structure rather than bulk curvature. The maximum thickness of the surface relief is typically equal to $2\lambda_0$ (for a substrate index of 1.5).

The surface profile between zones (e.g. like in a phase Fresnel zone plate) determines the amount of energy to be diffracted into a particular order. For the case of a binary phase Fresnel zone plate, approximately 81% of the incident illumination is shared by the +1 and -1 diffracted orders, equally. The remainder of the energy is appropriately distributed among the other diffracted orders; the relative amounts are determined by the square surface profile. The exact surface profile for a general diffractive lens is determined by the modulo 2π operation. However, experience in the manufacture of these lenses has shown that linear and quadratic approximations to the exact surface profile provide excellent results in many cases.

It is important to note that the period of the resulting grating structure at a particular spatial location is proportional to the rate at which the optical phase transformation goes through 2π [see Fig. 2-2]. If the desired phase change across the optic is small, then there will be few 2π phase jumps in the resulting kinoform element; the *minimum* grating spacing (or zone) can be quite large and the optic can be easily manufactured. However, if the diffractive element provides a large phase transformation (many 2π phase jumps), then there will be many zones and the minimum zone spacing can be quite small. For example, for the case of a cylindrical diffractive lens, the spacing of the outermost zone is equal to

$2\lambda_0 f/\#$, where λ_0 is again the design wavelength and $f/\#$ represents the f-number of the lens. For an $f/2$ lens at visible wavelengths, the grating spacing at the edge of the lens is $4\lambda_0$ or approximately $2\text{ }\mu\text{m}$. Recall that the proper height of the surface profile is of the order of twice the design wavelength. Blazed structures of this size have been fabricated using diamond turning methods for visible and infrared applications. The fabrication schemes for structures this small are quite complicated and currently require expensive machinery. However, as we will see later, diffractive lenses for HMD systems do not require extremely high-spatial frequency grating structures and should be, in general, easier to fabricate.

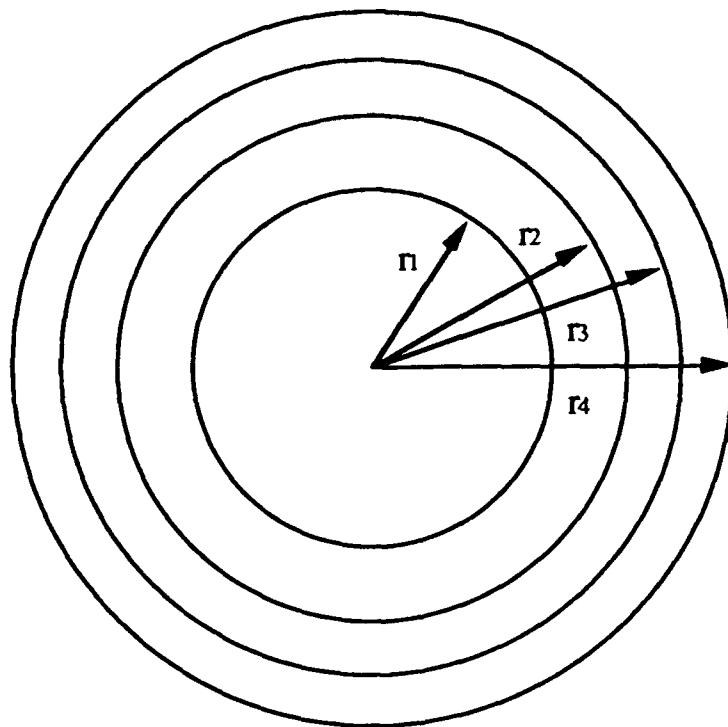


Fig. 2-2. Paraxial diffractive lens illustrating the radii of the first four zones, where $r_1 = \sqrt{2\lambda_0 F}$, $r_2 = \sqrt{4\lambda_0 F}$, $r_3 = \sqrt{6\lambda_0 F}$ and $r_4 = \sqrt{8\lambda_0 F}$. The zone radii are determined directly by the required phase transformation.

Surface-relief diffractive optics have a number of useful properties that include the following:

1. Arbitrary phase functions can be encoded and manufactured to help achieve optimum optical performance;

2. Diffractive lenses do not contribute to Petzval curvature (i.e. the effective refractive index is essentially infinite) and can provide for flat field imaging;
3. Wavelength dispersion is opposite in sign to that of conventional optical elements and the dispersion is quite large. This fact permits the correction of chromatic aberrations using diffractive/refractive hybrid elements;
4. Diffractive elements can be fabricated on thin substrates to help reduce system size and weight;
5. Diffractive optics can also be fabricated directly on the surface of a conventional optical element for aberration control thereby eliminating the need for the addition of extra optical elements.

Initial studies of the aberration properties of diffractive elements were commonly performed, in the past, by comparing the optical path or phase differences between an object point and an image point^{13,14,15,16}. In 1977, it was shown independently by Sweatt¹⁷ and Kleinhans¹⁸ that a diffractive lens is mathematically equivalent to a thin lens with an infinite refractive index. Using this thin lens analogy, it is possible to apply the results of geometrical optics to diffractive lenses without the need to calculate a special class of formula that applies only to diffractive optics. In particular, this analogy provides a method for discussing the aberration characteristics of diffractive structures in terms of the Seidel sums and the paraxial chromatic contributions. Conventional lens design software can be used to design systems that include diffractive components.

It is important to note that there are other useful methods beside the thin-lens-equivalent method to design diffractive elements with lens design software. We have also created diffractive surfaces that are described by phase polynomials such as

-
- 13 K. Kamiya, "Theory of fresnel zone plate," *Sci. Light* **12**, 35 (1963).
 - 14 R. W. Meier, "Magnification and third-order aberrations in holography," *J. Opt. Soc. Am.*, **55**, 987 (1965).
 - 15 E. B. Champagne, "Nonparaxial imaging, magnification, and aberration properties in holography," *J. Opt. Soc. Am.*, **57**, 51 (1967).
 - 16 M. Young, "Zone plates and their aberrations," *J. Opt. Soc. Am.*, **62**, 972 (1972).
 - 17 W. C. Sweatt, "Describing holographic and optic elements as lenses," *J. Opt. Soc. Am.*, **67**, 803 (1977).
 - 18 W. A. Kleinhans, "Aberrations of curved zone plates and Fresnel lenses," *Appl. Opt.* **16**, 1701 (1977).

$$\phi = \frac{2\pi}{\lambda_0} (s_1\rho^2 + s_2\rho^4 + s_3\rho^6 + s_4\rho^8 + s_5\rho^{10} + \dots) , \quad (2-1)$$

where

$$\rho^2 = x^2 + y^2 , \quad (2-2)$$

s_i represent the phase coefficients, ϕ is the optical phase transformation, ρ is the radial coordinate in the plane of the diffractive structure, and λ_0 is the design wavelength. Optical aberrations can be corrected through the use of phase transformations as described in Eq. (2-1) that are implemented using surface-relief profiles. Mathematical relationships of the form of Eq. (2-1) can be used to direct a coordinate generator in the fabrication process to effectively write the aspheric structure. We will refer to these surfaces more later.

Chromatic correction of the HMD optics has been a primary consideration in this investigation. As discussed earlier, diffractive/refractive hybrid elements can be constructed to correct for chromatic aberrations in much the same manner as refractive lenses are combined for achromatization purposes. Many successful applications of hybrid optics already exist.¹⁹ It is important to note, however, that it is theoretically impossible to produce an *achromatic real image* of a non-virtual object using *only* diffractive elements.²⁰

The axial chromatic contribution of the diffractive lens can be found by starting with the power of a diffractive lens. The power $\Phi_d(\lambda)$ at a given wavelength λ is given by

-
- 19 See, for example, S. J. Bennett, "Achromatic combinations of hologram optical elements," Appl. Opt. **15**, 542 (1976); R. E. Hufnagel, Achromatic holographic optical system, US Patent 4,550,973 (5 NOV 1985); T. Stone and N. George, "Hybrid diffractive-refractive lenses and achromats," Appl. Opt. **27**, 2960 (1988); D. Faklis and G. M. Morris, Achromatic imaging with combinations of holographic and conventional lenses," J. Opt. Soc. Am A **3** P53 (1986); D. A. Buralli and J. R. Rogers, "The use of Gaussian brackets in holographic optical design," J. Opt. Soc. Am. A **4**, P17 (1987); G. J. Swanson and W. B. Veldkamp, "Diffractive optical elements for use in infrared optical systems," Opt. Eng. **28**, 605 (1989); T. Stone, "Hybrid diffractive-refractive telescopes," SPIE **1212** (1990).
- 20 D. A. Buralli and J. R. Rogers, "The use of Gaussian brackets in holographic optical design," J. Opt. Soc. Am. A **4**, P17 (1987); D. A. Buralli and J. R. Rogers, "Some fundamental limitations of achromatic holographic systems," J. Opt. Soc. Am. A **6** 1863 (1989).

$$\Phi_d(\lambda) = \frac{\Phi_d(\lambda_o)\lambda}{\lambda_o} = \frac{\lambda}{\lambda_o f_d(\lambda_o)} \quad , \quad (2-3)$$

where Φ_o is the power of the diffractive lens when $\lambda = \lambda_o$. Note from Eq. (2-3) that a diffractive lens is indeed very dispersive and, in fact, the dispersion is obviously in the opposite direction relative to most conventional refractive elements.

To illustrate the concept of using diffractive lenses for color correction, the transverse axial chromatic aberration, TACH (i.e. a transverse measure of the axial color) of a hybrid doublet (i.e. a single piece of glass or plastic with a curved front surface and a diffractive rear surface) is described by

$$\text{TACH} = \frac{f}{2(f/\#)} \left(1 - \frac{K_{\text{ref}}(n_{\text{ref}}(\lambda) - 1) + \frac{\Phi_d(\lambda_o)\lambda}{\lambda_o}}{\Phi_o} \right) \quad , \quad (2-4)$$

where f is the focal length and if we minimize the RMS values for the TACH for three wavelengths we find that

$$K_1 = \Phi_o \frac{CD - EB}{AC - B^2} \quad (2-5)$$

and

$$\frac{\Phi_d(\lambda_o)}{\lambda_o} = -\Phi_o \frac{BD - AE}{AC - B^2} \quad (2-6)$$

where

$$\begin{aligned}
A &= \sum_{i=1}^3 (n_{\text{ref}}(\lambda_i) - 1)^2, \\
B &= \sum_{i=1}^3 (n_{\text{ref}}(\lambda_i) - 1)\lambda_i, \\
C &= \sum_{i=1}^3 \lambda_i^2, \\
D &= \sum_{i=1}^3 (n_{\text{ref}}(\lambda_i) - 1), \\
E &= \sum_{i=1}^3 \lambda_i.
\end{aligned} \tag{2-7}$$

If we choose the glass for the element as BK7 and correct the doublet over the visible spectrum, using the C, d and F' spectral lines, we find that

$$\Phi_{\text{ref}}(\lambda_o) = \Phi_o(1.8310)(n_{\text{ref}}(\lambda_o) - 1) \Big|_{\lambda_o = .586 \mu\text{m}} = \Phi_o(.94628), \tag{2-8}$$

and

$$\Phi_d(\lambda_o) = \Phi_o(0.092605)(\lambda_o \text{ in microns}) \Big|_{\lambda_o = .586 \mu\text{m}} = \Phi_o(.0527011). \tag{2-9}$$

A very important result of this calculation is that the optical power of both the refractive element and the diffractive surface are positive. This can allow the weight of the hybrid diffractive/refractive doublet to be reduced with respect to that of a *single-refractive-element monochromatic* lens. Note that the power of the diffractive surface is only 5% of the total optical power. This translates into a simplified manufacturing process since the minimum zone spacing can be quite large.

The TACH for a hybrid doublet using BK7 over the visible region of the spectrum is plotted in Fig. 2-3. In addition, the TACH for hybrid doublets using SF3 and FK54 is plotted. It is interesting to notice that the secondary spectrum of all the hybrid doublets is opposite in sign to that of conventional refractive doublets.

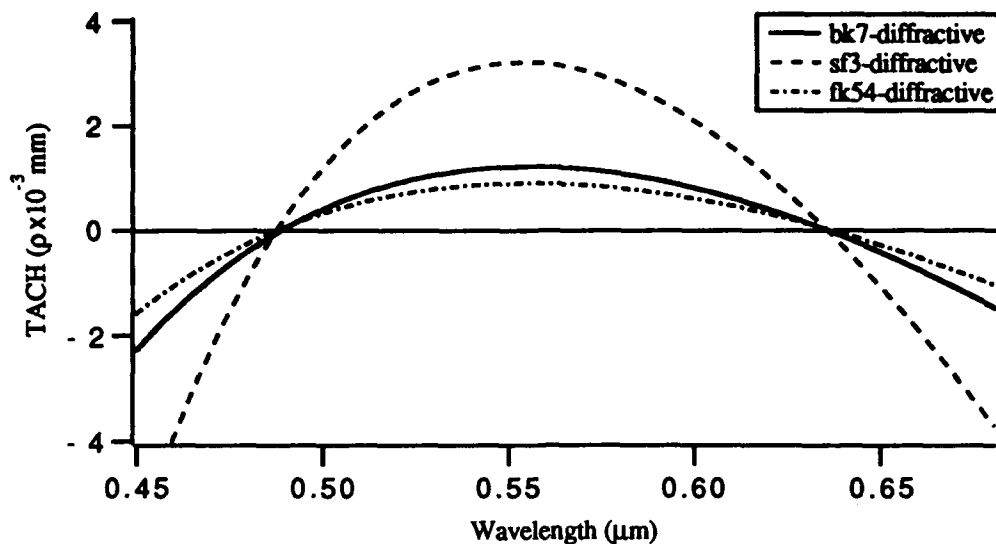


Fig. 2-3. TACH for a hybrid doublet over the visible region. Note that the secondary spectrum is opposite in sign relative to that of a conventional refractive achromatic doublet.

The effect of the secondary spectrum of the system can be reduced by combining the color correction of a refractive doublet with that of a diffractive doublet. Optical systems corrected for three wavelengths are commonly referred to as apochromatic. An apochromatic hybrid system can be designed by using the same technique as were employed to design the achromatic doublet. The TACH for this case is given by

$$\text{TACH} = \frac{f_\lambda}{2(f/\#)} \left[1 - \frac{K_{\text{ref}1}(n_1(\lambda) - 1) + K_{\text{ref}2}(n_2(\lambda) - 1) + \frac{\Phi_d(\lambda_o)\lambda}{\lambda_o}}{\Phi_o} \right] \quad (2-10)$$

Again, by minimizing the RMS TACH for the C, d and F' spectral lines using BK7 and SF3 combined with the diffractive structure, we find that the powers are given by

$$\begin{aligned} \Phi_{\text{bk}7}(\lambda_o) &= \Phi_o(3.0113)(n_{\text{bk}7}(\lambda_o) - 1) \Big|_{\lambda_o = 0.587 \mu\text{m}} = \Phi_o(1.5562) , \\ \Phi_{\text{sf}3}(\lambda_o) &= \Phi_o(-0.77048)(n_{\text{sf}3}(\lambda_o) - 1) \Big|_{\lambda_o = 0.587 \mu\text{m}} = \Phi_o(-0.57016) , \end{aligned} \quad (2-11)$$

and

$$\Phi_d(\lambda_o) = \Phi_o(0.02369)(\lambda_o \text{ in microns}) \Big|_{\lambda_o = 5.87 \mu\text{m}} = \Phi_o(0.013919) \quad (2-12)$$

For this system the first element has approximately 1.5 times the total system power. The extra power in the first element and the compensation in the second element will increase the system weight over the weight of the simple monochromatic singlet by approximately a factor of 2, this increase is still less than that of an achromatized refractive doublet. Figure 2-4 illustrates the performance of the hybrid lens.

The previous examples were used to illustrate the process by which diffractive surfaces are used to help correct for chromatic aberration. However, chromatic effects are not limited to the first order properties of the system. The third-order aberrations of the system are also affected by the element dispersions in the system. An example of the chromatic change of third-order aberrations is spherochromatism, a change in the magnitude of spherical aberration with wavelength. An example of spherochromatism results by examining the thin-lens Seidel sum for spherical aberration.

$$S_I = \frac{\rho^4 \Phi^3}{4} \left[\left(\frac{n}{n-1} \right)^2 + \frac{n+2}{n(n-1)^2} B^2 + \frac{4(n+1)}{n(n-1)} BT + \frac{3n+2}{n} T^2 \right] + 8G\rho^4(\Delta n) \quad (2-13)$$

In Eq. (2-13), $n = n(\lambda)$ is the index of refraction of the lens substrate, ρ is the paraxial marginal ray height at the lens, $\Phi = \Phi(\lambda) = (c_1 + c_2)(n-1)$ is the power of the lens, c_1 and c_2 are the curvatures of the two lens surfaces, G is the fourth-order aspheric deformation of a surface (if either or both surfaces are not spherical), $\Delta n = \Delta n(\lambda)$ is the change in refractive index on passing through the aspheric surface, and B and T are the dimensionless bending and conjugate parameters, respectively, defined by

$$B = \frac{c_1 + c_2}{c_1 - c_2} \quad T = \frac{u + u'}{u - u'} \quad (2-14)$$

In Eq. (2-14), u and u' are the paraxial ray angles for the paraxial marginal ray entering and leaving the thin lens. If we consider a single thin lens operating with the object at infinity ($T=-1$), the value for S_I is a minimum when

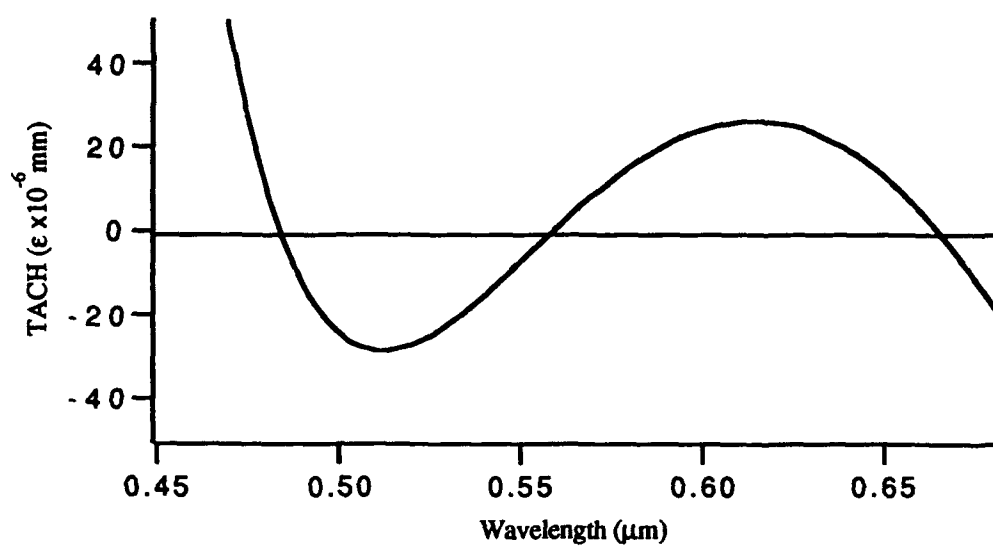


Fig. 2-4. TACH for an F/5 apochromatic system with $efl=10$ mm that utilizes hybrid refractive/diffractive elements. Note the change in scale from Fig. 2-3.

$$B = \left[\frac{(4n+1)(n-1)}{(2n+4)} \right] . \quad (2-15)$$

For this particular case to illustrate the concept of spherochromatism, the spherical aberration is given by

$$S_I = \frac{\rho^4 \Phi^3}{4} \left[\left(\frac{n}{n-1} \right)^2 - \frac{4n+1}{n+2} + \frac{3n+2}{n} \right] . \quad (2-16)$$

For a single spherical element with the object at infinity, the primary spherical aberration can never be zero, unless the index is infinite. The residual spherical aberration is typically corrected using an asphere on one surface. If the asphere is on the first surface, the expression for G is given by

$$G = -\frac{\Phi^3}{16(n-1)} \left[\left(\frac{n}{n-1} \right)^2 - \frac{4n+1}{n+2} + \frac{3n+2}{n} \right] . \quad (2-17)$$

This computation sets the value for S_I to zero for the *design* wavelength. It is obvious from Eq. (2-16) that for any wavelength other than the design wavelength the value for S_I will not be zero. Because of special dispersion characteristics, the wavelength-dependent spherical aberration produced by the diffractive structure helps reduce the spherochromatism of the system.²¹ The diffractive structure is described, in general, by Eq. (2-1). The values of the weighting parameters s_i and the optical performance are determined using established lens design methods.

The above discussion was presented to illustrate the important capability of diffractive optics to correct both the first- and higher-order aberrations. Although the discussion is limited to a few important cases (e.g. on-axis aberration), however, the method is quite general. To summarize, controlling the zone spacings of the diffractive element (i.e. the appropriate phase profile) allows correction of the lens aberrations.²² The form of the height profile allows the diffracted energy distribution to be controlled. In

²¹ A. P. Wood, "Using hybrid refractive-diffractive elements in infrared Petzval objectives," SPIE, Holographic Optics, 1354-21, Paris, June 1989.

²² D. A. Buralli and G. M. Morris, "Design of a wide field diffractive landscape lens," Appl. Opt. 28, 3950 (1989).

particular, it is possible to achieve high-optical performance and high-diffraction efficiency for a specific diffracted order.

2.3.2 Scope of Work

In the following Section, a detailed description of the HMD optical designs is presented. For the Federal SBIR Phase I feasibility study, we investigated diffractive correction for three main classes of HMD systems. These are 1) All-diffractive, monochromatic; (2) Centered, on-axis, color corrected; and (3) Off-axis, color corrected. Design tradeoffs, expected performance levels and a tolerance analysis are reported. In Section 4.0, the investigation of fabrication techniques for the diffractive elements is presented. Both photolithographic and single-point diamond turning techniques are considered. A brief analysis of substrate materials and replication schemes is reported. In Section 5.0, we present the results of an investigation of methods to characterize the performance of the diffractive components of the HMD. We report a study of the diffraction efficiency issue of diffractive optics and we present a discussion of the effects of imperfect diffraction efficiency on the modulation transfer function over the field-of-view.

3.0 Helmet-Mounted Display Design Using Diffractive Optics

3.1. Introduction

This section discusses the investigation of optical designs for helmet-mounted displays utilizing diffractive optics. The first system considered is an all-diffractive design, the primary advantage of this is extremely lightweight. The remaining systems are hybrid diffractive/refractive systems that are color corrected over an extended wavelength range. Of the hybrid designs, both on-axis and off-axis designs have been investigated.

3.2 All-diffractive HMD Design

We have considered the design of an all-diffractive relay lens for use with an on-axis combiner system to investigate the feasibility of the class of on-axis, all-diffractive HMDs. The motivation for considering this system design is that an all-diffractive HMD that consists of planar optics can be *extremely* lightweight. Our goal is to minimize the head-borne weight of the system while maintaining acceptable performance, thus decreasing the problems associated with HMD center of gravity.

The design parameter that likely has the greatest impact on the optical performance of the all-diffractive relay lens is the spectral bandwidth of the illumination source. An increase in the illumination bandwidth reduces significantly the imaging performance in an all-diffractive system due to the large dispersion of the diffractive components [see, for example, Section 2.3 and Section 5.0]. It is now known that there are no combinations of diffractive elements only that will give rise to an achromatic real image of an object. As we will report later, the spectrum of the phosphor source must be properly filtered to provide narrowband illumination. This may seem to be a severe drawback, however, the all-diffractive solution may be quite useful for the case of future systems that may use miniature laser scanners or bright narrowband phosphors to display avionics symbology. In any case, the required degree of monochromaticity will be discussed with regards to the overall effect on system performance.

We have completed two all-diffractive relay lens designs for an on-axis HMD system configuration. Our effort includes an investigation of the effect of CRT size on system performance. The design information for the two relay-lens systems, designated system A and system B, is found in Appendices A and B, respectively. For the first design

(system A), the diameter of the CRT active area is 19 mm and in the second design (system B) the CRT active area is 23 mm in diameter. Note that the CRT size will certainly affect the optical performance however, the two resulting optical system designs are not merely scaled versions of each other. The effect of the CRT diameter on the system performance will be discussed with respect to both the monochromatic and the polychromatic MTF of the system.

For the present analysis, it is assumed that the image produced by the CRT is on the outside of the faceplate. The image of the CRT may be projected to the outside surface of the faceplate through the use of a fiber-optic imaging bundle. We have chosen to curve the faceplate of the CRT to help correct for the field curvature caused by the curved combiner. As discussed briefly in Section 2.3, diffractive elements cannot be used to correct field curvature because they do not contribute to the Petzval sum. An alternate method for correcting the field curvature in these systems is to use a refractive field flattening element placed at the image plane. Refractive field flatteners are commonly used in refractive relay systems and are used in the hybrid refractive/diffractive relays discussed later.

The class of all-diffractive relay lenses considered in this study is composed of two planar diffractive elements. In our investigations, we have determined that the monochromatic performance can be improved through the addition of a third diffractive element. However, because acceptable narrowband performance can be achieved (see Section 2.2) with two diffractive elements, the three-element diffractive relay is not discussed in detail in this report.

The on-axis combiner geometry was specifically chosen to examine the feasibility of using an all-diffractive relay lens in a HMD. For this combiner configuration, we have chosen a full FOV of 50° in the horizontal direction and 37.5° in the vertical direction. This choice of FOV was made because it represents the larger (i.e. more difficult design) of the two FOVs that are of current interest to AL. The unvignetted EPD for this system was chosen to be 19 mm. The unvignetted EPD was chosen using an instantaneous EPD of 5 mm and an allowed helmet motion of ± 3 mm with respect to the eye of the wearer.

We have chosen a combiner design that is similar to that of the baseline HMD configuration shown in Fig. 3-1. The combiner consists of a spherical visor with a radius of curvature of 150 mm, which is located 125 mm in front of the pupil of the eye, and a beamsplitter that folds the light path down to the relay lens and the CRT. The large eye

relief (125 mm) chosen for this combiner is required to provide sufficient clearance away from the face for the beamsplitter. The relay lens is located at the image of the eye pupil produced by the spherical combiner. The optical path length from the visor to the image of

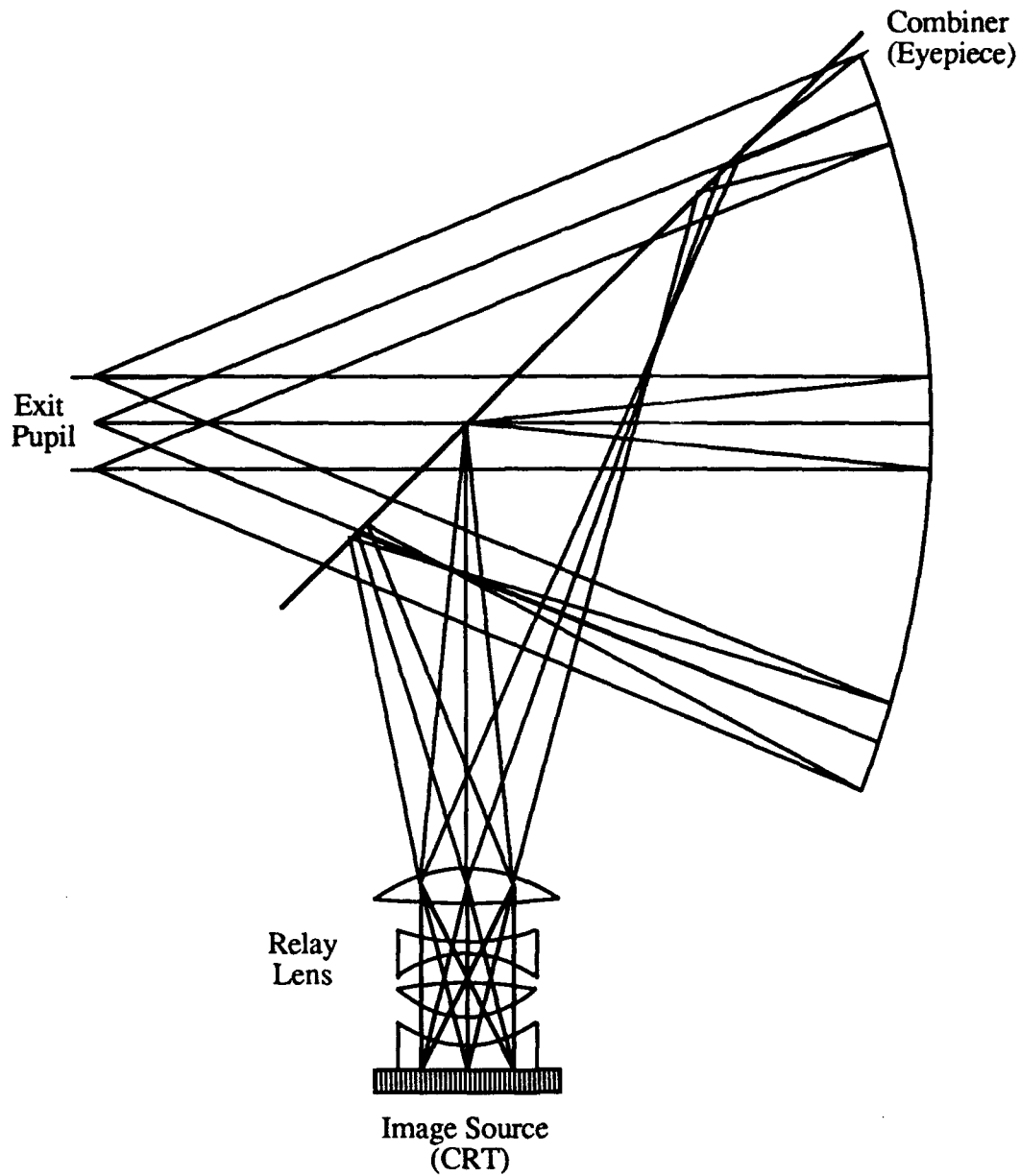


Fig. 3-1. Baseline configuration of the optical train for a HMD using an on-axis combiner and relay system. The components have been drawn in simply to illustrate the geometry and do not represent actual design data.

the eye pupil is 187.5 mm; this distance will allow this on-axis combiner to be mounted to a helmet. One possible mounting configuration for this combiner geometry is shown in Fig. 3-2. Placing the relay lens in this position will help to reduce the size of the refractive or diffractive elements required to produce the large unvignetted system exit pupil.

The diameter of the visor element D for a given half FOV in the horizontal direction Φ and eye relief ER is given by

$$D = 2ER \sin \Phi \quad (3-1)$$

Equation (3-1) gives a visor diameter for this system ($\Phi=25^\circ$, $ER=125$ mm) of 106 mm, this is larger than the minimum interpupillary distance IPD, of 52 mm given in Section 2.2. The interpupillary distance in this case limits the allowed overlapped FOV. The overlapped FOV of this visor in a binocular system is given by

$$OFOV = 2 \arcsin \left(\frac{IPD}{2ER} \right) \quad (3-2)$$

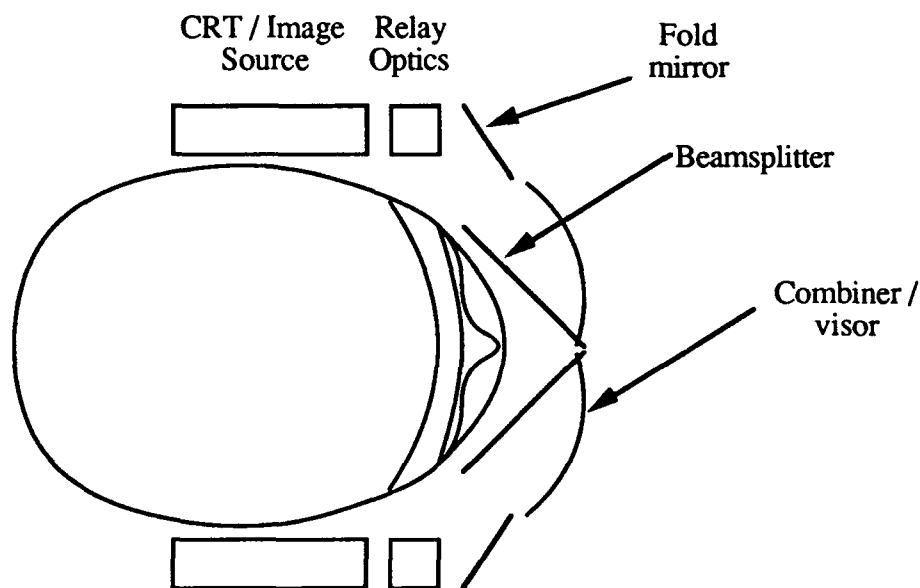


Fig. 3-2. Head-mounted, on-axis combiner/visor system. One possible configuration of the all-diffractive on-axis HMD.

Equation (3-2) effectively places a constraint on the overlapped FOV to no more than 20°, which results in a full FOV equal to 80°. The overlapped FOV and the full FOV of a binocular system using this combiner configuration are shown in Fig. 3-3.

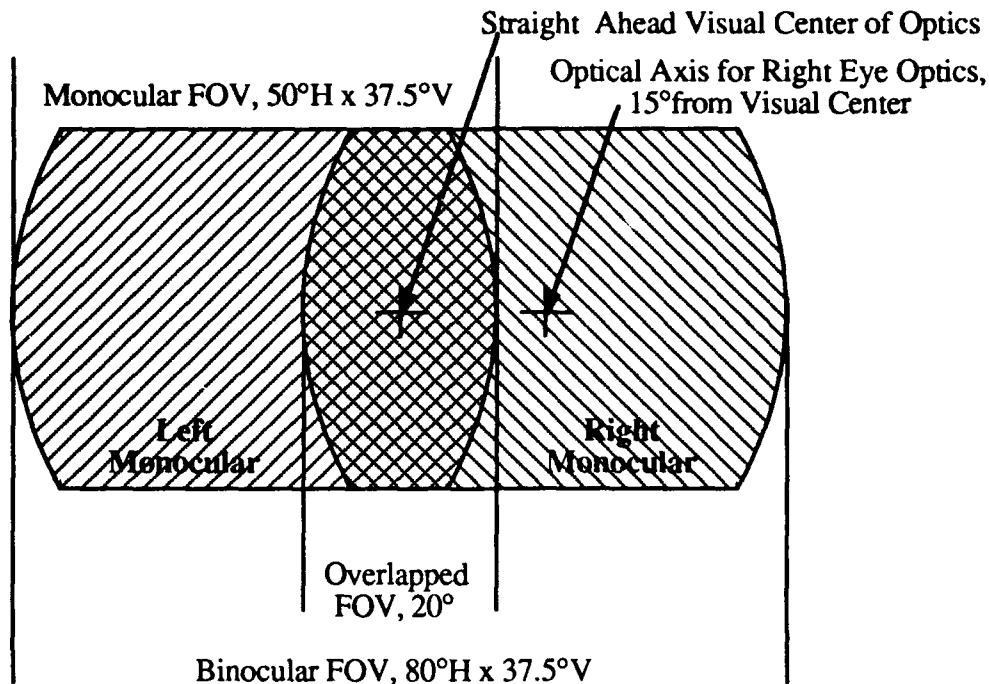


Fig. 3-3. Binocular FOV of on-axis combiner, illustrating maximum allowable overlapped FOV.

Using this combiner in a binocular system with a partially overlapped FOV places an additional constraint on the optical system that requires the mapping of the CRT to the pupil of the eye to follow the F-theta condition. The deviation from the F-theta condition will be specified for each system in terms of the percent linearity (%lin). The percent linearity is defined as

$$\%lin = \frac{h}{F_{rms} \Theta} - 1 \quad , \quad (3-3)$$

where h is the real image height for the field angle Θ and F_{rms} is chosen to minimize the RMS percent linearity over the field. The percent linearity for the system designs considered here are less than 1%.

The throughput of the combiner can be approximated by considering the output spectrum of the image source to be monochromatic. For a monochromatic source, we assume that the coating on the visor is designed to have a reflectivity of unity over a very small wavelength band (~ 20 nm) centered around the design wavelength and a reflectivity of approximately 0.2 over the rest of the spectrum. Similarly, we assume that the beamsplitter has a reflectivity of 0.5 over a small bandwidth and a reflectivity of 0.2 over the rest of the spectrum. These assumptions give a combiner transmission of 64% from the outside world and a transmission of 25% for the light that is coming from the relay lens.

Unfolded diagrams of system A and system B are shown in Figs. 3-4 and 3-5, respectively. The substrates chosen for the diffractive elements in both of these systems are curved, 2 mm-thick BK7 windows. In the design, we have chosen to allow the diffractive element substrates in the all-diffractive systems to be curved or bent. Bending the diffractive elements adds a useful degree of freedom to the system.

The actual length of the relay lens for system A is approximately 88 mm and that of system B is approximately 102 mm. The overall length of the all-diffractive relay lenses studied here is rather large. Although two elements give acceptable performance, the addition of a third element may be used to decrease overall length and allow for a system that is easier to integrate.

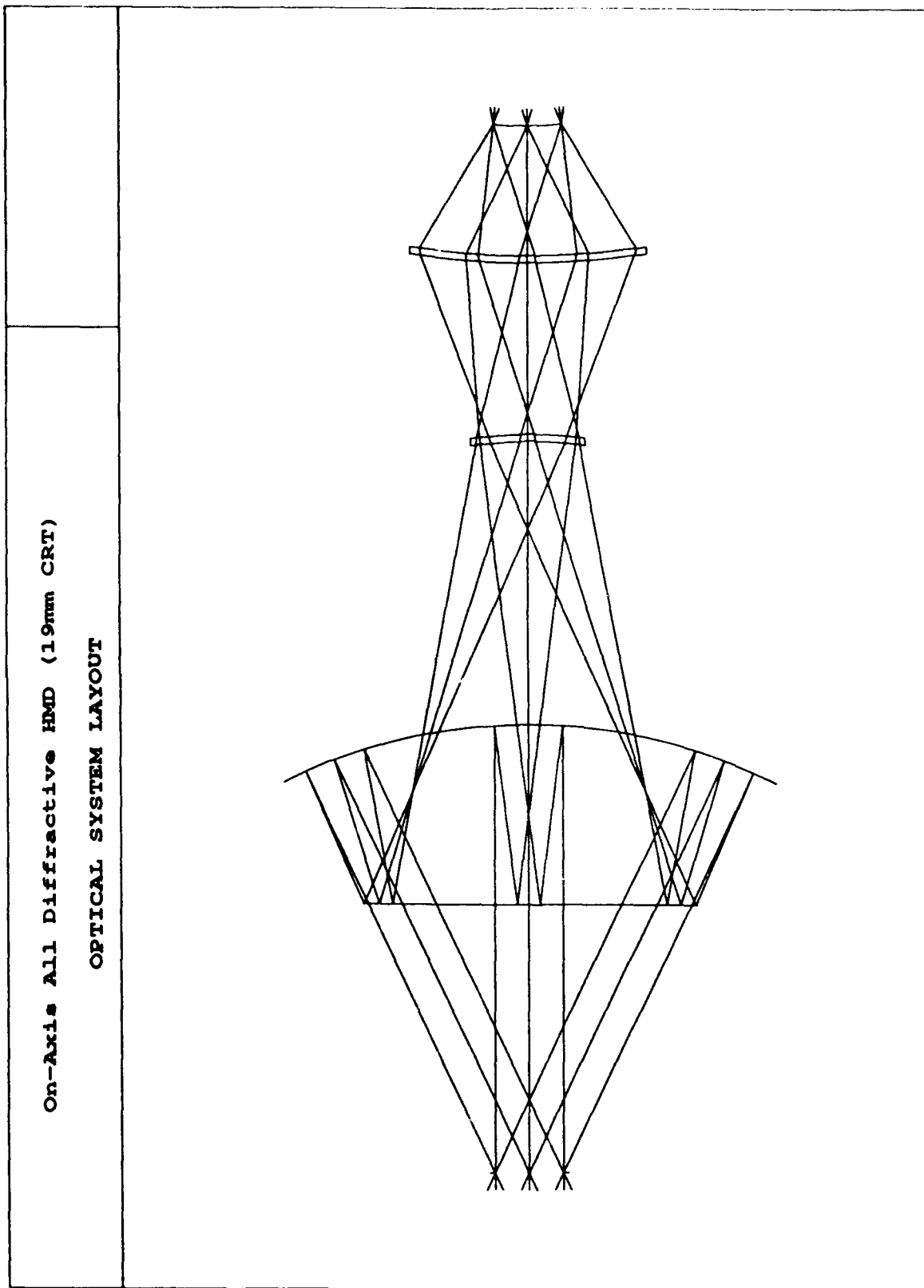


Fig. 3-4. Unfolded system diagram for system A. The illustration represents an on-axis HMD using an all-diffractive relay lens with a 50° FOV, 19 mm EPD and 19 mm-diameter CRT.

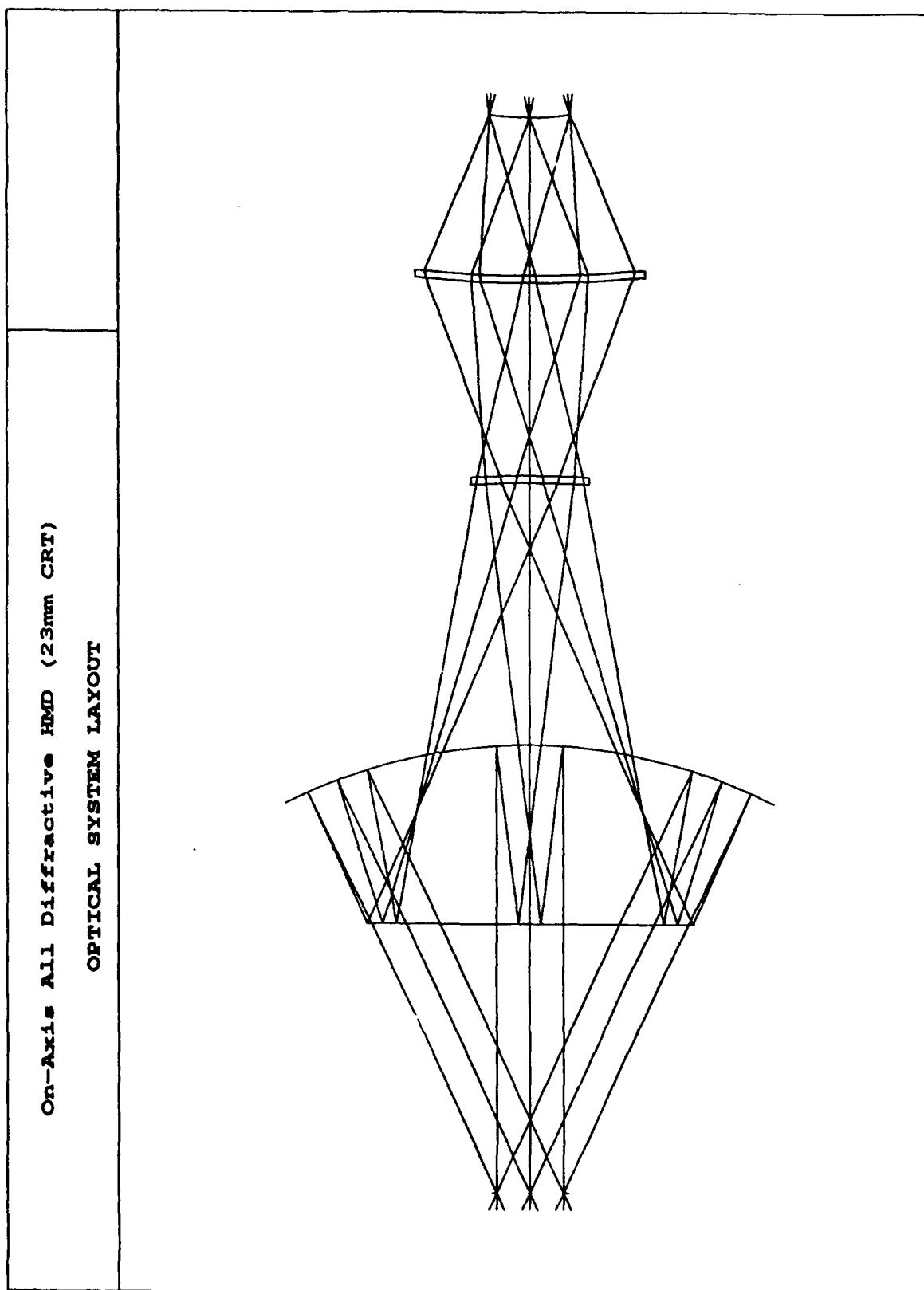


Fig. 3-5. Unfolded system diagram for system B. The illustration represents an on-axis HMD using an all-diffractive relay lens with a 50° FOV, 19 mm EPD and 23 mm-diameter CRT.

The monochromatic performance of system A is shown in Figs. 3-6 and 3-7. The monochromatic performance of system B is illustrated in Figs. 3-8 and 3-9. The two plots for each system correspond to two rotations of a 5 mm-diameter eye pupil. The first set of MTF curves corresponds to the wearer looking straight ahead (straight-ahead viewing). When the wearer is looking straight ahead with this combiner geometry, the eye pupil is rotated away from the optical axis of the viewing system by 15° . The MTF plots for this eye pupil rotation are for straight ahead or 0° , full field or $+10$ degrees and -15° . The second set of MTF curves are for the eye pupil rotated to the axis of the combiner and relay (on-axis viewing). The eye pupil rotation required so that the eye pupil is centered on the optical axis is 15° away from straight-ahead viewing. The eye positions and field angles used to evaluate the performance of the on-axis combiner systems are shown in Figs. 3-10 and 3-11.

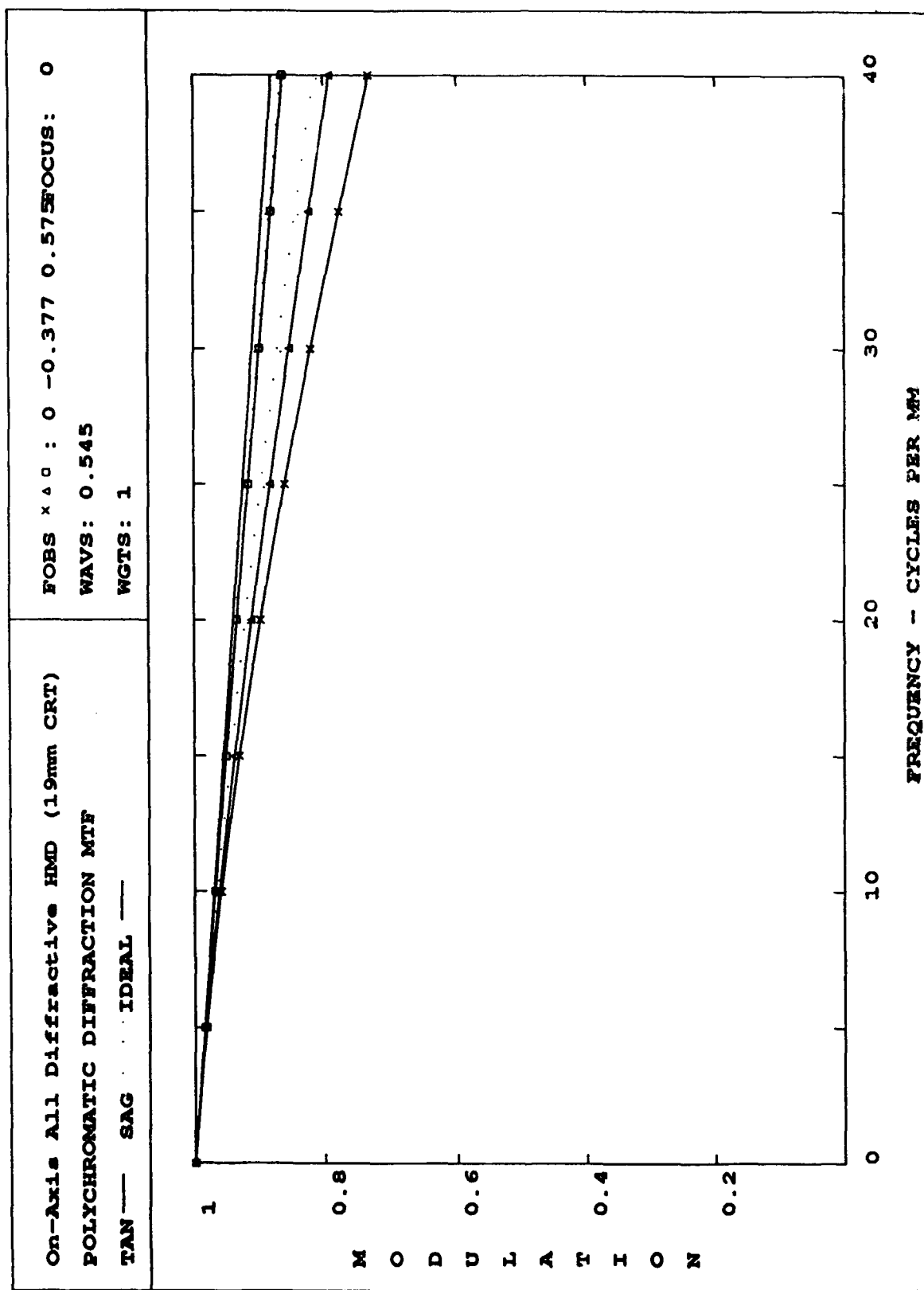


Fig. 3-6. Monochromatic performance for system A with a 5 mm eye pupil in the straight-ahead viewing configuration.

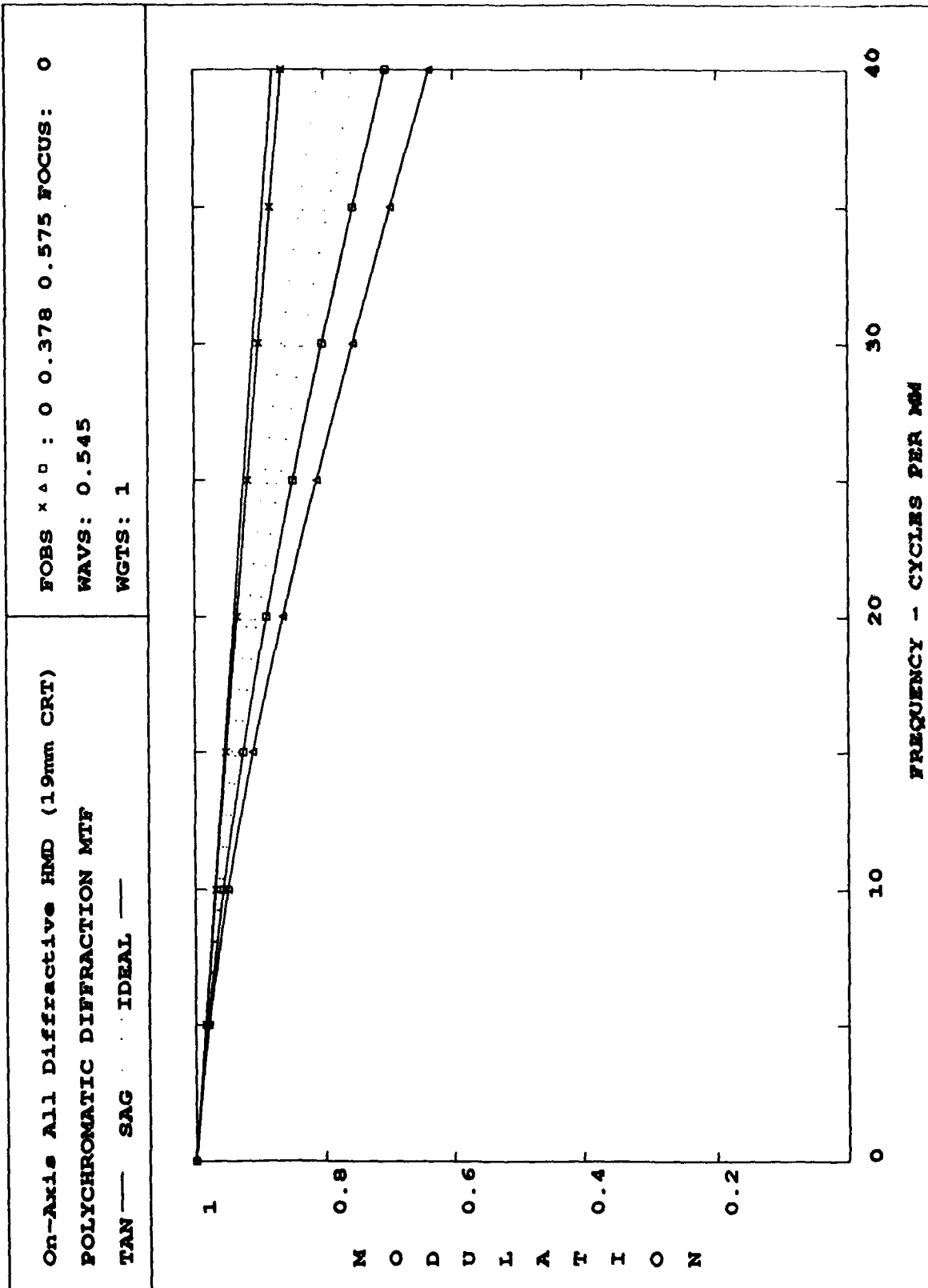


Fig. 3-7. Monochromatic performance for system A with a 5 mm eye pupil in the on-axis viewing configuration.

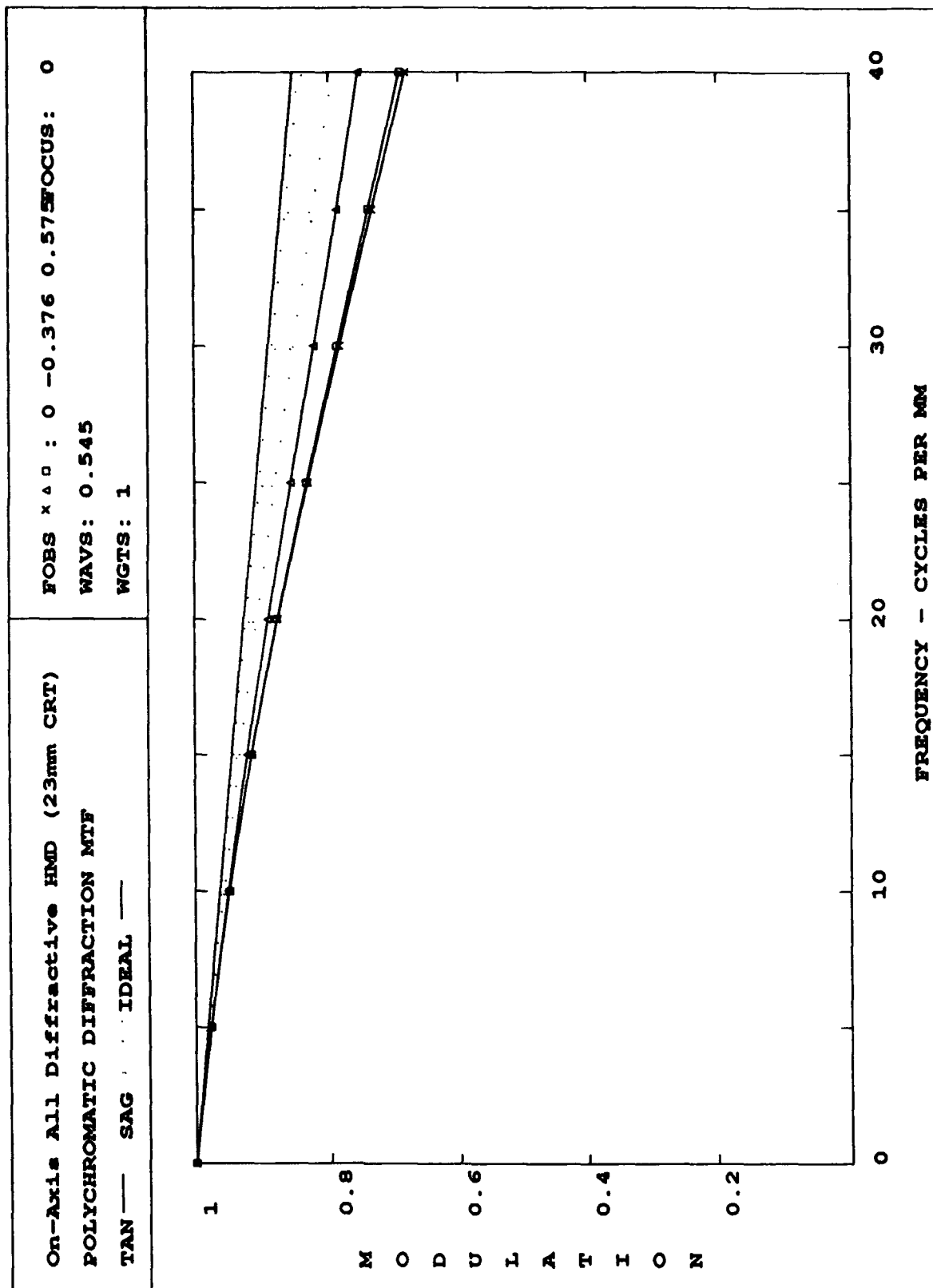


Fig. 3-8. Monochromatic performance for system B with a 5 mm eye pupil in the straight-ahead viewing configuration.

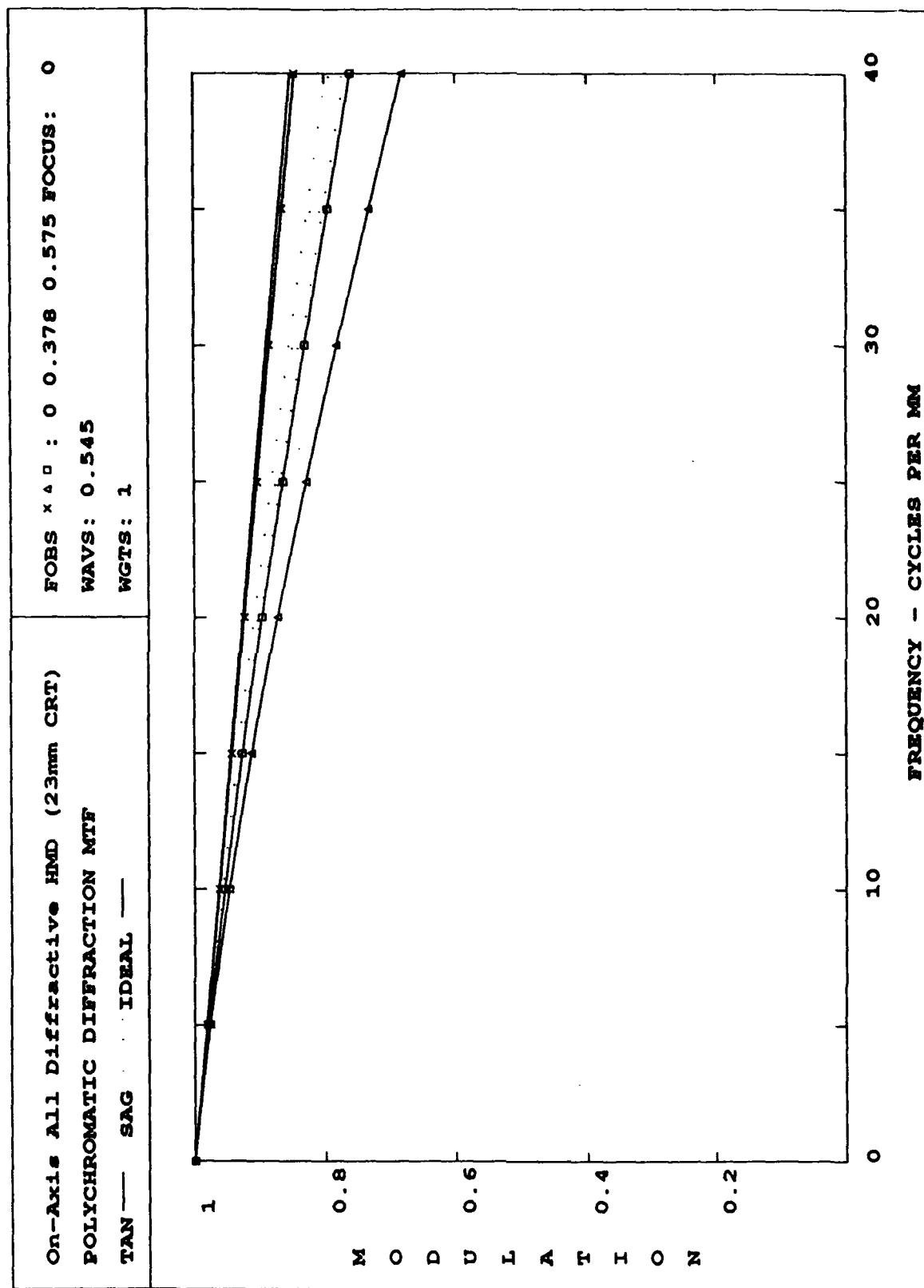


Fig. 3-9. Monochromatic performance for system B with a 5 mm eye pupil in the on-axis viewing configuration.

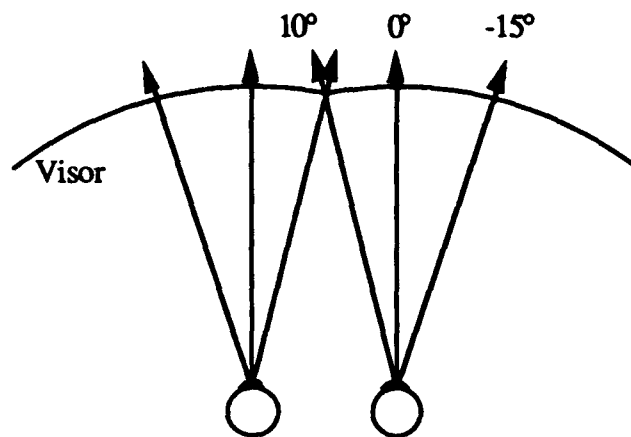


Fig. 3-10. Eye rotation for viewer looking straight-ahead (straight-ahead viewing). The desired instantaneous field-of-view is 10° (inward) and -15° (outward).

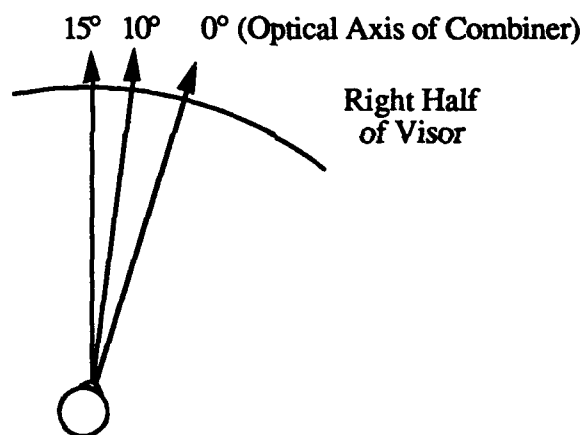


Fig. 3-11. Eye rotation for a viewer looking along the optical axis of the system (on-axis viewing), which is 15° outward from straight-ahead viewing. Hence, for on-axis viewing, straight-ahead corresponds to 15° in the field.

The polychromatic MTF for straight-ahead viewing has been plotted for system A in Figs. 3-12 - 3-14 for a full width at half maximum spectral bandwidth of 0.5 nm, 1.0 nm, and 1.5 nm, respectively. The polychromatic MTF for straight-ahead viewing has been plotted for system B in Figs. 3-15 - 3-17 for the same spectral bandwidths as system A. From the polychromatic MTF plots of the all-diffractive systems, we can see that the spectral bandwidth of the CRT illumination source must be filtered significantly to achieve

satisfactory system performance. The tangential MTF at 20 lp/mm for the 0° field for straight-ahead viewing versus the spectral bandwidth is plotted for system A and system B in Fig. 3-18. From this graph, it is clear that the maximum spectral bandwidth of the illumination source that can be tolerated for the all-diffractive relay system is approximately 1 nm. This limits the potential sources for an all-diffractive relay system to lasers.

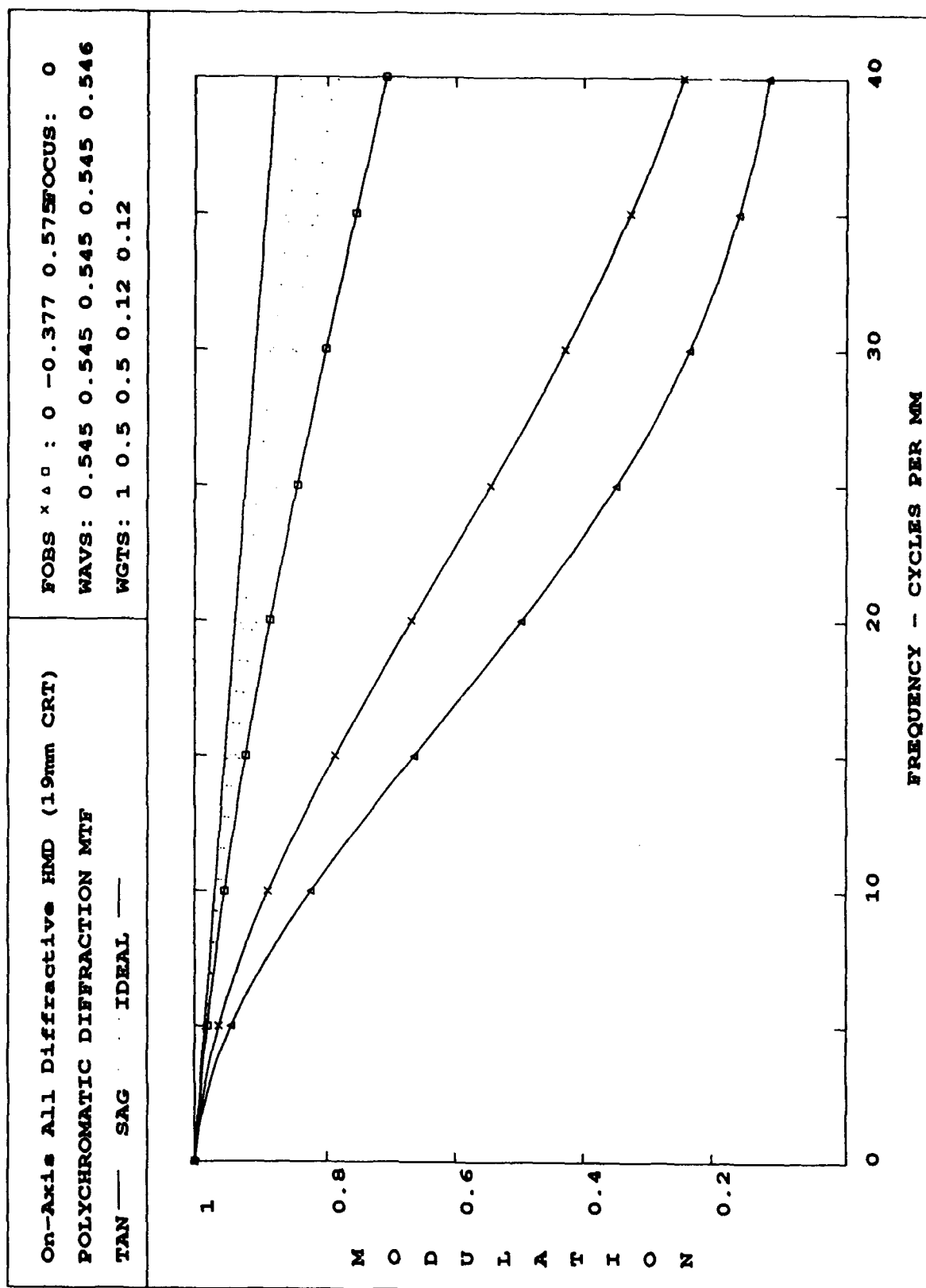


Fig. 3-12. Polychromatic performance for system A with a spectral bandwidth of 0.5 nm FWHM and a 5 mm eye pupil in the straight-ahead viewing configuration.

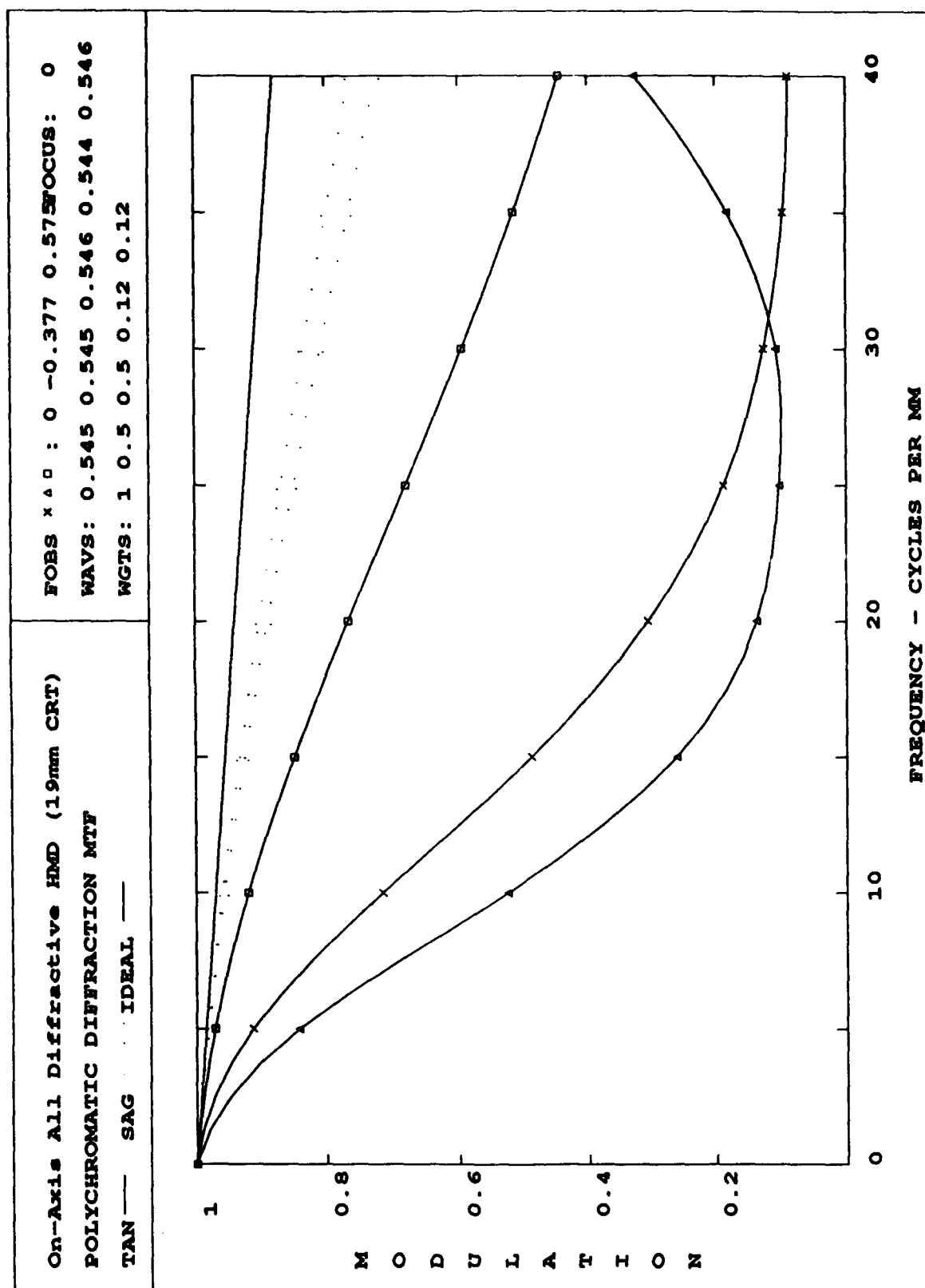


Fig. 3-13. Polychromatic performance for system A with a spectral bandwidth of 1.0 nm FWHM and a 5 mm eye pupil in the straight-ahead viewing configuration.

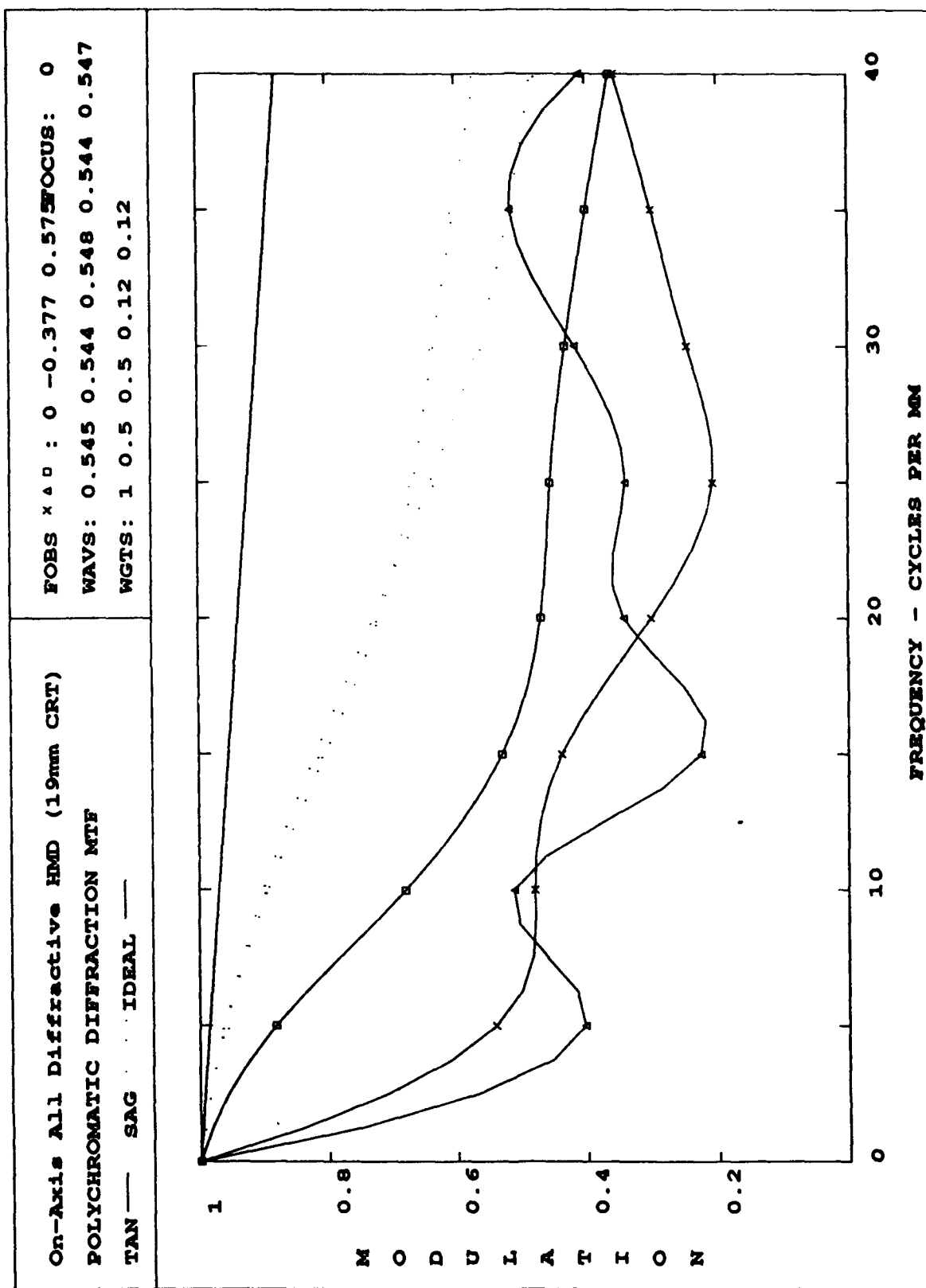


Fig. 3-14. Polychromatic performance for system A with a spectral bandwidth of 1.5 nm FWHM and a 5 mm eye pupil in the straight-ahead viewing configuration.

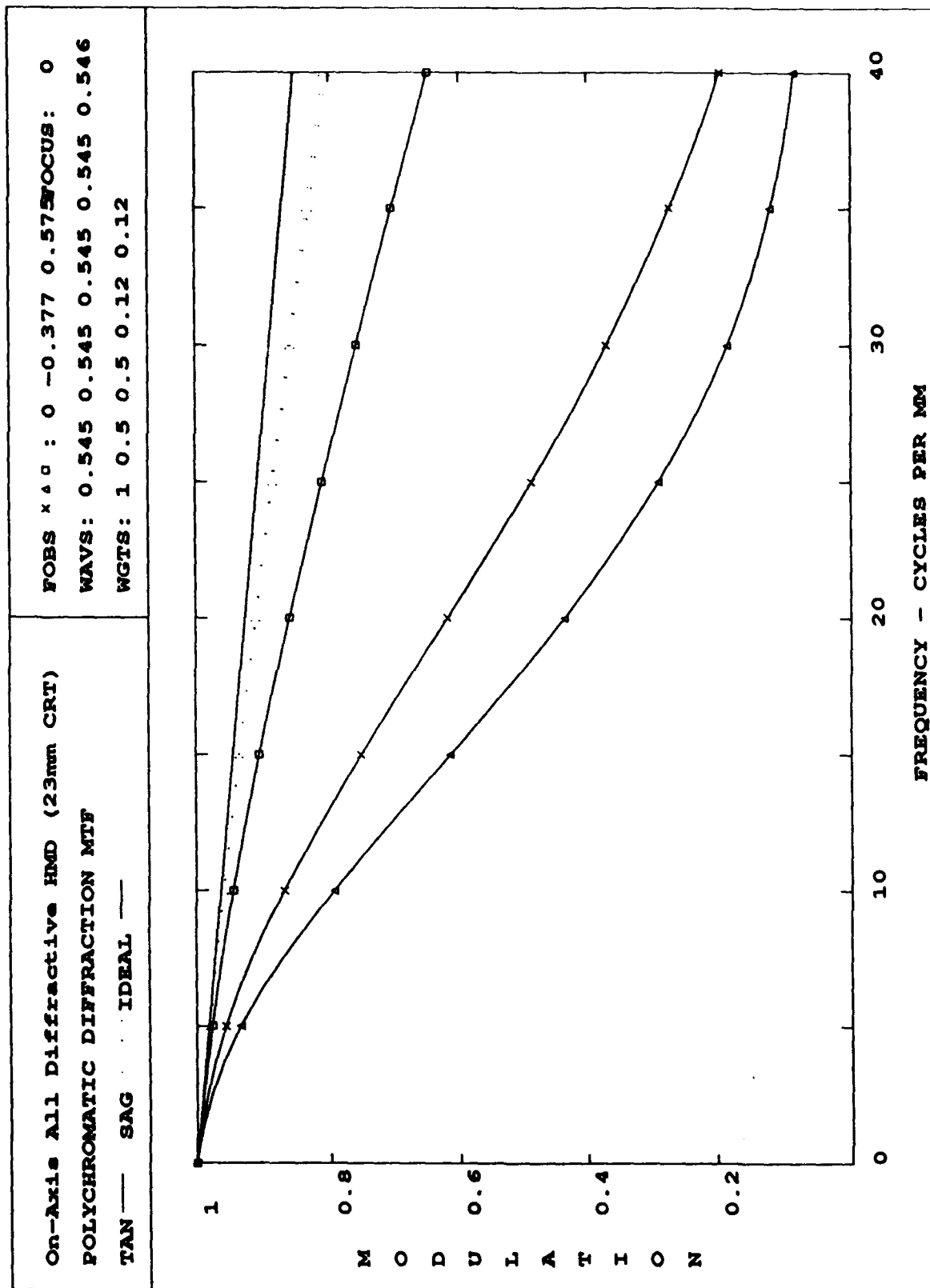


Fig. 3-15. Polychromatic performance for system B with a spectral bandwidth of 0.5 nm FWHM and a 5 mm eye pupil in the straight-ahead viewing configuration.

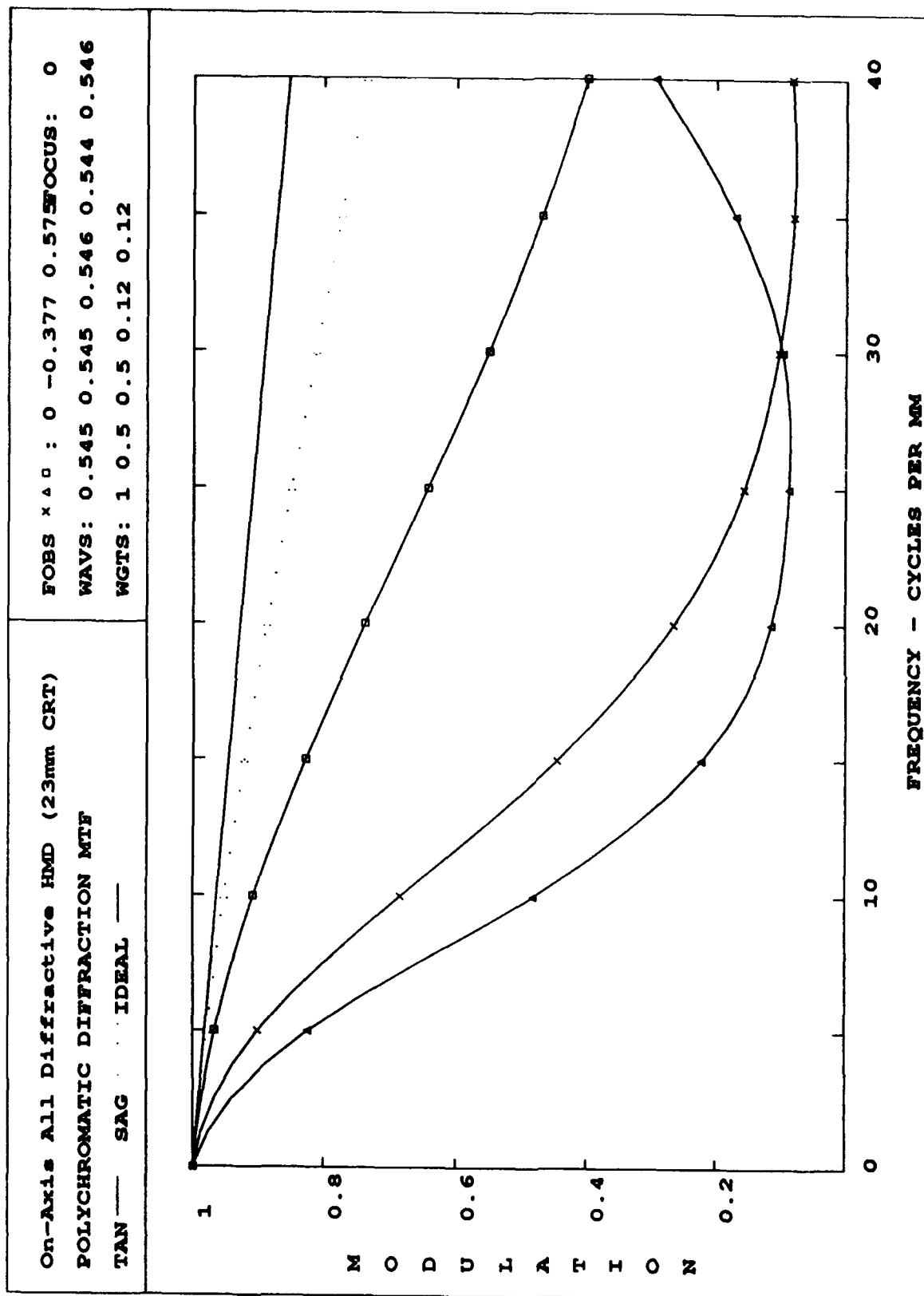


Fig. 3-16. Polychromatic performance for system B with a spectral bandwidth of 1.0 nm FWHM and a 5 mm eye pupil in the straight-ahead viewing configuration.

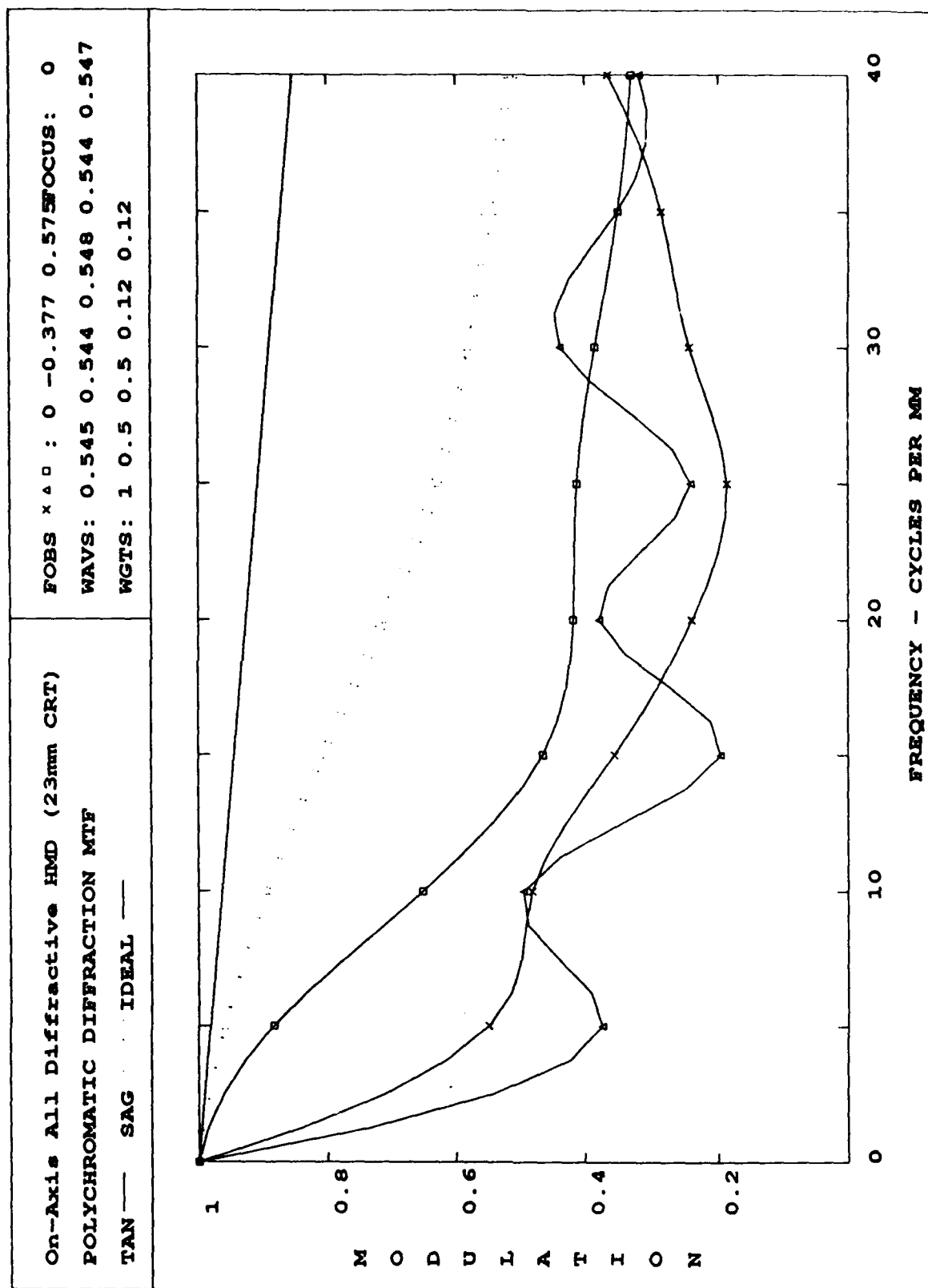


Fig. 3-17. Polychromatic performance for system B with a spectral bandwidth of 1.5 nm FWHM and a 5 mm eye pupil in the straight-ahead viewing configuration.

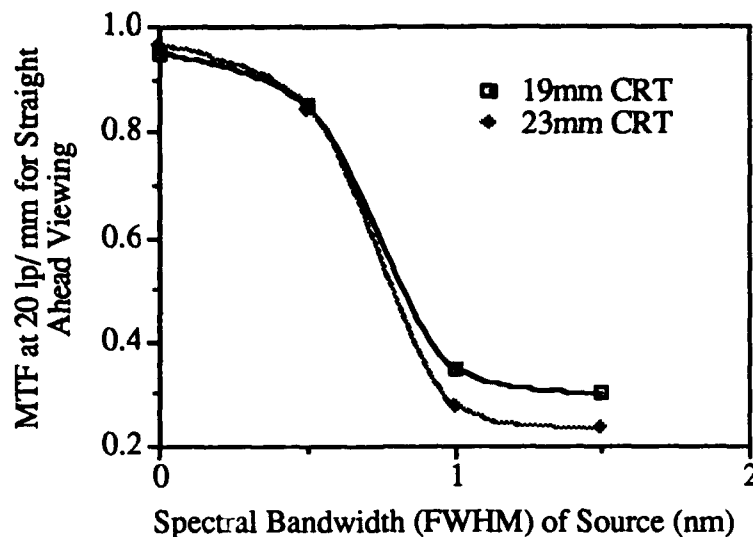


Fig. 3-18. Effect of the spectral bandwidth of the illumination source on polychromatic MTF at 20 lp/mm for 0° field angle with the eye pupil in the straight-ahead viewing configuration.

From the comparison of the monochromatic and polychromatic MTFs of system A and system B, we can see that the monochromatic performance of system B is better than that of system A, whereas the polychromatic performance of system A is better than that of system B. The differences in performance between the two systems is due to the difference in CRT size between system A (19 mm) and system B (23 mm). Increasing the CRT size of the system while holding the FOV constant has two effects. The first effect of increasing the CRT size is that the focal length of the system is proportionately increased. The second effect is that the $f/\#$ of the system is also increased. The increase in the $f/\#$ of system B over that of system A is the reason that the monochromatic performance of system B is enhanced over that of system A. The differences between the two systems are summarized in Table 3-1. In general, as the $f/\#$ of an optical system is increased, some of the geometrical aberrations of the system are decreased. The aberrations that are affected the most by increasing the $f/\#$ of the system are spherical aberration and coma since they are inversely proportional to $(f/\#)^4$ and $(f/\#)^3$, respectively. The reason that the polychromatic performance of system A is better than that of system B is because the dominant aberration of the polychromatic systems is the transverse chromatic aberration. The transverse chromatic aberration of system B is increased over that of system A because it is directly proportional to the product of the FOV of the system and the system focal length. The dependence of the transverse chromatic aberration on the product $F\Theta$ shows that the

polychromatic performance of an all-diffractive HMD can be increased by decreasing the size of the CRT. Obviously, there are design tradeoffs between monochromatic performance and color correction.

In summary, we have found as a result of our investigations, that the two-element all-diffractive relay lens can be lightweight and still offer good monochromatic performance. (Specific details regarding the system designs are located in Appendices A-D). As expected, for a system that consists solely of diffractive elements, chromatic aberrations remain. We have shown that for limited spectral bandwidths, on the order of 1 nm, the polychromatic performance of this system meets the requirements. For larger illumination bandwidths, the system fails to meet design requirements. All-diffractive designs can be feasible when used in conjunction with laser illumination sources which may be present in future architectures.

	System A	System B
CRT Size	19 mm	23 mm
Full Field of View	50°	50°
Focal Length	21.77 mm	26.36 mm
Entrance Pupil Diameter	19 mm	19 mm
System F#	f/1.14	f/1.38
Monochromatic Spot Size at Full Field	9.55 μm	6.85 μm
Transverse Chromatic Aberration at Full Field for a 2 nm FWHM Source Bandwidth	55 μm	59 μm

Table 3-1. Design parameters associated with systems A and B.

3.3 On-axis Aspheric Hybrid Refractive/Diffractive HMD Design

With reference to the previous discussion, it has been shown that for the case of an on-axis combiner system, an all-diffractive relay lens system cannot provide acceptable

polychromatic performance when used in combination with a broadband phosphor-based CRT. In this Section, we will investigate the use of combinations of refractive and diffractive elements in the relay lens to provide color correction. The feasibility of color-corrected HMD systems using hybrid refractive/diffractive systems is investigated by considering the design of color-corrected hybrid relay lenses for the on-axis combiner configuration used in systems A and B above. The spectral band used for color correction is obtained from the emission curve for P53 phosphor. The spectral energy distribution for P53 is shown in Fig. 3-19. With regard to Fig. 3-19, the three primary wavelengths used for color correction are 490 nm, 545 nm and 590 nm. These wavelengths were chosen because they correspond to the three major spectral peaks of P53.

In consideration of a color-corrected on-axis combiner system, we have designed two color-corrected, hybrid refractive/diffractive relay lenses to investigate the effect of CRT size on the system performance. For comparison purposes, the CRT sizes that have been considered are 19 mm and 23 mm, designated systems C and D, respectively. The complete design information for these systems is located in Appendices C and D, respectively.

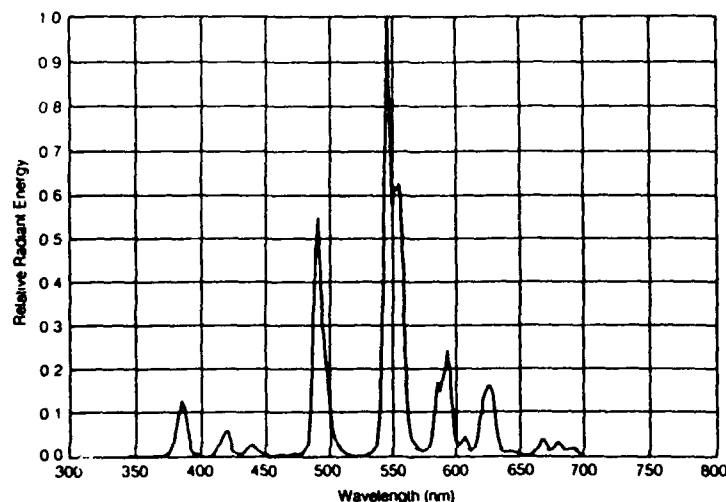


Fig. 3-19. The spectral energy distribution for P53 phosphor.

Combiner Efficiency

The relay lenses utilized in systems C and D have been designed using three refractive elements; two refractive aspheres and one spherical field flattener that is either cemented to the CRT faceplate or incorporated into the faceplate [see Figs. 3-20 and 3-21]. Refractive aspheric elements were used at this stage in the design to minimize weight and to produce a well-corrected system using a minimum number of elements. As outlined in Section 2.3, color correction is provided by a diffractive phase structure on the object side of the refractive element furthest from the CRT (for specific detail, see Appendices C and D).

The final designs for both systems C and D are very similar in appearance and construction [see Fig. 3-20 and 3-21]. The optical glasses that are used for the design are BK10 for the field flattening element, FK5 for the aspheric element closest to the image source and SF56 for the aspheric element with the diffractive surface. It has been determined that for a system that has been constrained to three elements, glasses of this type are necessary to control both the first-order chromatic aberrations (longitudinal axial chromatic aberration and transverse chromatic aberration) and the higher-order chromatic aberrations (spherochromatism, chromatic coma and chromatic astigmatism). Note that it is necessary to correct most of the higher-order chromatic aberrations in a HMD to allow the eye pupil to make use of the entire system pupil without affecting the optical performance.

The effect of higher-order chromatic aberrations can be seen from Figs. 3-22 and 3-23. The chromatic ray error plot is shown in Fig. 3-22. This system is corrected for first-order chromatic aberrations and spherical aberration. The primary aberration remaining is spherochromatism. When the viewer's 5 mm-pupil is moved, the effect is to select a particular 5 mm-section of the whole pupil shown in Fig. 3-22. If the viewer's pupil is moved to the very edge, then the resulting aberrations would be shown in Fig. 3-23. The spherochromatism has been effectively translated to transverse chromatic and axial chromatic aberration.

On-Axis Aspheric Hybrid HMD (19mm CRT)

OPTICAL SYSTEM LAYOUT

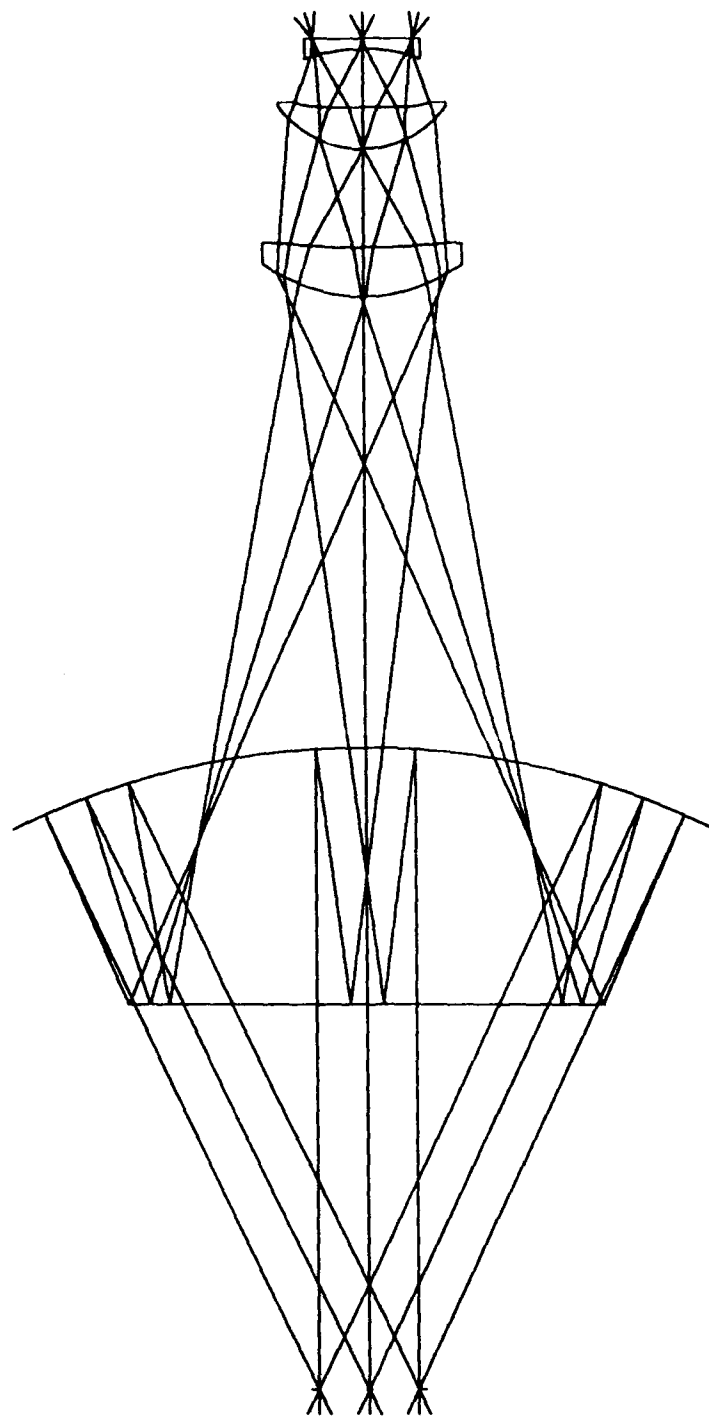


Fig. 3-20. Unfolded system diagram for system C. On-axis HMD using a hybrid refractive/diffractive relay lens with a 50° FOV, 19 mm EPD and 19 mm diameter CRT.

On-Axis Aspheric Hybrid HMD (23mm CRT)

OPTICAL SYSTEM LAYOUT

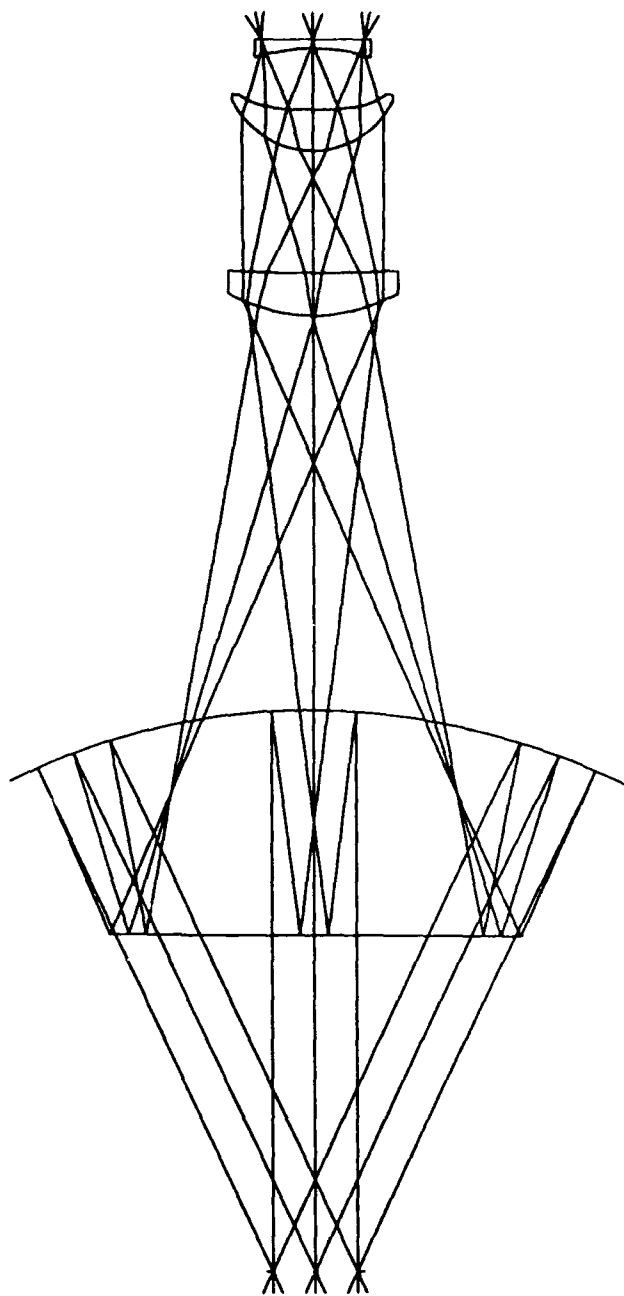


Fig. 3-21. Unfolded system diagram for system D. On-axis HMD using a hybrid refractive/diffractive relay lens with a 50° FOV, 19 mm EPD and 23 mm diameter CRT.

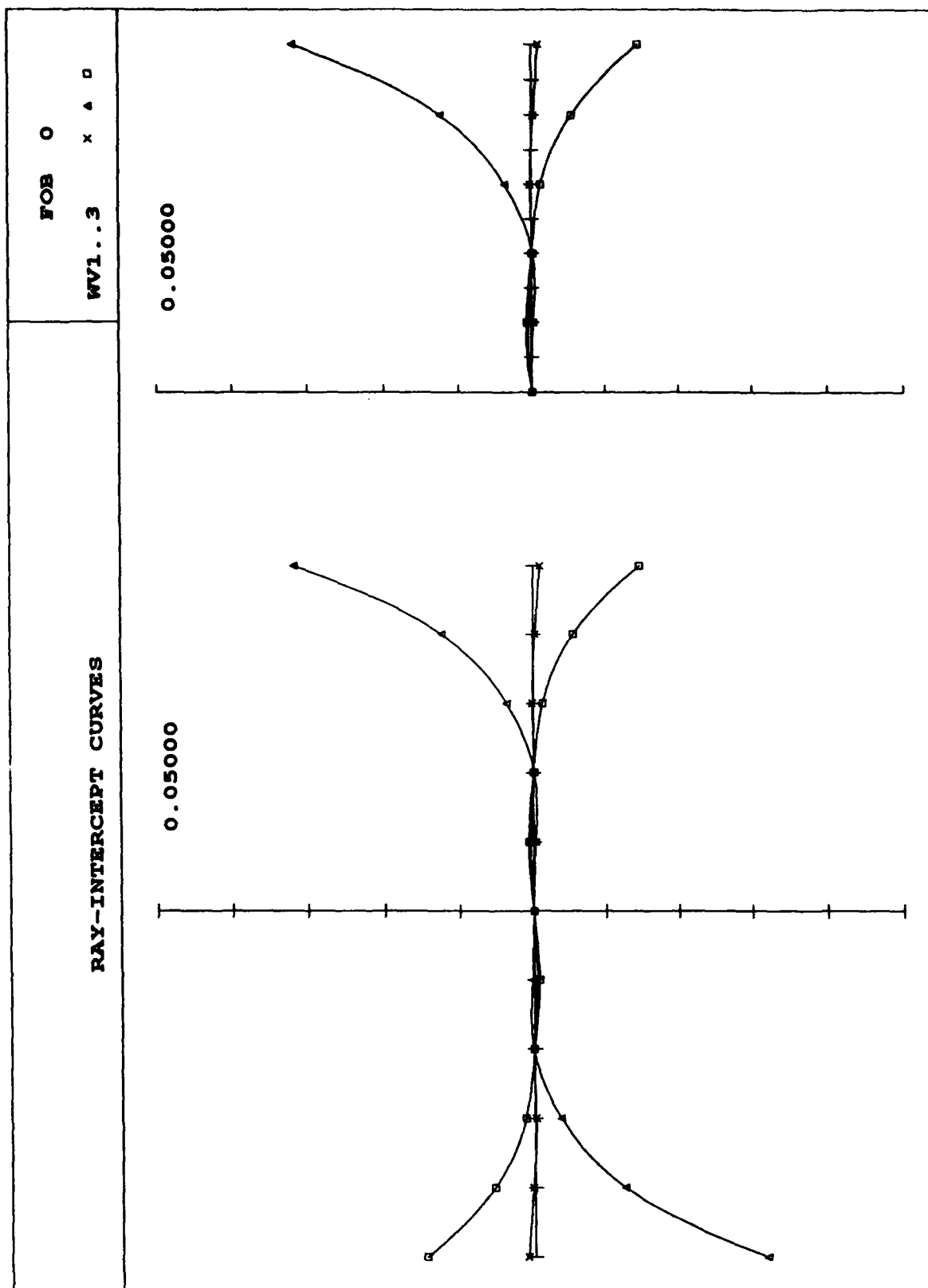


Fig. 3-22. Chromatic ray error plot exhibiting spherochromatism. The design is a centered optical system with a 19 mm pupil that is corrected for longitudinal and transverse chromatic aberrations as well as all monochromatic aberrations.

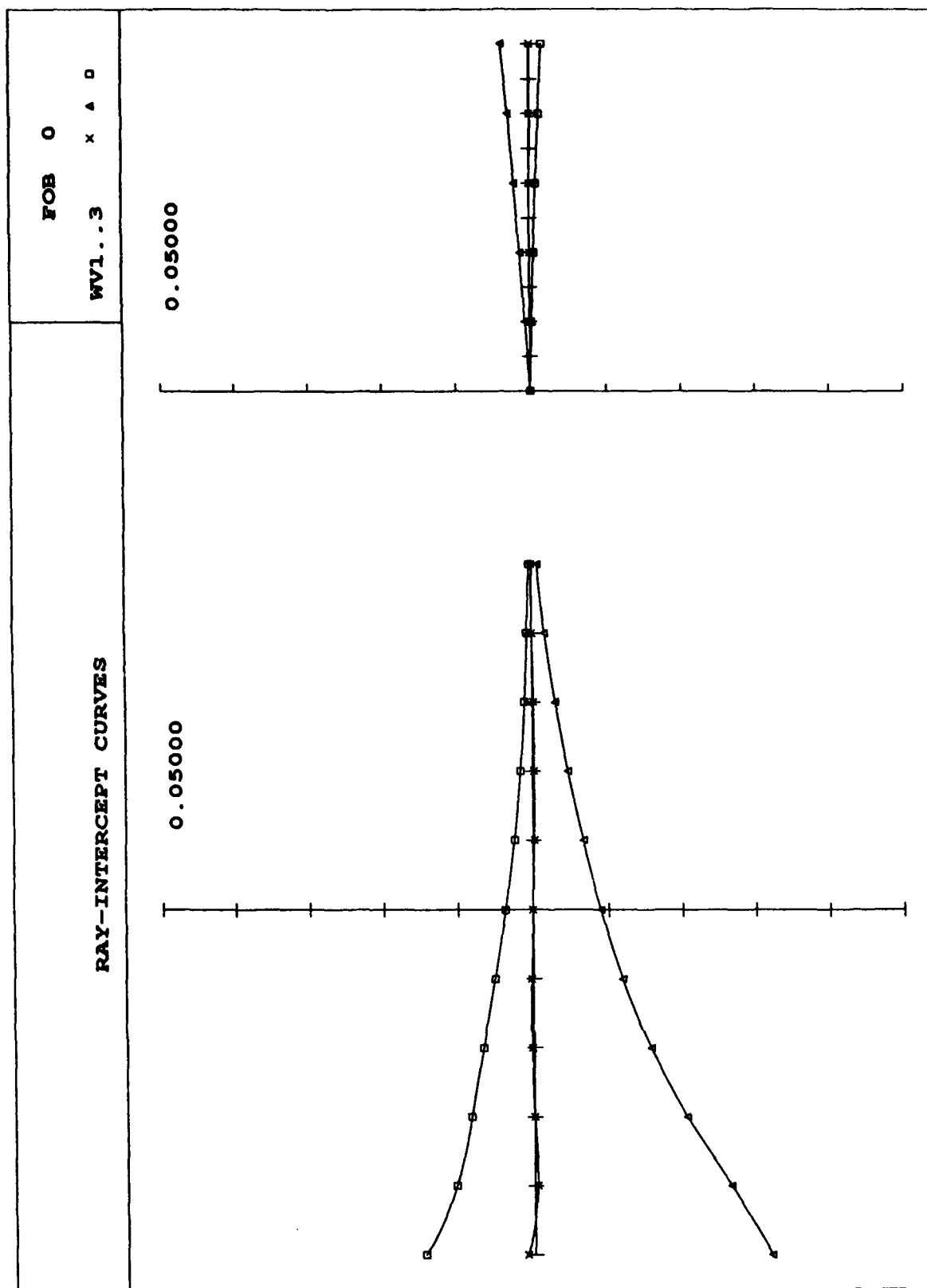


Fig. 5-23. Effect of spherochromatism, for a 5 mm pupil decentered from the axis by 7 mm.

The polychromatic MTF plots for systems C and D are shown in Figs. 3-24 - 3-27. The plots represent the straight-ahead viewing case and the on-axis viewing case as discussed previously. The chromatic weightings used to calculate the polychromatic MTF of the color-corrected relay lenses are shown in Table 3-2. They are calculated by first calculating the total power in each of the five spectral peaks of the P53 phosphor. This is then multiplied by the photopic response of the eye and the diffraction efficiency of the diffractive element. The diffraction efficiency is discussed in Section 5.0. The spectral efficiency of the coatings on the beamsplitter and combiner have not been utilized. Previously, spectrally-selective coatings on the beamsplitter and combiner have been used to attenuate the CRT emission at wavelengths other than 545 nm. However, their use in a color-corrected design may reduce the overall throughput and reduce the advantages of a color-corrected system. Evaluation of the proper wavelength selectivity for the beamsplitter and combiner is highly dependent on the final application, and tradeoffs between color correction and overall throughput can only be made with knowledge of the total system goals.

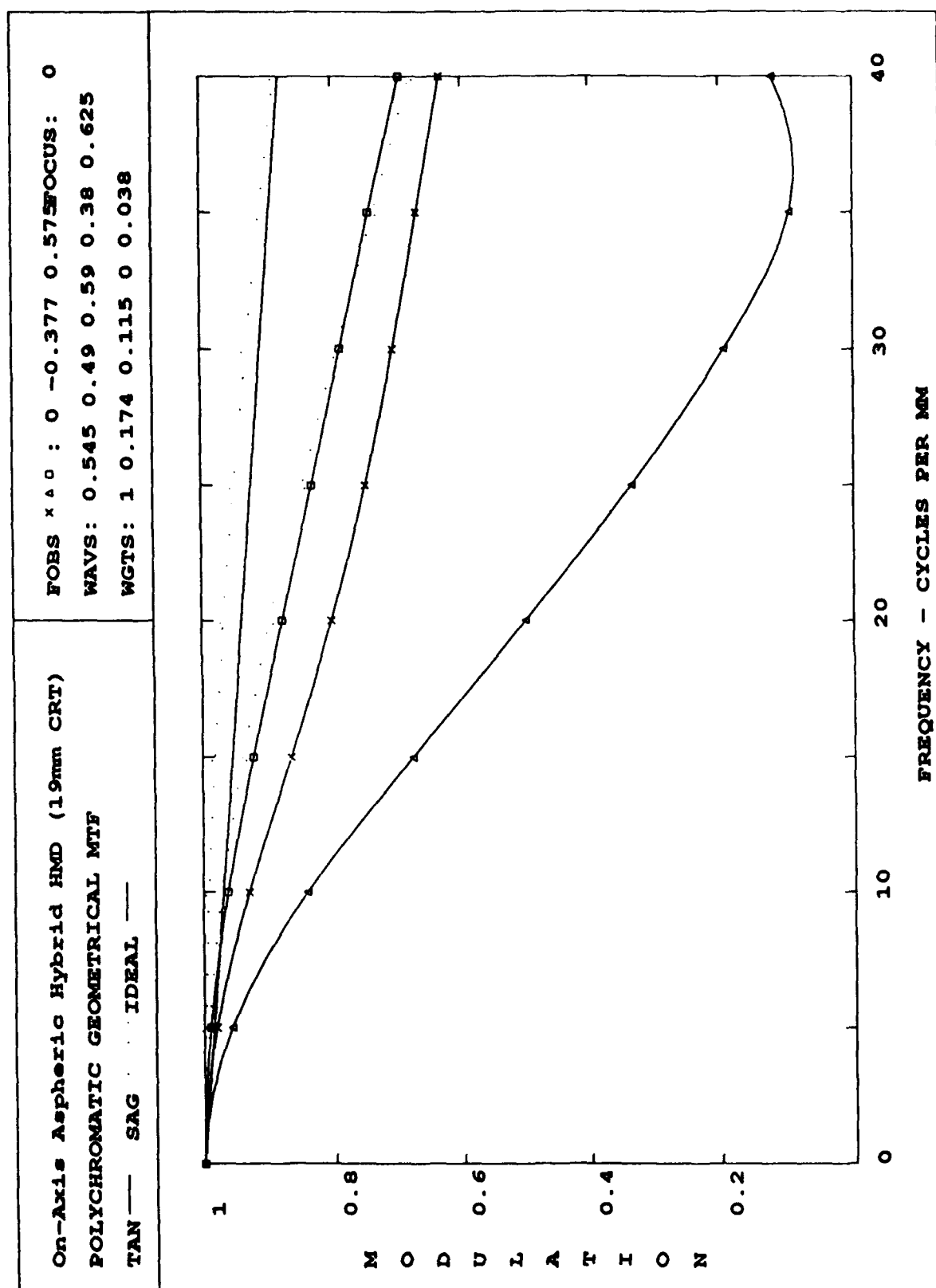


Fig. 3-24. Polychromatic performance for system C with a 5 mm eye pupil in the straight-ahead viewing configuration.

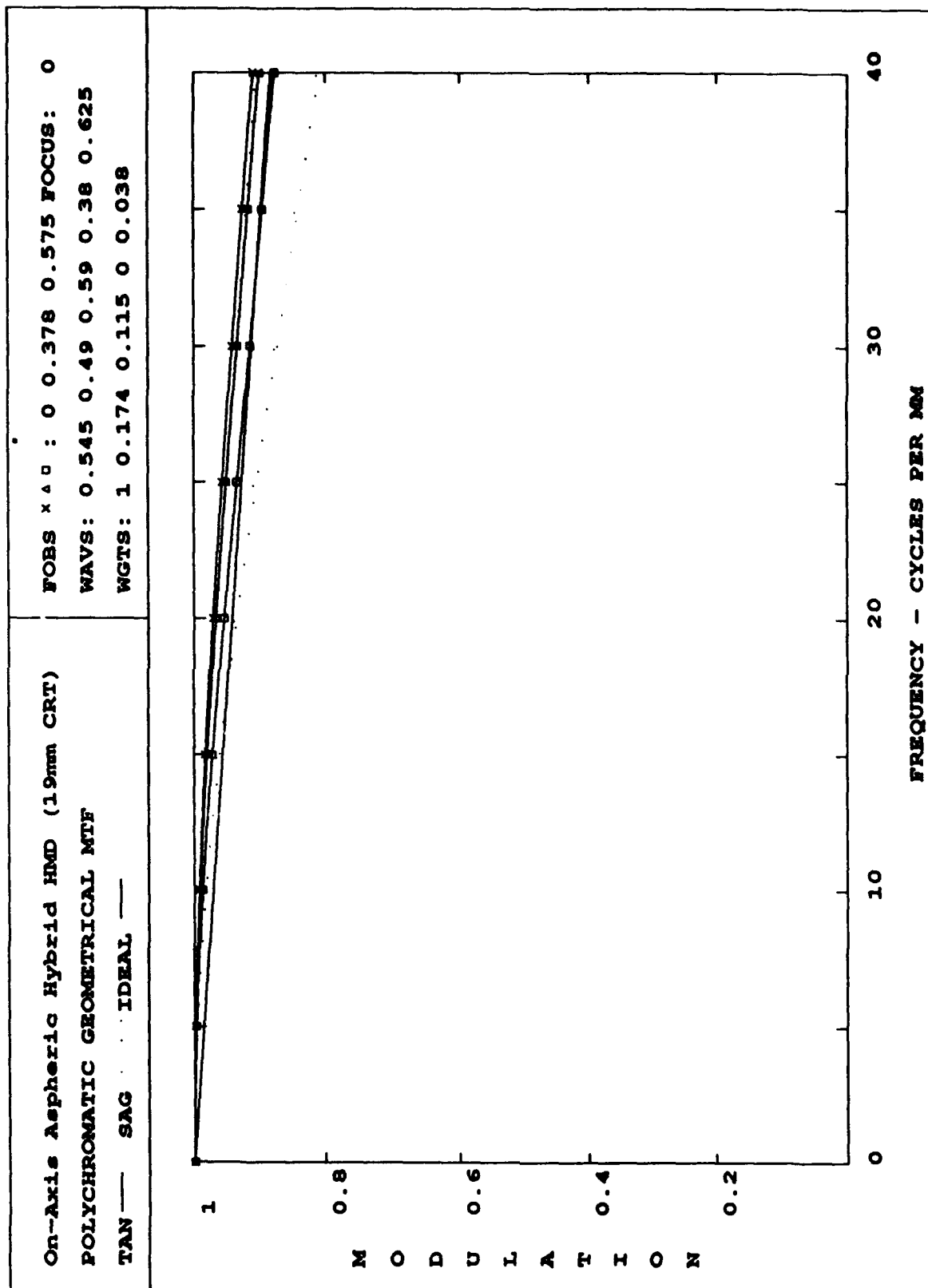


Fig. 3-25. Polychromatic performance for system C with a 5 mm eye pupil in the on-axis viewing configuration.

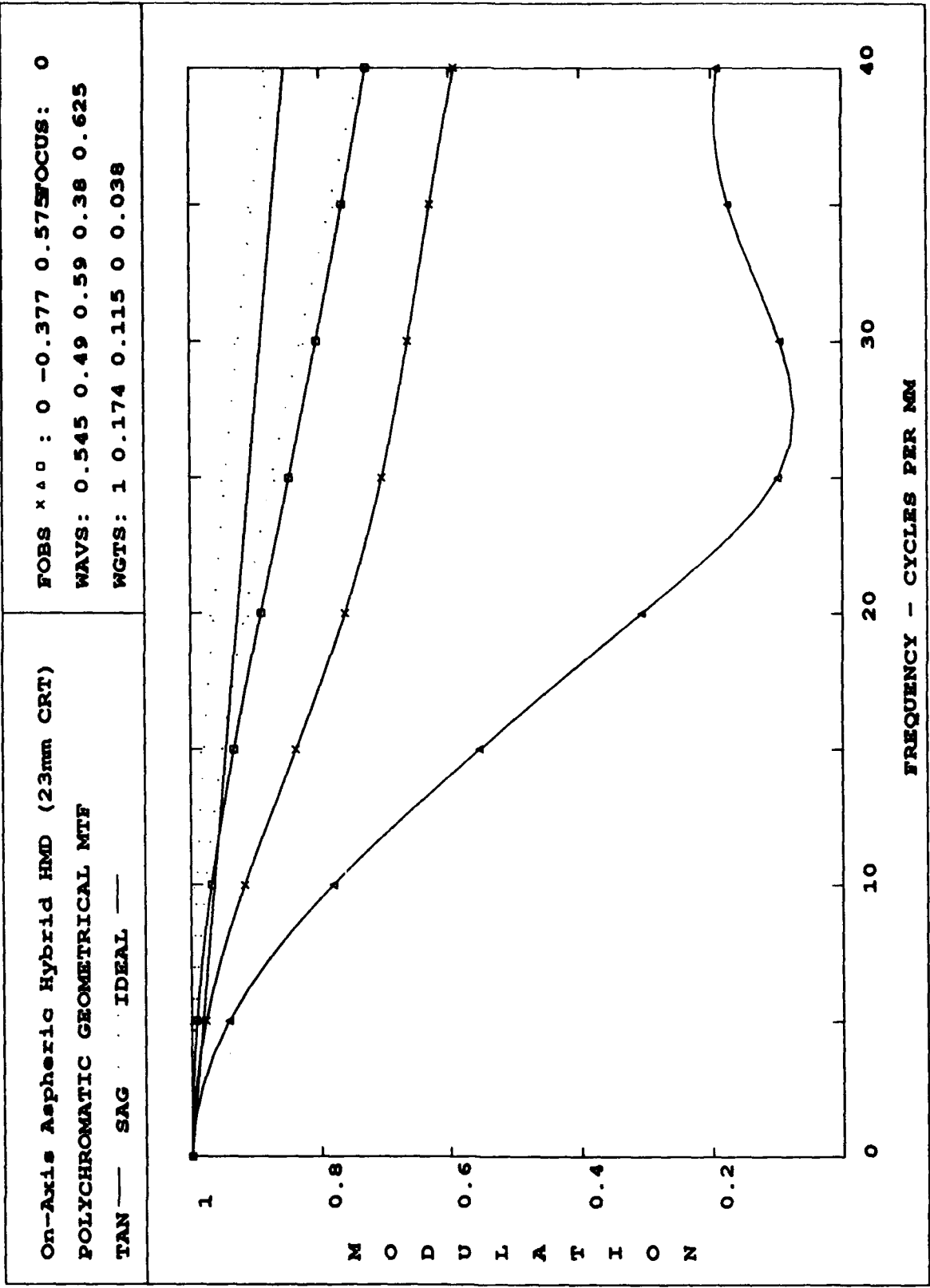


Fig. 3-26. Polychromatic performance for system D with a 5 mm eye pupil in the straight-ahead viewing configuration.

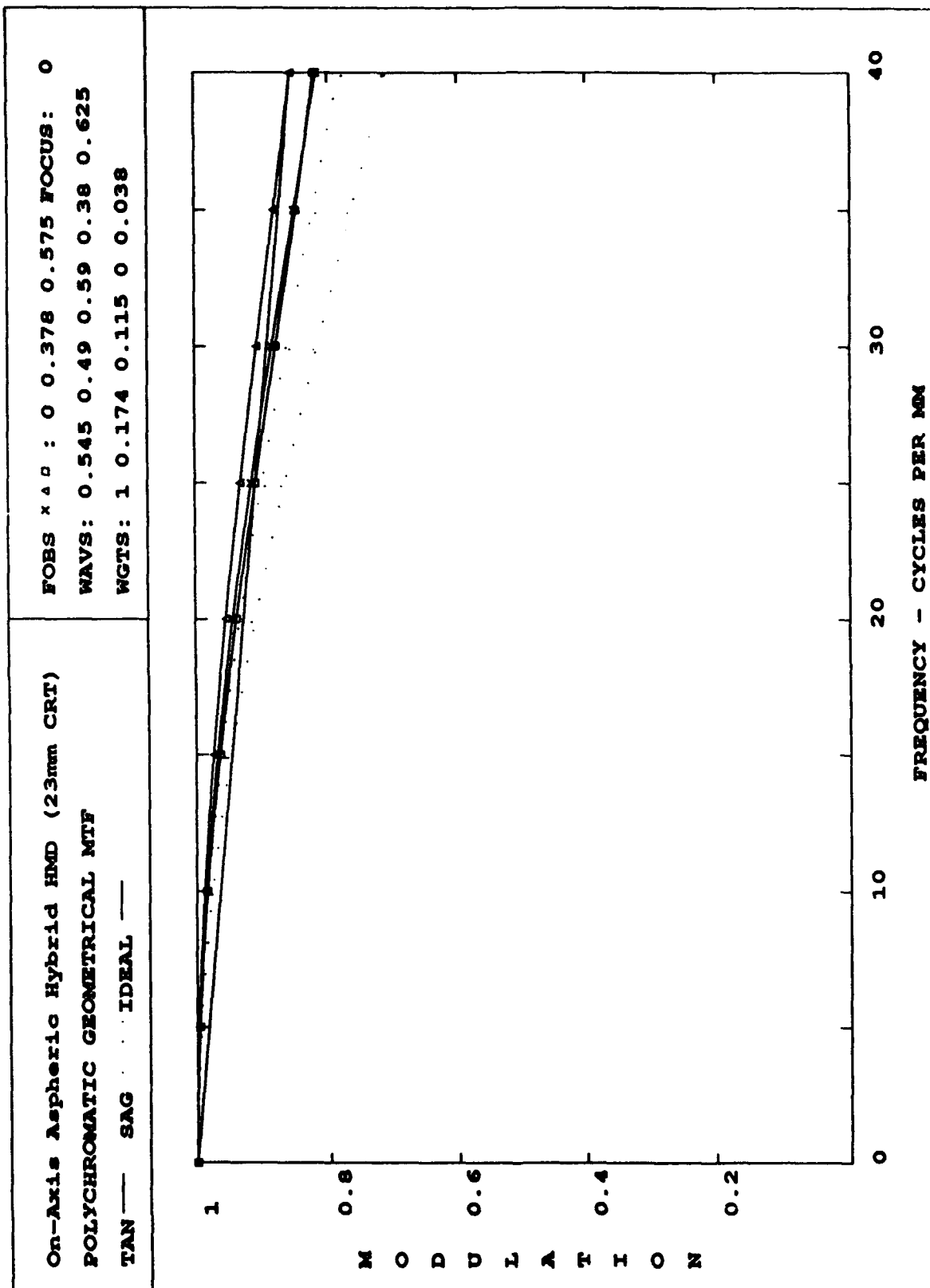


Fig. 3-27. Polychromatic performance for system D with a 5 mm eye pupil in the on-axis viewing configuration.

	Normalized Spectral Power	Photopic Response	Grating Efficiency	Weighted Normalized Power	Percentage Power in Each Band
490 nm	0.602	0.3	0.962	0.174	13.1
545 nm	1.000	1.0	1.000	1.000	75.4
590 nm	0.168	0.7	0.976	0.115	8.67
625 nm	0.134	0.3	0.936	0.038	2.86

Table 3-2. Generation of the spectral weighting function.

Systems C and D, as illustrated in Figs. 3-24 - 3-27, are well corrected over the required spectral bandwidth. The limiting field point in this system corresponds to the full field-of-view (10° inward) of the combiner for the straight-ahead viewing eye pupil position. The performance for this field point is reduced by the presence of higher-order chromatic aberrations.

The higher-order chromatic aberrations can be reduced through the use of higher-order aspheric terms. For these investigations, we have made use of only the first four aspheric coefficients. The sag of the aspheric surface is described by

$$\text{Sag} = \frac{y^2 / r}{1 + \sqrt{1 - (CC + 1)y^2 / r^2}} + ADy^4 + AEy^6 + AFy^8 + AGy^{10} \quad , \quad (3-4)$$

where y is the distance away from the optical axis, r is the radius of curvature of the surface, CC is the conic constant of the surface, and AD , AE , AF and AG are the fourth-, sixth-, eighth- and tenth-order aspheric coefficients of the surface.

Comparison of the performance of the two systems shows that they are approximately equivalent. A larger CRT allows the focal length of the system to increase, which improves the monochromatic aberrations. However, since this system is not monochromatic, the increased field size leads to increased lateral chromatic aberrations. It may be possible that higher-order aspheric terms may be used to allow an increase in CRT size while maintaining correction of lateral chromatic aberration.

3.4 On-axis Refractive/Diffractive Relay Lens: Throughput Analysis

The goal of color correcting the relay lens with diffractive optics is obviously valuable only if the addition of diffractive elements will improve overall system performance. To show the usefulness of color correction, Table 3-3 shows throughput efficiencies for a typical relay lens with a P53 phosphor.

For the case of an all-refractive lens shown in the top table, filters were used to reject the light outside of the 545 nm band. It may be desirable to add even more filters to reduce the component at 590 nm, which represents 12% of the total illumination. The hybrid refractive/diffractive case is shown in the bottom table; the only loss is from the reduced grating efficiency at wavelengths other than the design wavelength (545 nm) [see Section 5.0]. As is evident from the last column, the total amount of light through the diffractive system is almost twice that of the refractive case. Furthermore, nearly all of this light is useful since the system is color corrected at 490, 545, and 590 nm.

The next step is to consider the effect of the beamsplitter and combiner on the throughput. A typical on-axis design will have a transmission efficiency for the CRT image of $E = R_V R_B (1 - R_B)$, where R_B is the reflection coefficient of the beamsplitter and R_V is the reflection coefficient of the visor. The best case is for $R_B = 0.5$, so only 25% of the light is getting through. However, this analysis is highly dependent on the coatings used for the beamsplitter and the combiner. The primary motivation behind this work has been to investigate color correction of the relay lens using diffractive optics. For that reason, we have not placed a large emphasis on the role of the beamsplitter and combiner. Off-axis combiners that do not use a beamsplitter offer the advantage of higher throughput. The performance of a color-corrected system utilizing off-axis combiners will be highly dependent on the coatings available.

The use of diffractive optics in the relay lens offers greater throughput because of the color correction that can be achieved *without* filters. In certain situations such as some simulator displays, where the display is not superimposed on an external scene, the benefit of increased brightness and color correction is immediate. Furthermore, it may be possible to use a diffractive relay lens in a color display system. For those cases where the viewer is viewing the display superimposed on an ambient scene, the design of the beamsplitter

Wavelength, nm	Relative Luminance @CRT	Transmission, longpass filter, (Schott OG515)	Transmission, bandpass filter, (Schott VG-4)	Relative luminance after relay lens
490	0.31	0.01	0.70	0.002
545	0.53	0.98	0.84	0.442
590	0.09	0.99	0.60	0.054
625	0.07	0.99	0.50	0.03

Wavelength, nm	Relative Luminance @CRT	Grating efficiency, m=1 order	Relative luminance after relay lens
490	0.31	0.963	0.30
545	0.53	1.000	0.53
590	0.09	0.976	0.08
625	0.07	0.936	0.07

Table 3-3. The relative throughput for the relay lens, using typical values for glass filters (top) and a diffractive element without any filters (bottom). From the last column, the total amount of throughput in the diffractive case is almost twice that of the system with filters. The hybrid diffractive refractive relay lenses discussed in the text are corrected at 490, 545, and 590 nm. All refractive designs are corrected at 545 nm. only.

and combiner must now be optimized for the new (i.e. wider) input spectrum. Because previous systems have emphasized quasimonochromatic performance, the design goals of the beamsplitter and combiner were straightforward. However, full utilization of the wider spectrum will only be possible with careful design of the beamsplitter and combiner, which will require further investigation of the possible coatings.

3.5 Off-Axis Aspheric Hybrid Refractive/Diffractive HMD Design

Since it is well known that an off-axis combiner system can be more light efficient than an on-axis system, we present an investigation of a preliminary design for a color-corrected, hybrid refractive/diffractive off-axis system. It is also well known that off-axis, binocular HMDs represent a very significant optical design and manufacturing challenge. Because of the potentially large impact of color-corrected off-axis HMD geometries, we have attempted to generate a viable design framework for diffractive off-axis systems during this feasibility study. It is our intention to generate preliminary off-axis designs during Phase I and to propose a detailed development effort for the SBIR Phase II program. In Phase II, we plan to assemble an experienced team to generate advanced off-axis designs that will lead to a laboratory prototype.

For the preliminary system, we have chosen a combiner design that, for the primary configuration, consists of an off-axis elliptical visor with a radius of curvature of 150 mm, that is located approximately 100 mm in front of the pupil of the eye [see Fig. 3-28]. The conic constant chosen for the ellipse is such that the eye pupil and the exit pupil of the relay lens are located at the two foci that define the ellipse. The conic constant chosen for the visor combiner is -0.25. The bend angle used to fold the light path back to the relay lens and the CRT has been chosen to be 60° . The relay lens is located at the image of the eye pupil in the system. The relay lens position was chosen to be at the image of the eye pupil to reduce the size of the refractive elements required to produce a large unvignetted system exit pupil (16 mm). The CRT size chosen for this system is 19 mm.

We have produced an initial design for the off-axis system that is an extension of the designs used previously. The form of the design is similar to that studied by Buchroeder²³ where an on-axis design is extended to an off-axis design by using an eccentric correction element in front of the on-axis relay lens and a combiner that is not spherical but rather is an off-axis portion of an ellipse. Other designs have used off-axis sections of confocal parabolas.²⁴ For the current design, we have concentrated on correcting the longitudinal and transverse chromatic aberrations in the system and have allowed the higher-order chromatic aberrations to remain uncorrected. The transverse chromatic aberration (lateral color) of the system is illustrated in Fig. 3-29. It is anticipated that the higher-order chromatic aberrations may be corrected by optimizing the eccentric correction element. The correction element is currently represented by a very weak cylindrical lens.

The polychromatic performance of the current off-axis HMD system for an on-axis 5 mm eye pupil at three field points (0°, 10° and 15° inward) is shown in Fig. 3-30. The configuration used in the evaluation of the system performance is shown in Fig. 3-31. We have not shown the performance of the current design for other eye pupil positions because the lens performance for off-axis pupil positions is influenced by the presence of higher-order chromatic aberrations.

The weight of the optics in the relay lens, including the field flattener at the faceplate of the CRT, is approximately 145 grams. The weight for this color-corrected design is comparable to other *monochromatic* off-axis designs.

23 R. A. Buchroeder, "Helmet-mounted displays," SPIE-OE/LASE, Los Angeles, CA T72 (1989).

24 J. E. Melzer and E. W. Larkin, "An integrated approach to helmet display system design," SPIE 778, 83 (1987).

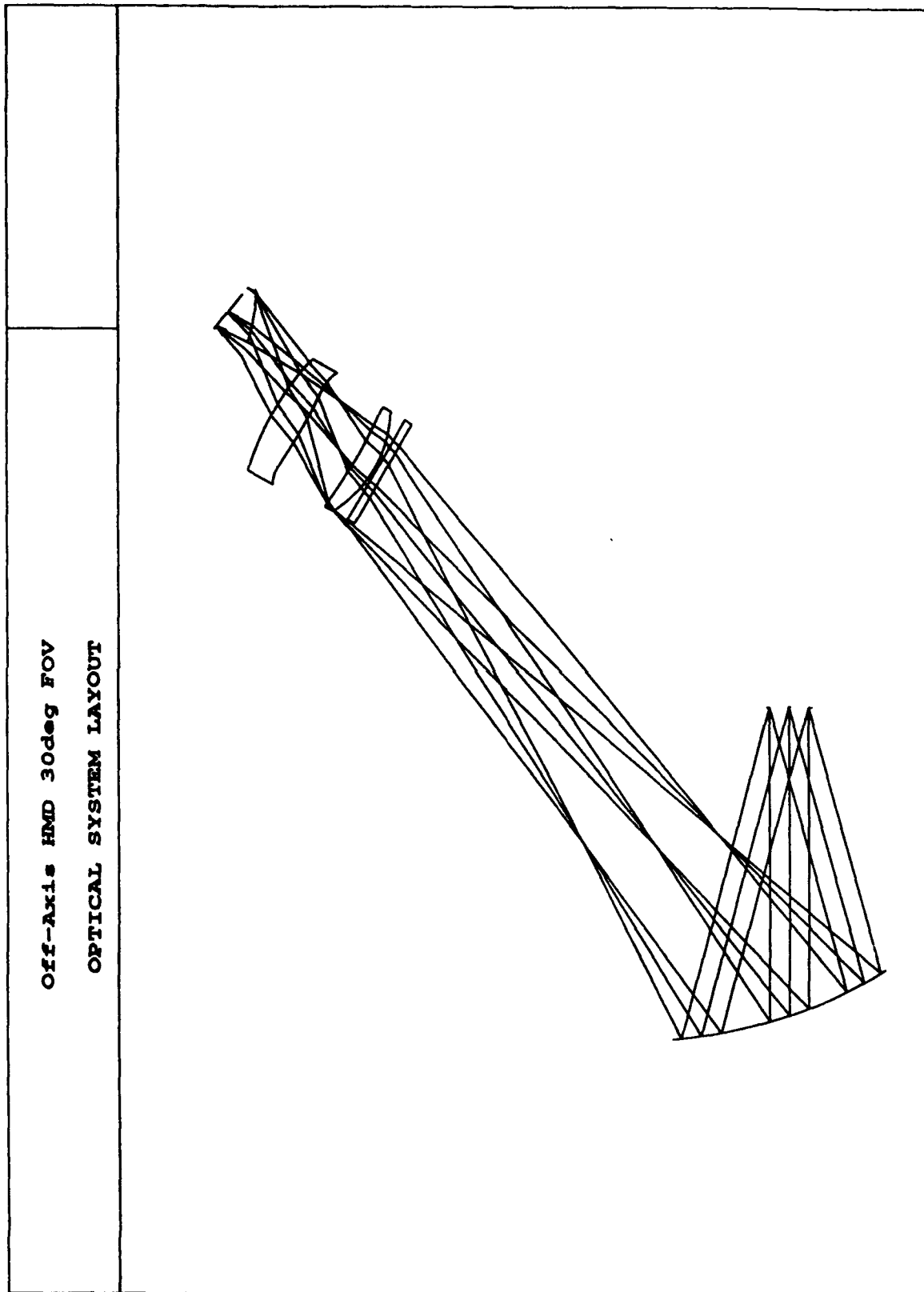


Fig. 3-28. Off-axis HMD configuration using an off-axis ellipsoidal combiner, 30°FOV, 15 mm EPD and a 19 mm CRT.

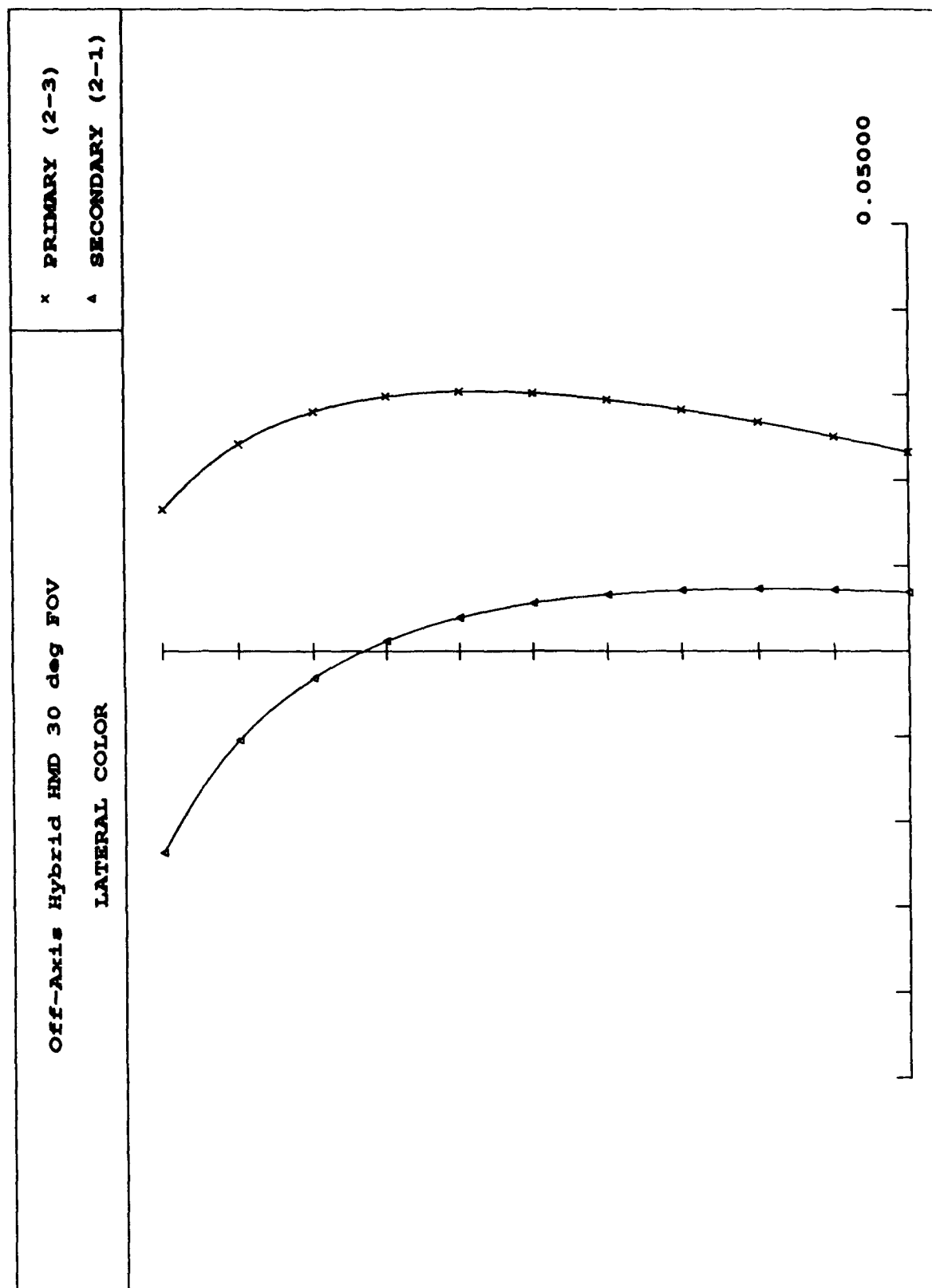


Fig. 3-29. Plot showing the transverse chromatic aberration (lateral color) across the field of the system. The plot extends across the complete field of the HMD.

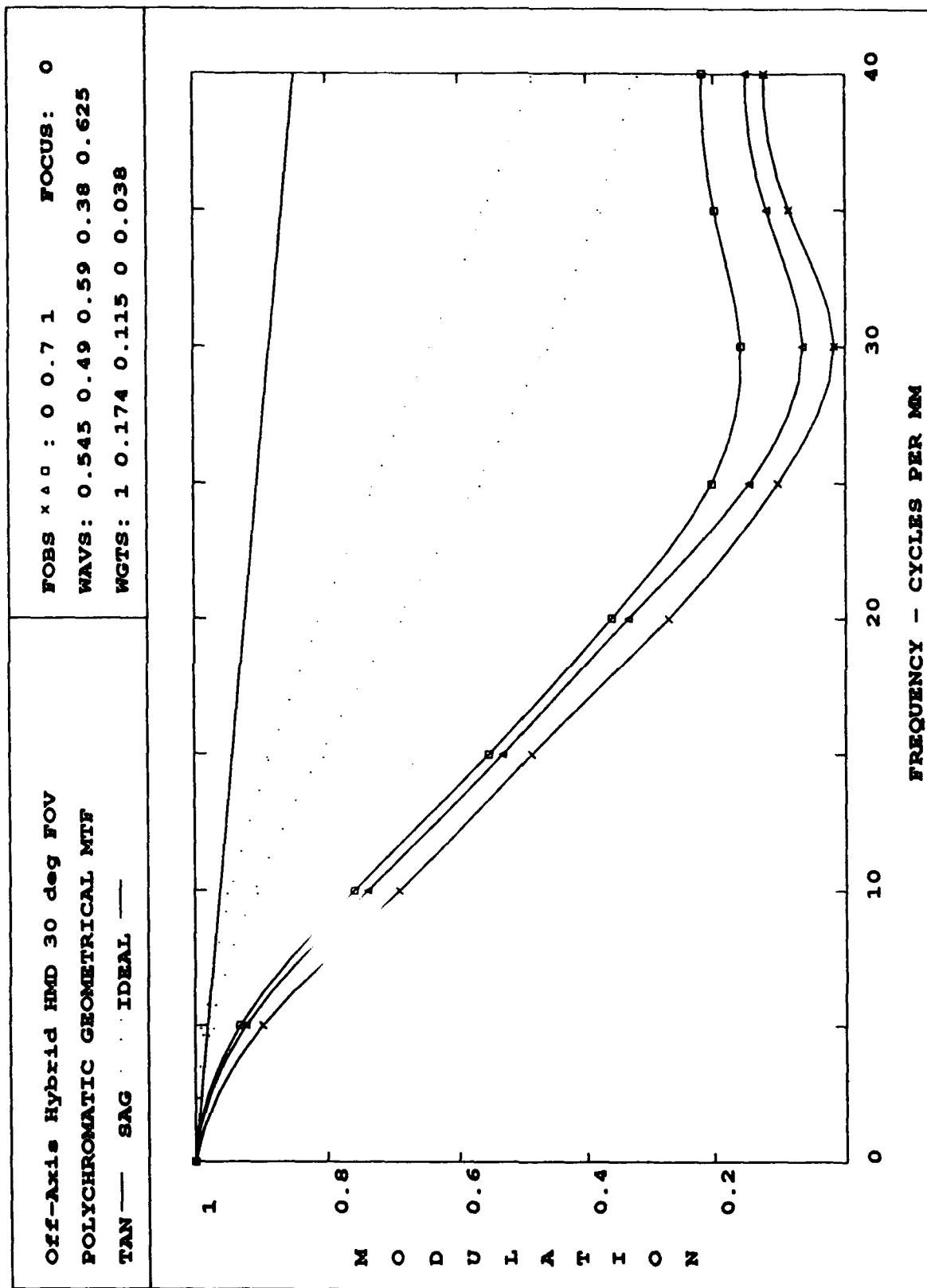


Fig 3-30. Polychromatic MTF of the off-axis HMD system with the viewer looking straight ahead for three field points as shown in Fig. 3-31.

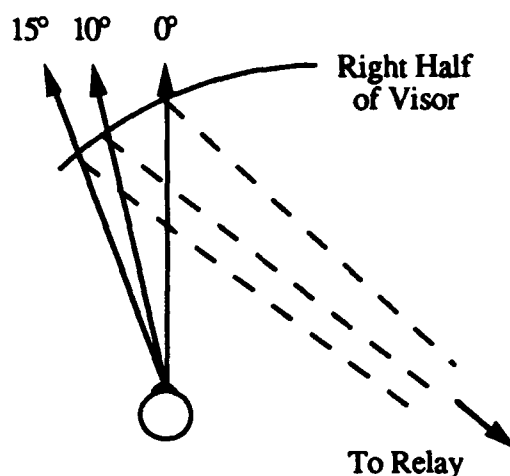


Fig. 3-31. Configuration for evaluation of system performance for off-axis HMD system.

The diameter of the visor element required to produce a $\pm 15^\circ$ FOV in the horizontal direction for this system is approximately 56 mm thus allowing a design of a fully overlapped system and to ignore the F-theta mapping condition. However, because this system is off-axis, there is some keystone distortion in the mapping of the CRT to the exit pupil. The distortion that is produced can be corrected with the electronics associated with the CRT. The required mapping of the image on the CRT is shown in Fig. 3-32.

An additional degree of freedom that can be used to correct the aberrations in the system is to allow the elliptical combiner to include a diffractive surface. We have found that introducing a diffractive asphere on the visor of the color-corrected system can have a positive effect on both the transverse chromatic aberrations and the higher-order chromatic aberrations. The diffractive asphere structure introduced is rotationally symmetric about the axis of the ellipse. We have also found that rotationally symmetric aspheric terms added to the shape of the combiner element can be used to aid in the correction of the monochromatic aberrations. From our investigations, it appears that diffractive structures placed on the surface of the combiner element can improve the performance of the combiner element in an off-axis system.

We have produced a good starting point for an off-axis hybrid refractive/diffractive color-corrected HMD system and have identified some of the key variables that can be used to improve the performance of the design. The starting design is corrected for both longitudinal and transverse chromatic aberrations. The performance of this system is currently limited by the presence of higher-order chromatic aberrations.

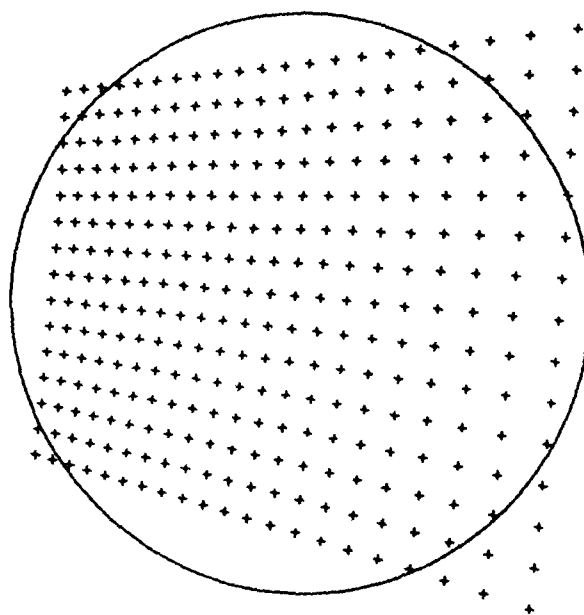


Fig. 3-32. Distortion mapping required on the CRT face for keystone distortion correction.

3.6 On-axis Refractive/Diffractive Relay Lens: Tolerance Analysis

To illustrate system specifications, a tolerance analysis has been performed for system C. The method used to develop a tolerance budget for this system is the root sum of squares (RSS) method for statistical addition of the tolerance effects described by Smith.²⁵ The RSS method is implemented by perturbing the individual parameters of the system to the limit of the proposed tolerance and calculating the change caused by the perturbation on some merit function. The most commonly used merit function is an RMS spot size. The individual changes t_i , are statistically added using

$$\text{RSS sum} = \sqrt{\sum (t_i)^2} \quad (3-5)$$

to find the RSS sum. The RSS tolerance method provides a simple method for relating the effects of individual tolerances to the performance of the completed system.

The RSS method is used to develop a tolerance budget in which the individual contributions are tabulated and adjusted by varying the tolerances. The goal of this process is to develop a set of tolerances that will allow a system to meet specifications while minimizing overall cost. We have developed a tolerance budget for system C to show that the tolerances required to realize a hybrid refractive/diffractive system that uses diffractive optics for color correction are reasonable. We have considered tolerances for the power and irregularity of the surfaces, the thickness, refractive index and dispersion, and tilts and decenters of the individual elements. In addition, the decenter of the diffractive surface is toleranced. The function of merit used for this tolerance analysis is the RMS combination of the ray errors for all three wavelengths introduced for on-axis viewing with a 5 mm EPD for three field angles (0°, 17.5° and 25°). A goal for the RSS sum of the individual contributions in the tolerance analysis is to allow up to a 10% increase in the tolerance merit function. The final tolerance budget for system C is shown in Table 3-4.

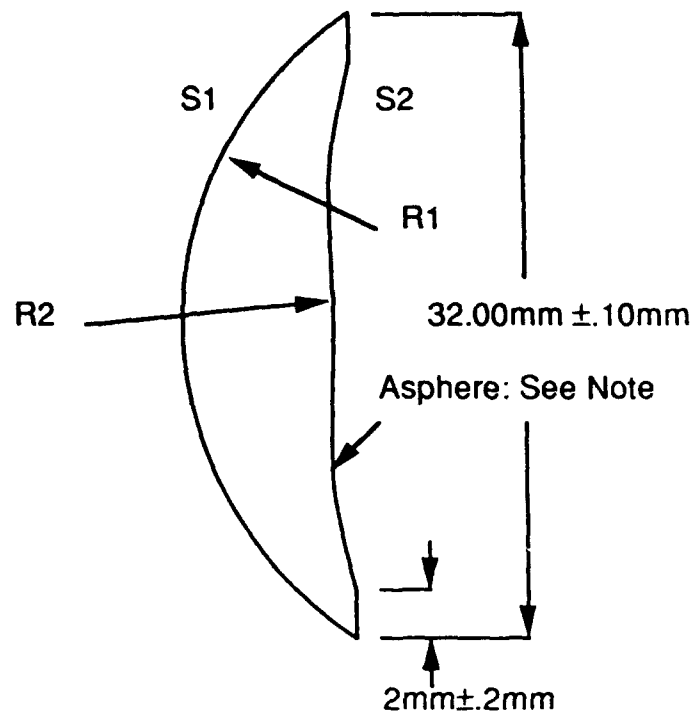
25 W. Smith, "Fundamentals of establishing an optical tolerance budget," SPIE, 531 (1985).

Surface Number	Fringes of Power	Fringes of Irregularity	Thickness (mm)	Index	Abbe Number	Element Decenter (mm)	Element Tilt (deg)
Surface 6	5	2	0.2	0.0005	0.5%	0.05	0.06°
% change	0.18%	0.60%	0.94%	0.79%	3.94%	1.75%	1.31%
Surface 7	5	2	0.2				
% change	0.15%	0.43%	3.32%				
Diffraction Surface						0.025	
% change						1.02%	
Surface 8	5	2	0.2	0.002	0.8%	0.05	0.3°
% change	0.08%	0.37%	3.95%	0.62%	1.93%	0.22%	1.75%
Surface 9	5	2	Focus Compensator				
% change	.002%	0.001%					
Surface 10	5	2	0.2	0.002	0.8%	.05	0.3°
% change	0.02%	0.30%	2.90%	0.01%	0.22%	0.22%	1.12%
Surface 11	5	2					
% change	0.14%	0.003%					
RSS sum	0.28%	0.77%	5.99%	1.00%	4.39%	2.05%	2.46%
% change							

Table 3-4. Tolerance budget for an on-axis HMD. The % change refers to the change in the RMS ray errors. These are summed over all three wavelengths and at three filed angles, for the case of on-axis viewing with a 5mm EPD. RSS total for all tolerances: 8.19%

The goal for this tolerance budget was to allow the RMS ray errors to increase by no more than 10%; the goal has been met with reasonable optical tolerances. The tolerances specified for the elements in this system have been used to generate engineering drawings for a manufacturable relay lens system. The individual element drawings along with associated engineering data are shown in Figs. 3-33 - 3-35. The total weight for the three elements was computed to be 46.3 grams, over 66% of the weight is from the SF56 element. This total weight compares favorably with regard to similar *monochromatic* designs.

To summarize our results, we have shown the feasibility of using diffractive optics for color correction in a hybrid refractive/diffractive relay lens system in an on axis HMD.



Notes:

1. Material: Schott FK5 Standard Grade or equivalent.
2. Aspheric Surface Specification (S2):
Aspheric Coefficients
D= 4.1152e-5 E= -4.5152e-8 F= 2.4337e-10 G= 3.2535e-13
3. Sag Equation

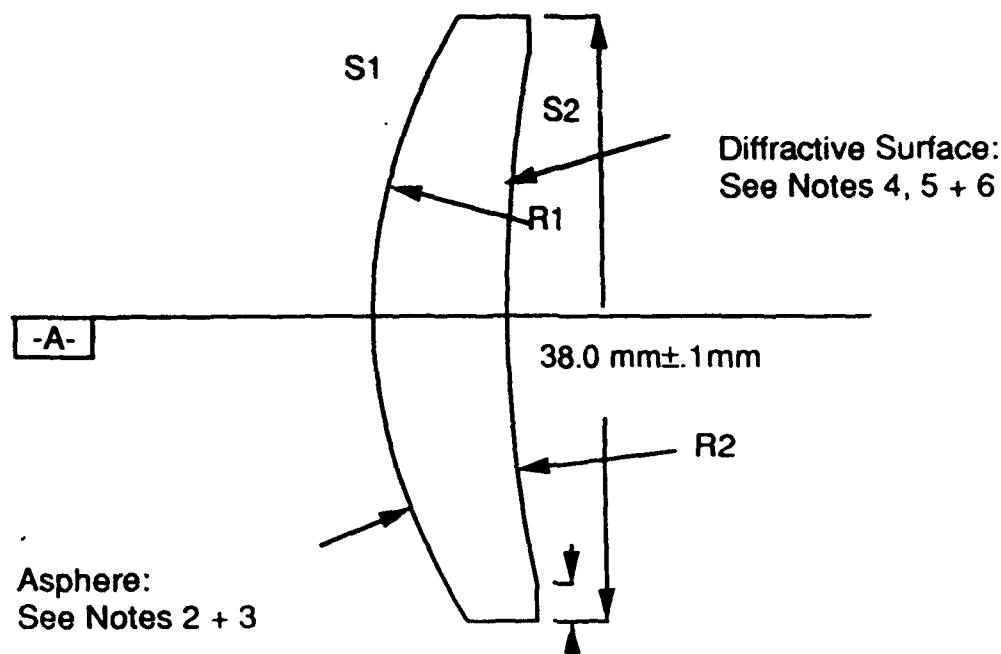
$$\text{Sag} = \frac{y^2 / r}{1 + \sqrt{1 - (k + 1)y^2 / r^2}} + Dy^4 + Ey^6 + Fy^8 + Gy^{10}$$

Rochester Photonics Corp
80 O'Connor Rd, Fairport, NY 14607

OSH502A1D-2

Fig. 33

All units in mm	Surface 1 (S1)	Surface 2 (S2)
Radius	R1= 19.50mm	R2= -423.60mm
Clear Aperture	CA1=28mm	CA2=26mm
Figure Tolerance(Fringes)	5/2	5/2
Beauty Defects (Mil-0-13830)	60-40	60-40
Center Thickness	8.000mm ± .100mm	
Centration	3 arc minutes	
Coating	MgF2 centered at 545nm	



Notes:

1. Material: Schott SF56 Grade 3 or equivalent. 2mm ± 2mm
2. Aspheric Surface Specification (S1):
Conic constant K = -0.60615
Aspheric Coefficients
D = 9.2864e-7 E = -7.1144e-9 F = 1.5729e-11 G = -4.3414e-14

3. Sag Equation

$$\text{Sag} = \frac{y^2 / r}{1 + \sqrt{1 - (k + 1)y^2 / r^2}} + Dy^4 + Ey^6 + Fy^8 + Gy^{10}$$

4. Diffractive Surface Specification (S2):

Phase Coefficients

P1 = -2.2979e-3 P2 = 4.9053e-6 P3 = -5.7925e-8 P4 = 6.8330e-10
P5 = -5.3210e-12 P6 = 2.3689e-14 P7 = -5.6374e-17 P8 = 5.5333e-20

5. Phase Function

$$\Phi = \frac{2\pi}{\lambda} \left(P_1 y^2 + P_2 y^4 + P_3 y^6 + P_4 y^8 + P_5 y^{10} + P_6 y^{12} + P_7 y^{14} + P_8 y^{16} \right)$$

$\lambda = .545 \mu\text{m}$

Diffracted Order 1

6. Phase Function concentric to optical axis -A- ±.025mm.

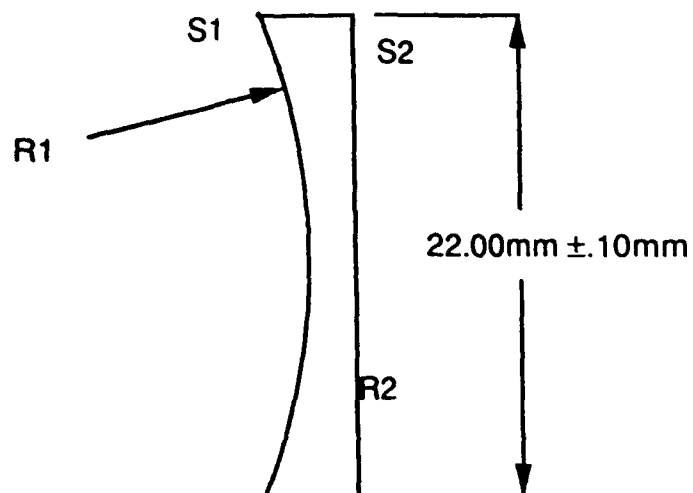
Fig. 34

Rochester Photonics Corp

80 O'Connor Rd, Fairport, NY 14607

OSH502A1D-1D

All units in mm	Surface 1 (S1)	Surface 2 (S2)
Radius	R1 = 29.00mm	R2 = 137.00mm
Clear Aperture	CA1 = 34mm	CA2 = 32mm
Figure Tolerance (Fringes)	5/2	5/2
Beauty Defects (Mil-0-13830)	60-40	60-40
Center Thickness	9.500mm ± .100mm	
Centration	3 arc minutes	
Coating	MgF2 centered at 545nm	See Notes



Notes:

1. Material: Schott F2 Standard Grade or equivalent.

Rochester Photonics Corp
80 O'Connor Rd, Fairport, NY 14607

OSH502A1D-3

Fig 35

All units in mm	Surface 1 (S1)	Surface 2 (S2)
Radius	R1= 19.50mm	R2= ∞
Clear Aperture	CA1=20mm	CA2=20mm
Figure Tolerance(Fringes)	5/2	5/2
Beauty Defects (Mil-0-13830)	40-30	40-30
Center Thickness	2.000mm \pm .100mm	
Centration	3 arc minutes	
Coating	MgF2 centered at 545nm	

The investigation proceeded by generating designs that met the design goals set forth by the AL mission. A tolerance study of one particular design suggests that we have achieved a manufacturable condition.

3.7 Hardware Requirements for HMD System.

We have performed a preliminary assessment of the required equipment for developing a prototype HMD system utilizing diffractive optics for color correction. The following is a brief discussion of some of the key components. Additional information is presented in the Federal SBIR Phase II proposal.

The cathode ray tubes manufactured by Thomas Electronics and Hughes Display Products Corporation appear to be applicable to the HMD system. Both sources have CRT products with P53 phosphors that would be appropriate for use in a HMD. The characteristics are summarized in Table 3-5. Further analysis will be required to determine if the larger 23 mm diameter is useful for color-corrected systems.

Model No.	Useful Screen Area	Outside dimensions	Weight (grams)	Cost
Hughes MH1425	15mm dia.	23 mm dia. x 110 long	90	\$4,000
Hughes MH1426	19 mm dia.	27 mm dia. x 110 long	100	\$4,000
Thomas 1M83P-MFO	19.05 x 12.7 mm.	20.4 mm dia. x 100 long	100	\$2,700

Table 3-5. Summary of CRT data appropriate for HMDs. These CRTs are tabulated for comparison only and do not necessarily represent units that will be used in a prototype system.

Regarding the visor/combiner, we have been in contact with Dr John Masso at American Optical Corporation (AOC) to discuss the feasibility of generating prototype combiners. AOC, Precision Products Business, has been and is currently involved with programs to fabricate components for HMD systems. AOC can bring the following technologies to bear on HMD development:

- 1) The ability to injection mold, cast and coat plastic optical elements. Optical plastics that can be molded include polycarbonate, acrylic and styrene. CR-39 can be cast in glass molds.
- 2) The ability to coat plastic optics with scratch resistant coatings, vapor deposited coatings and holographic narrowband coatings.
- 3) Fabrication of aspheric surfaces using proprietary processes.

Dr Masso indicated that CR-39 can be a low cost alternative for a proof-of-concept program prior to generating expensive tooling for injection molding. The group at AOC are very interested in working with RPC to develop novel combiner hardware during Phase II.

Because high performance off-axis geometries may require specialized combiner coatings, we have contacted Dr James Rancourt of OCLI to discuss the application of angle-sensitive coatings to HMD systems. While conventional HMD bandpass coatings may provide acceptable performance, we are still investigating with OCLI, the potential for special coatings in different HMD designs.

Concerning the aspheric surfaces, we have contacted several companies that specialize in the optical fabrication of aspheres. J. A. Optical and Tinsley have considered the aspheres required for the on-axis, color-corrected case. Both firms were interested in fabricating the parts, however, the unit price is quite high. It is our intention to fabricate the diffractive components in-house. However, for a second source, we have contacted the 3M Company, which is also capable of fabricating the diffractive surfaces.

3.8 Summary

In this Section, several HMD geometries were investigated with special emphasis given to the correction of chromatic aberration through the use of surface-relief diffractive optics. We have considered the design of an all-diffractive relay lens for use with an on-axis combiner system to investigate the feasibility of the class of on-axis, all-diffractive HMDs. Results indicate that, while an all-diffractive system can be rather lightweight, there are severe limitations on the spectral bandwidth of the illumination source [see Fig. 3-18]. The all-diffractive relays may be useful for future systems that utilize laser sources. We have also investigated the use of combinations of refractive and diffractive elements in the relay lens to provide color correction. The feasibility of color-corrected HMD systems using hybrid refractive/diffractive systems was investigated by considering the design of color-corrected hybrid relay lenses for on-axis and off-axis combiner configurations. The

spectral band used for color correction was obtained from the emission curve for P53 phosphor. For the case of the on-axis combiner geometry [see Figs. 3-1 and 3-2], an acceptable hybrid, color-corrected relay weighs less than two ounces. The chromatic aberration was corrected for the entire spectrum of P53 and not just for the green spectral peak of P53. The preliminary design for the off-axis geometry also indicates that diffractive optics can play an important role in extending the operational bandwidth and in reducing the weight of HMD systems.

4.0 Fabrication of Diffractive Optical Elements

4.1 Introduction

This section of the report covers key developments in the fabrication of diffractive optics. Both photolithographic and single-point diamond turning techniques are considered. A brief analysis of substrate materials and replication schemes is reported.

Diffractive optical elements can be generated interferometrically using coherent wavefronts or directly using computer-controlled hardware. For the case of interferometric generation, a suitable recording medium is placed at the intersection of two mutually coherent waves. The resultant fringe pattern is thereby stored in the photosensitive material in a manner closely related to conventional holography. In this fashion, diffractive elements that are described by arbitrary phase functions can be generated. For example, a particular phase function may describe either a wide-field diffractive imaging lens or a null corrector for the optical testing of an aspheric system. For the case of interferometric generation, the realizability of a particular diffractive element is primarily dependent on the realizability of the pair of coherent wavefronts. The wavefronts may be produced using conventional optical elements or computer-generated holograms.

The fabrication of diffractive elements using computer-controlled hardware is typically completed using a point-by-point process where the prescribed phase function is opto-mechanically recorded onto the desired substrate. Common methods include photolithographic (mask-and-etch) techniques and schemes based on single-point diamond turning. Most high-performance diffractive lenses are fabricated using techniques based on one of these direct-write technologies.

4.2 Photolithographic Techniques

Common photolithographic fabrication methods can be divided into two parts; microelectronics-based and optical direct write. Here we report on the features of the microelectronics-based method with regard to the applicability to the HMD program.

4.2.1 Fabrication Using Microelectronics Technology

In the design of diffractive optical systems, a mathematical description of the required phase profile of a particular diffractive element is generated using commercially available lens design code or proprietary software. In the fabrication process, this representation of the required phase profile is then transferred into (or onto) a suitable substrate.

A set of lithographic (binary) masks can be created using the mathematical description of a particular design. The binary masks are designed to approximate the theoretical phase profile using a staircase approximation. The number of mask levels that are required depends on the level of approximation that is required to accurately describe the surface profile.

The masks are created using standard pattern generators from the integrated circuit industry. These pattern generators, whether optical or electron beam, expose a thin layer of photoresist that is coated on a chrome-covered quartz substrate. The exposed photoresist is then washed off the chrome-covered substrate, leaving the pattern in the remaining unexposed photoresist. The pattern is then transferred to the chrome by etching away the chrome that remains uncovered by photoresist. After the chrome has been appropriately patterned, the remaining photoresist is cleared. This removal process gives rise to a finished-lithographic mask. The complete set of masks is used to approximate the ideal phase profile of the computer generated diffractive element. What remains is to transfer and convert the amplitude pattern contained in the mask set into a surface-relief pattern on an appropriate substrate.

To illustrate the fabrication process, Fig. 4-1 describes the steps needed to construct a binary phase grating. A substrate of the desired material is coated with a thin layer of prescribed thickness of a photoresist. The lithographic mask is then placed in intimate contact with the substrate material and is illuminated from above using a source of ultraviolet light. The photoresist is developed by clearing away the exposed layer and leaving the binary grating pattern in the remaining photoresist. The photoresist acts as an etch stop, as in the lithographic mask process, except that now the substrate material is etched instead of the chrome layer.

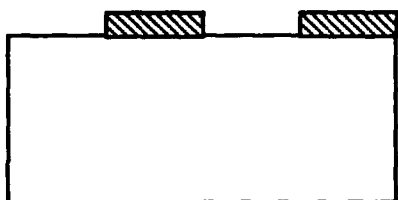
Mask 1



Binary Amplitude Mask



Photoresist
Substrate



Development



Reactive Ion Etch



Photoresist Removal

Fig. 4-1. Describing the fabrication process for a binary phase grating.

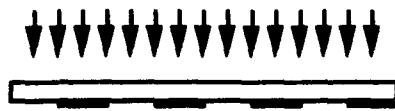
A reactive-ion etch process is then used to completely transfer the pattern into the substrate material so as to form a surface-relief profile. The depth of the etch must be accurately controlled. It is the depth of the surface relief that essentially controls the diffraction efficiency of the element. After the etch process, the residual photoresist is removed leaving a binary surface-relief grating in the substrate material.

If the process is repeated using the other members of the mask set, a staircase approximation to the ideal surface profile is realized. Figure 4-2 illustrates how the next mask in the set is transferred into the substrate. The binary phase structure described previously is recoated with photoresist and exposed using the appropriate lithographic mask that has a frequency twice that of the first mask. After development, the substrate is again subjected to the reactive-ion process. The depth of the etch is chosen to be half that achieved during the first etch. The removal of the residual photoresist results in a four-level surface relief structure that represents a boxcar approximation to the desired ideal profile. The process is repeated using the other members of the mask set until a satisfactory approximation is obtained.

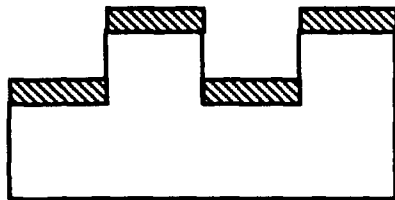
Note the importance of accurate mask alignment in the fabrication process. Commercially available mask aligners available in the microelectronics industry are used to achieve submicron tolerances. Mask misalignment has the deleterious effect of altering the surface height from the ideal. The primary result is a decrease in the diffraction efficiency of the element. Element cost is directly related to the number of masks that need to be precisely positioned; the cost function is somewhat nonlinear.

The fabrication of surface-relief diffractive optics using photolithographic techniques requires a set of amplitude masks and a microelectronics-type facility. A set of N binary masks properly aligned gives rise to a surface profile with 2^N phase levels. The current minimum feature size for this technology in production (not state-of-the-art) is approximately $0.7\text{ }\mu\text{m}$ and the alignment tolerance results in approximately an $0.8\text{ }\mu\text{m}$ feature. If three masks provide acceptable diffraction efficiency, then the minimum zone spacing is of the order of $6.5\text{ }\mu\text{m}$. This technology is adequate and can be used for some HMD corrective elements.

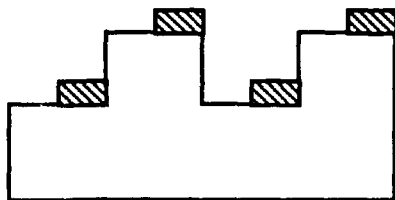
Mask 2



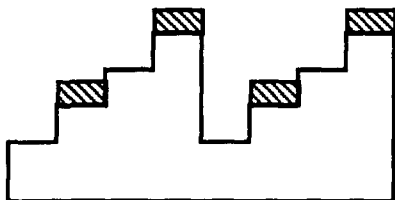
Binary Amplitude Mask



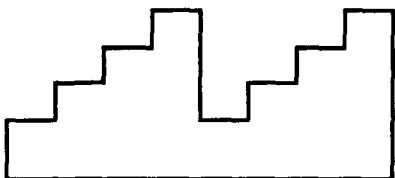
Photoresist
Substrate



Development



Reactive Ion Etch



Photoresist Removal

Fig. 4-2. Implementation of an additional lithographic mask for the fabrication of a multi-level phase grating.

4.3 Single-Point Diamond Turning

Computer-controlled milling machines and lathes (mechanical direct-write) can be used for the fabrication of surface-relief diffractive optics. In particular, techniques to generate the surface structure based on single-point diamond turning have been implemented by several laboratories.²⁶ A microscopic diamond-tipped tool is controlled by a host computer. The three-dimensional surface profile is calculated and then stored in computer memory. Using CNC standards, the computer directs the diamond tool to transfer the mathematical representation to a physical 3D profile in an appropriate material. These precision machine tools utilize optical interferometers on each axis to produce blazed phase profiles with submicron accuracy.

Using direct-write or indirect molding from a master element, blazed diffractive elements have been generated using diamond turning in a wide variety of metals and plastics. Rotationally symmetric and linear gratings have been fabricated. Figure 4-3 is a series of scanning electron micrographs of different radial locations on the surface of an $f/3$ ($\lambda = 587$ nm) diffractive lens. The lens was fabricated by the Optics Technology Center at the 3M Company. Note from the figure that the finest zone spacing is approximately $3\text{ }\mu\text{m}$. 3M produced a blazed master element using diamond turning in a metal. The lens itself was created in PMMA (acrylic) using the master and a compression molding process.

Single-point diamond-turning allows the fabrication of blazed gratings with smaller periods than those fabricated using conventional photolithography (mask-and-etch). Diamond turning allows a surface profile that is continuous while mask-and-etch processes only allow a discrete staircase approximation to the continuous case. The current state-of-the-art feature size including the effects of mask alignment are of the order of $0.5\text{ }\mu\text{m}$ for VLSI-type photolithography. If sixteen levels are required to synthesize the blaze, then the minimum period allowed is $8\text{ }\mu\text{m}$. At visible wavelengths, this minimum spacing corresponds to an ability to fabricate $f/8$ (and slower) diffractive lenses. Diamond turning methods, on the other hand, offer the ability to generate $f/1.5$ optics for use in the *visible*

²⁶ P. P. Clark and C. Londono, "Production of kinoforms by single point diamond machining," *Optics News*, p.39 Dec. 1989; C. Londono and P. P. Clark "The design of achromatized hybrid diffractive lens systems," *Int'l. Lens Design Conf.*, June 1990.

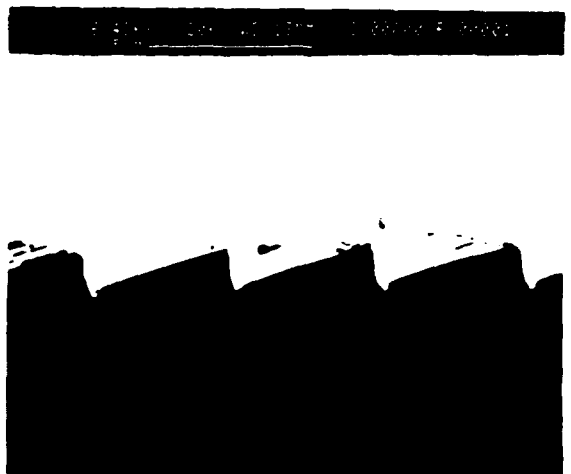
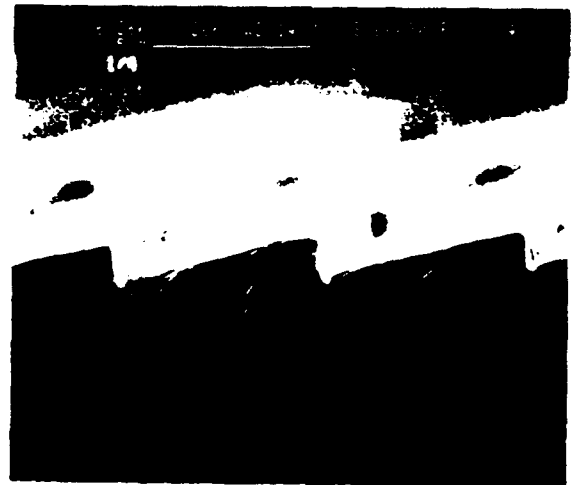
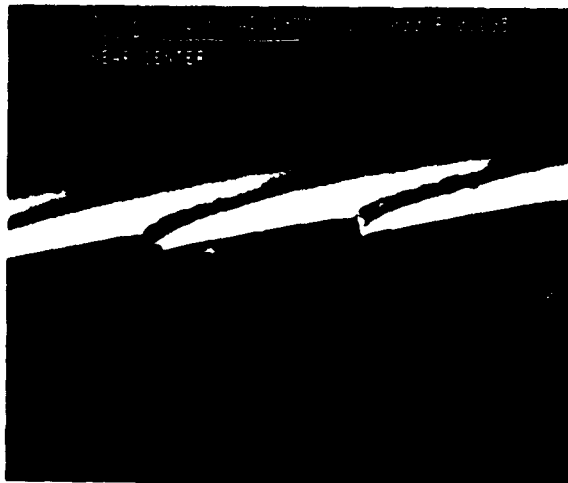


Fig. 4-3. Electron micrographs of a replica from a diamond-turned diffractive master.

region. Diamond turning techniques may be used to fabricate the elements in the HMD system.

4.4 Element Replication

The surface-relief profile associated with the master diffractive element can be replicated using several techniques. Methods based on injection or compression molding have been reported. The lens generated by 3M [see Fig. 4-3] was produced using a compression-molding technique. Several companies replicate surface-relief pictorial holograms using embossing processes.

Another method based on the cast-and-cure of photopolymers has also been used. In this process, a substrate that is covered with a small amount of photopolymer is made to come into intimate contact with the master element. Ultraviolet light is used to polymerize the thin layer and the master is separated from the replica. The replica now resides on a mechanically stable substrate. A wide variety of substrates can be used including fused silica and a large range of optical glasses. There appear to be few limitations on the choice of substrate material; the substrate is still subject to mechanical considerations.

One of the most important properties for the replication process is that the resulting replica element must have excellent dimensional stability with respect to the master. Obviously, the zone spacing and the height of the surface profile control the operation of the diffractive element. Materials and processes currently exist to help ensure that the replica conforms to the master over a wide range of operating conditions. We have identified several UV-polymerizable coatings that have excellent optical and mechanical properties. However, there is still a significant need for further development in the area of element replication. Philips, 3M, and DuPont currently have development programs to advance the state of replication for diffractive and refractive aspheric lenses. There appear to be no fundamental limitations that may preclude the replication of the diffractive elements in the HMD system in the production phase.

5.0 Characterization and Testing of the Diffractive Components of the HMD

In this Section, we present the results of an investigation of methods to characterize the performance of the diffractive components of the HMD. We report a study of the diffraction efficiency issue of diffractive optics and we present a discussion of the effects of imperfect diffraction efficiency on the modulation transfer function over the field-of-view.

5.1 Introduction

As a direct result of the research and development presented in the previous sections, it is clear that diffractive optics can play an important role in the development of color-corrected HMD systems. However, unlike conventional optical elements, diffractive lenses generate an exiting field distribution that generally contains more than a single diffracted order. The existence of multiple orders has the effect of decreasing the contrast of the image. For the SBIR Phase I feasibility study, it is important to investigate the effects of the nonunity diffraction efficiency on imaging performance over the wavelength band of interest. From a broader perspective, since diffraction into unwanted orders occurs, RPC has identified and is currently developing methods to test the diffractive components for diffraction efficiency and modulation transfer function.

Fundamentally, diffractive optical elements are designed through the application of particular constraints to a general diffraction grating. The constraints consist of parameters such as grating period and optical path length delay across a given period (commonly referred to as a "blaze"). For the case of a diffractive lens, the dependence of the grating period on the radial coordinate determines the focusing properties of the lens. The grating period is, in general, described by a higher-order polynomial in the radial coordinate. The coefficients of the various terms in the polynomial determine the first-, third-, fifth- and higher orders of the exiting wavefront that is produced on transmission or reflection from the surface. The particular form of the surface-relief profile or blaze determines the amount of energy that is diffracted into a particular diffraction order. Lenses can be blazed to focus nearly all the incident energy into any one diffraction order. It is also possible to choose a blaze profile such that the lens diffracts certain amounts of energy into several orders simultaneously. For most cases of practical interest, the optical designer chooses to concentrate all the energy into the first diffracted order. If the blaze is chosen correctly, it is theoretically possible (in the scalar domain) to focus 100% of the incident light into the first

order beam. If the blaze is not chosen correctly or if the lens is not fabricated properly, one expects less than 100% of the light to be diffracted into the first order. The remainder of the incident energy is shared appropriately among all the other diffraction orders. The deviation from ideal that results from poor design or manufacture causes structured, stray light to be present in the optical system.

The amount of energy that is diffracted into the order of interest is represented as a percent of the total diffracted energy and that ratio is called "diffraction efficiency." The designer and fabricator must now control both the grating period as a function of the radial coordinate and the (blazed) surface-relief profile. Furthermore, he must understand how to accommodate situations where the diffraction efficiency is less than 100% since this is almost always the case in real systems. In fact, as we will see, outside the scalar domain, electromagnetic (vector) effects may make it virtually impossible to obtain 100% efficiency for some lenses.

There are many problems that can arise from low transmission characteristics at a surface. The most important problem to consider is that of veiling glare. Veiling glare is caused by diffraction into orders, other than the primary order, that reaches the image plane of a system and does not come to a sharp focus. The following represents a detailed analysis of diffraction efficiency as it applies to the HMD program.

5.2 Diffraction Efficiency

5.2.1 Theory

An important design parameter of a diffractive element is the throughput of the element. There are two components to the efficiency. The first component is the Fresnel reflections at each surface of the element.²⁷ The Fresnel reflections can be reduced by applying conventional multi-layer coatings to each of the two surfaces. The second contribution results from the diffractive surface-relief profile.

The efficiency of the diffractive surface is dependent on both the profile of the grooves and to a lesser extent (although the relationship is quite complicated) their spacing. For many cases, the diffraction efficiency of the groove profile can be determined from

²⁷ M. Born and E. Wolf, *Principles of Optics*, (Pergamon Press, 6th ed. 1987) p. 69.

scalar diffraction theory^{28,29} This method allows the magnitude of individual diffracted orders to be calculated from the Fourier transform of the phase function of the diffractive element.

Diffractive lenses are typically designed to diffract a maximum amount of energy into one particular order. Once the zone structure (grating period as a function of radius) of the lens is computed to achieve an acceptable level of wavefront performance, the surface profile is blazed in a manner equivalent to a blazed diffraction grating to provide maximum diffraction efficiency. The resulting blazed structure is equivalent to a blazed, chirped (variable period) diffraction grating.

As long as the grating period across the diffractive lens aperture remains much greater than the illumination wavelength, ordinary scalar diffraction theory is sufficient to describe the expected diffraction efficiency. If the grating period takes on values on the order of the illumination wavelength at any point on the lens surface, the scalar approximation becomes invalid and a (vector) electromagnetic treatment is required to predict the diffraction efficiency. For example, a blazed diffractive lens operating at $f/2$ has a minimum grating period of four waves. Using scalar theory, the expected diffraction efficiency in the first order for this lens is 100%. However, since the grating period at the edge of the lens is of the order of the wavelength, scalar theory offers incorrect results. Actually, the integrated efficiency of the $f/2$ diffractive lens taking into account the electromagnetic treatment is approximately 85%. Fortunately, the characteristic spacing of the diffractive elements in the HMD system is larger and will allow a higher integrated efficiency.

We have determined in our investigations that the blaze profile generated using scalar diffraction theory is the proper profile only in the regime where scalar diffraction remains a valid approximation. For lenses faster than about $f/5$, computer simulations have shown that vector diffraction theory must be used to predict the distribution of diffracted energy. At RPC, we make use of a rigorous coupled wave approach to calculate expected diffraction efficiencies. We have applied these concepts to the HMD design.

28 J. Goodman, *Introduction to Fourier Optics*, (McGraw-Hill, CA 1968) p. 30.

29 G. J. Swanson, "Binary optics technology: The theory and design of multi-level diffractive optical elements," MIT Lincoln Laboratory Tech. Rep. 854, (1989).

As we discussed earlier, there are actually two measures of efficiency for a diffractive element. The two measures are referred to as relative efficiency and absolute efficiency³⁰. Relative efficiency measurements refer to the diffractive component of the efficiency only and ignore any Fresnel losses that occur at the surfaces. The absolute efficiency of an element is a measure that includes any Fresnel losses.

The imaging performance of a diffractive element will, in general, be degraded by the presence of undiffracted light in the system. The definition of undiffracted light used in this analysis is any light that is not diffracted into the order of interest, or in this case the first order. The reason that we use the term undiffracted is that most of the energy not in the first diffracted order is, in general, in the zeroth order. In the analysis that follows, we assume that the energy in all orders other than one or zero is small. The effect of this light in the system has recently been treated as either a veiling glare or background noise in the image plane³¹.

For the case of a single diffractive element used with an infinitely distant object, the background noise can be treated using Fourier optics techniques. Consider the pupil function given by

$$P(u,v) = t_1(u,v)e^{ikW_1(u,v)} + t_u(u,v)e^{ikW_u(u,v)}, \quad (5-1)$$

where $t_1(u,v)$ is the local transmission function of the first order, $t_u(u,v)$ is the local transmission function of the undiffracted light, $W_1(u,v)$ is the wavefront function for the first-order light and $W_u(u,v)$ is the wavefront function for the undiffracted light. These wavefront functions represent the deviation of the wavefronts from a perfect spherical wave centered at the paraxial focus.

Again, at this point in the calculation, we assume that any background light in the system results from the zero order. This approximation is equivalent to stating that *most* of the noise results from light that passes directly through the lens, which occurs in many instances. Noise from other orders is assumed to be negligible compared to that produced

30 C. Londono and P. P. Clark "The design of achromatized hybrid diffractive lens systems," Int'l. Lens Design Conf., June 1990.

31 D.A. Buralli and G. M. Morris, "Performance of diffractive lenses with nonunity diffractive efficiency," OSA Ann. Mtg., OSA Tech. Dig., **15**, (OSA, Wash, DC 1990).

by the zero order. The local diffraction efficiency of the diffractive element $\eta(u,v)$, is related to the transmission function of the first order by

$$\eta(u,v) = |t_1(u,v)|^2 \quad . \quad (5-2)$$

The law of conservation of energy provides that the transmission function of the undiffracted light and the local diffraction efficiency are related through

$$(1 - \eta(u,v)) = |t_u(u,v)|^2 \quad . \quad (5-3)$$

For any pupil function defined by Eq. (5-1), it has been shown that the point spread function is given by

$$I(x,y) = |\text{FT}\{P(u,v)\}|^2 \quad . \quad (5-4)$$

For the case under examination, the wavefront function of the undiffracted light is equal to

$$W_u(u,v) = \frac{1}{2f}(u^2 + v^2) \quad . \quad (5-5)$$

Equation (5-5) gives the Fourier transform of the undiffracted light as the Fresnel diffraction pattern formed by a circular aperture. For this analysis, the diffraction pattern can be approximated as being identical to the local transmission function of the undiffracted light. This approximation allows us to ignore any cross terms that exist between the impulse response functions of the diffracted light $h_1(x,y)$, and the undiffracted light $h_u(x,y)$, where the impulse response function of an optical system is defined as the Fourier transform of the pupil function. The point spread function is then given by

$$I(x,y) \equiv |h_1(x,y)|^2 + |h_u(x,y)|^2 \quad . \quad (5-6)$$

The energy in the point spread function has been normalized to unity which gives

$$\int_{-\infty}^{\infty} \int_{-\infty}^{\infty} |h_1(x,y)|^2 dx dy + \int_{-\infty}^{\infty} \int_{-\infty}^{\infty} |h_u(x,y)|^2 dx dy = 1 \quad . \quad (5-7)$$

The optical transfer function (OTF) of the system and the point spread function are known to be a Fourier transform pair. This can be written as

$$\text{OTF}(f_x, f_y) = \iint_{-\infty}^{\infty} I(x, y) \exp[-i2\pi(f_x x + f_y y)] dx dy . \quad (5-8)$$

At this point it is useful to define a quantity called the integrated efficiency of the element η_i . η_i is a measure of the total amount of energy that is diffracted into the first order of the system and is defined by

$$\eta_i = \frac{\iint_{\text{pupil}} \eta(u, v) du, dv}{A} = \frac{\iint_{\text{pupil}} |t_1(u, v)|^2 du, dv}{A} , \quad (5-9)$$

where A is the area of the pupil. Application of Parseval's theorem implies that

$$\eta_i = \iint_{-\infty}^{\infty} |h_1(x, y)|^2 dx dy , \quad (5-10)$$

and by Eq. (5-7) above we can write

$$\iint_{-\infty}^{\infty} |h_u(x, y)|^2 dx dy = 1 - \eta_i . \quad (5-11)$$

This definition allows us to find the limiting value of the OTF, using

$$\text{OTF}(0, 0) = \iint_{-\infty}^{\infty} |h_1(x, y)|^2 dx dy + \iint_{-\infty}^{\infty} |h_u(x, y)|^2 dx dy = 1, \quad (5-12)$$

which gives

$$\text{OTF}(0, 0) = \eta_i + (1 - \eta_i) \quad (5-13)$$

Equation (5-13) shows that the limiting value, or the value for zero frequency, of the OTF for the focused or first-order component of the point spread function is equal to the integrated efficiency of the diffractive element. This is a remarkable result. The result implies that the modulation transfer function is scaled by the integrated efficiency. Low values of integrated efficiency correspond to poor imaging.

If we assume that the undiffracted component of the point spread function extends over a much larger area than the first order component, then the undiffracted component contributes to the OTF only when the spatial frequency is equal to zero. This allows us to write the approximate OTF of the system as

$$\text{OTF}(f_x, f_y) = \iint_{-\infty}^{\infty} |h_1(x, y)|^2 \exp[-i2\pi(f_x x + f_y y)] dx dy + (1 - \eta_i) \delta(f_x = 0) \delta(f_y = 0) \quad (5-14)$$

If we use the definition for η_i we find

$$\text{OTF}(f_x, f_y) = \frac{\eta_i \iint_{-\infty}^{\infty} |h_1(x, y)|^2 \exp[-i2\pi(f_x x + f_y y)] dx dy}{\iint_{\text{pupil}} |t_1(u, v)|^2 du, dv} + (1 - \eta_i) \delta(f_x = 0) \delta(f_y = 0) \quad (5-15)$$

Simplification gives³²

$$\text{OTF}(f_x, f_y) = \eta_i \text{OTF}_1(f_x, f_y) + (1 - \eta_i) \delta(f_x = 0) \delta(f_y = 0) \quad (5-16)$$

or the optical transfer function of this system is equal to the optical transfer function defined by the diffracted light in the point spread function, scaled by the integrated efficiency, plus a delta function at zero spatial frequency scaled by $(1 - \eta_i)$, which normalizes the function to unity.

An example of this result is found when the blaze angle of an $f/20$ diffractive element (with no aberrations), is incorrect. For the case of an $f/20$ lens, the efficiency of the element is approximately constant across the aperture. If all of the undiffracted light is in the zero order, then the OTF of the element is equal to the OTF of the element if the efficiency were one then scaled down by the integrated efficiency [see Fig. 5-1].

³² J. Goodman, *Introduction to Fourier Optics*, (McGraw-Hill, Inc., San Francisco, CA, 1968) p. 114.

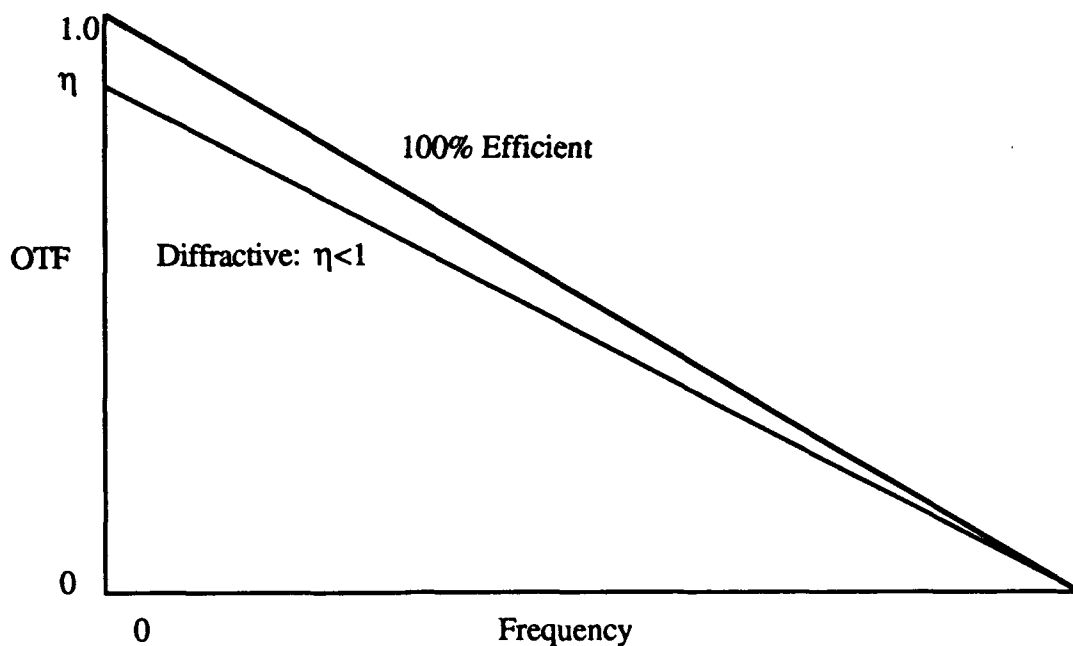


Fig. 5-1. The optical transfer function (OTF) for a 100%-efficient diffraction-limited imaging system vs. the OTF of the same system with an integrated efficiency equal to η , where η is less than 100%.

It is clear that the imaging performance of systems containing diffractive elements will be degraded by the presence of undiffracted light in the system. Undiffracted light is caused by a number of factors as discussed earlier. In addition to these factors, the diffraction efficiency can be affected by errors in the manufacturing process. The most obvious of these errors can occur through the encoding of incorrect groove depth. This can be seen from the efficiency of a blazed diffraction grating with a phase profile similar to Fig. 5-2, where α is equal to 1 for 100% efficiency in the first order. The diffraction

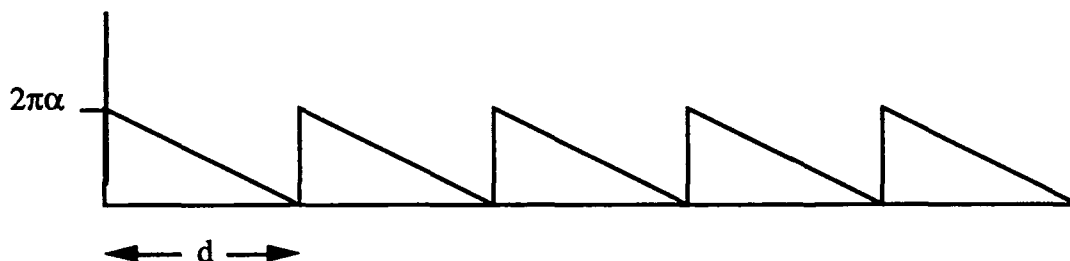


Fig. 5-2. Sawtooth blaze profile, where α is the maximum phase deviation produced by the grating.

efficiency as a function of wavelength for this grating is described by³³

$$\eta_\lambda = \text{sinc}^2(\alpha + m) \quad (5-17)$$

where

$$\text{sinc}(x) = \frac{\sin(\pi x)}{\pi x} \quad (5-18)$$

It can be shown that for diffraction into the first order ($m=1$), the parameter α is given by

$$\alpha = \frac{\lambda_0 [n(\lambda) - 1]}{\lambda [n(\lambda_0) - 1]} \quad (5-19)$$

where the index of refraction at a given wavelength λ , is given by $n(\lambda)$, and the center design wavelength is λ_0 . It is apparent from Eqs. (5-17) - (5-19) that the diffraction efficiency decreases in the presence of wavelength detunings.

The wavelength dependence of diffractive elements becomes a concern when the optic is to be used in a system that operates over an extended wavelength band. There are two wavelength-dependent effects unique to diffractive structures. The first effect results from the well-known fact that the diffraction angle is wavelength dependent. With reference to the grating equation, longer wavelengths are diffracted to larger angles, or the optical power of a diffractive lens is linearly proportional to the illumination wavelength. The second effect is the wavelength dependence of the diffraction efficiency, as discussed in this section.

Figure (5-3a) illustrates the functional form of the wavelength-dependent efficiency given by Eq. (5-17) for the $m=1$ order. The efficiency for the $m=0$ and $m=2$ orders is shown in Fig. (5-3b). The average diffraction efficiency in the $m=1$ order remains above approximately 95% for fractional bandwidths of up to 40%. This reduction in the diffraction efficiency for wide-band illumination restricts the usefulness of diffractive optics for some systems. Again, the light that is not diffracted into the design order is diffracted into other orders. This misdirected light can cause reductions in the image contrast. The

33 G. J. Swanson, "Binary optics technology: The theory and design of multi-level diffractive optical elements," MIT Lincoln Laboratory Tech. Rep. 854, (1989)

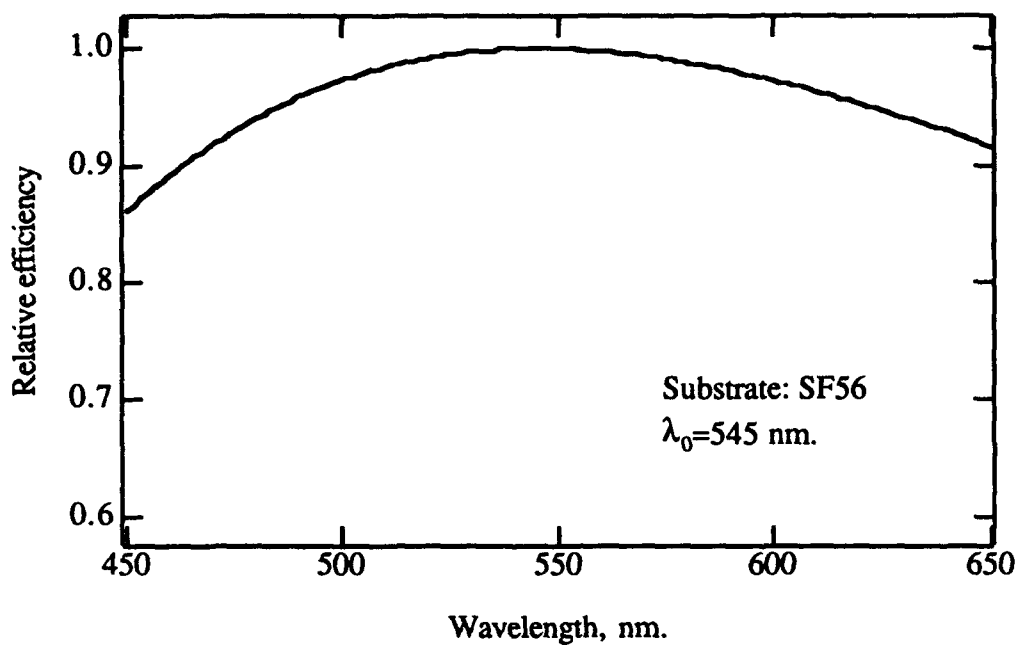


Fig. (5-3a). The relative efficiency for the $m=1$ order. The efficiency peaks at the design wavelength, and falls off to either side.

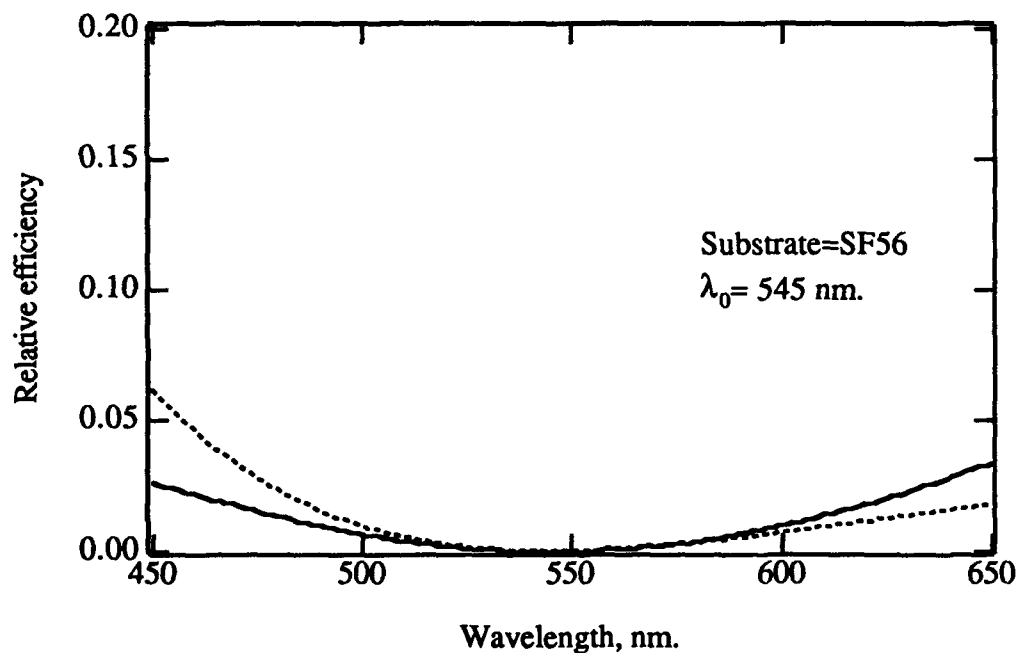


Fig. (5-3b). The relative amounts of power diffracted into the $m=0$ and $m=2$ orders. This light constitutes a background that decreases the overall system performance.

efficiencies for the primary wavelengths in the P53 spectrum are shown in Table 5-1. Also important is the effect of angular detunings (i.e. non-normal angles of incidence) on the diffraction efficiency. Fortunately, for angles of incidence less than approximately 30°, it has been shown that the diffraction efficiency is insensitive to angular detuning.

Wavelength, nm.	$\eta(m=0)$	$\eta(m=1)$	$\eta(m=2)$
490	0.0099	0.9627	0.0157
545	0.0000	1.0000	0.0000
590	0.0085	0.9763	0.0060
625	0.0255	0.9357	0.0144

Table 5-1. The grating efficiencies for the primary wavelengths of the P53 phosphor.

5.3 Stray Image Analysis for Diffractive Optics.

The previous section discussed the amount of power that is diffracted into orders other than the $m=1$ order. In the analysis of imaging systems, it is important to consider where the images formed by the extraneous diffracted orders are located. Throughout this report, the only extraneous orders considered are $m=0$ and $m=2$.

The location of these images is shown in a simplified diagram in Fig. (5-4). The figure shows the desired case of the $m=1$ order, the object is imaged at infinity for the viewer. The other two orders will also form images, however these images will be greatly out of focus compared to the $m=1$ order. The amount that the extraneous images are defocused depends on the paraxial power in the diffractive surface. If the diffractive power is weak, then all of the images will be nearly in focus. If the diffractive power is strong, then there will be a large amount of defocus between the images.

For the hybrid refractive diffractive designs presented in Section 3, the location of the extraneous images is shown in Fig. (5-4). For the case of the $m=0$ image, the distance d is 110 mm. This small distance will make it difficult for the viewer to focus on this image. The image from the $m=2$ order is located on the "other side" of infinity, i.e. the rays are converging towards the viewer. This image can not be brought to a focus by the viewer.

The relative luminance of the images is given by using Table (5-1), which shows the diffraction efficiency for the $m=0$ and $m=2$ orders as a function of wavelength. For example, the $m=0$ image at 490 nm will have a relative luminance of 0.99% compared to the $m=1$ image at 545 nm. Since the diffractive surface is 100% efficient at the design wavelength, the extraneous images will exist only at wavelengths other than the design wavelength.

The extraneous images discussed in this section will be produced in any system utilizing diffractive optics. Fully characterizing their effect with experimental data has not been reported, and will be required in future work.

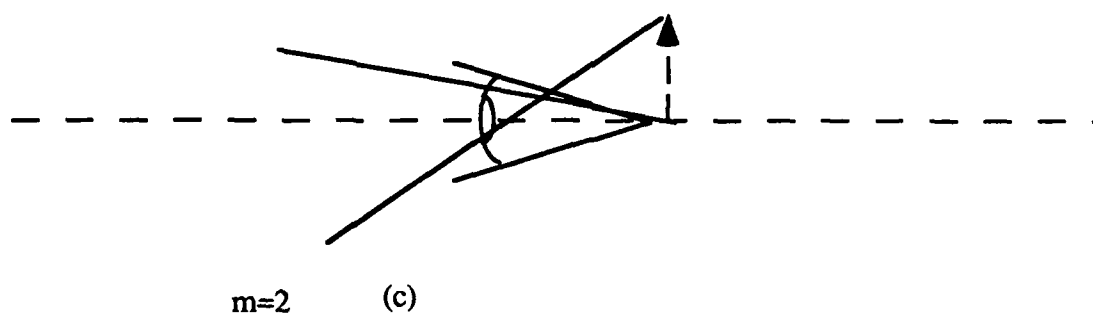
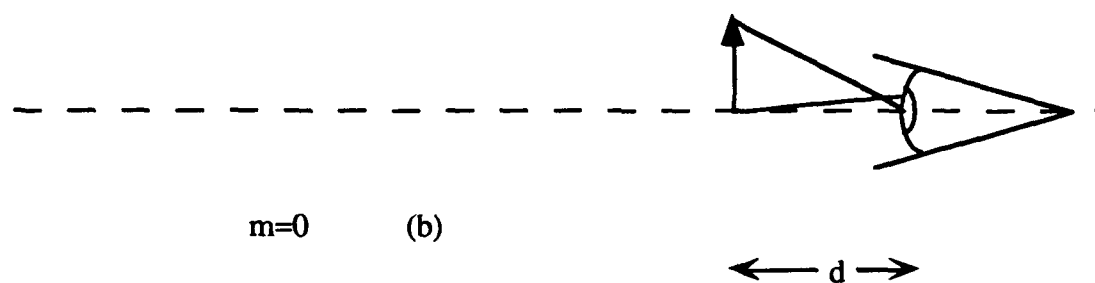
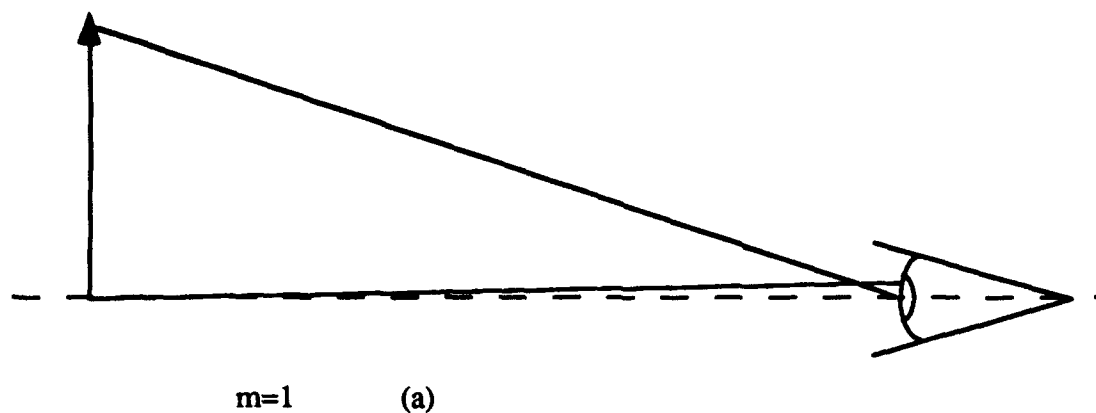


Fig. (5-4). Images formed in a system with diffractive optics, at infinity (a), near viewer (b), and beyond infinity (c).

5.4 Summary

This Section reported on some inherent characteristics of systems that employ diffractive optical elements. Diffraction efficiency is clearly a critical parameter in the design and implementation of diffractive elements. The optical performance is definitely effected by the undiffracted illumination [see Fig. 5-1]. Unfortunately, the amount of undiffracted light that a human observer can tolerate from an HMD over extended periods of time is an unknown quantity. RPC is currently developing sophisticated testing protocols and hardware for advanced measurements of diffraction efficiency and image quality of diffractive systems.

6.0 Future Research

During the Federal SBIR Phase I research and development effort, several HMD system designs were analyzed. It was found that through the use of surface-relief diffractive optics technology, HMD systems that are color corrected and operate over wide fields-of-view are feasible and can be implemented with commercially-available hardware.

We have thoroughly investigated the key optical components in the relay optical assembly and in the combiner. All-diffractive, centered on-axis and off-axis geometries were studied and color-correction principles were employed. Size and weight characteristics of the HMD system were given high priority in the design. Designs that utilize a minimum of optical components while maintaining high performance were identified to minimize overall system weight and alignment complexity.

In this Section 3.0, several HMD geometries were investigated with special emphasis given to the correction of chromatic aberration through the use of surface-relief diffractive optics. We have considered the design of an all-diffractive relay lens for use with an on-axis combiner system to investigate the feasibility of the class of on-axis, all-diffractive HMDs. Results indicate that, while an all-diffractive system can be lightweight, there are severe limitations on the spectral bandwidth of the illumination source [see Fig. 3-18]. The all-diffractive relays may be useful for future systems that utilize laser sources. We have also investigated the use of combinations of refractive and diffractive elements in the relay lens to provide color correction. The feasibility of color-corrected HMD systems using hybrid refractive/diffractive systems was investigated by considering the design of color-corrected hybrid relay lenses for on-axis and off-axis combiner configurations. The spectral band used for color correction was obtained from the emission curve for P53 phosphor. For the case of the on-axis combiner geometry (see Figs. 3-1 and 3-2), an acceptable hybrid, color-corrected relay weighs less than two ounces. The chromatic aberration was corrected for the broad spectrum of P53 and not just for the green spectral peak of P53. The preliminary design for the off-axis geometry also indicates that diffractive optics can play an important role in extending the operational bandwidth and in reducing the weight of HMD systems.

Techniques for the fabrication of the diffractive components were investigated. In all of our designs, we have included fabrication constraints and applied design-for-manufacture procedures. Methods based on photolithographic techniques and single-point diamond turning may be used to fabricate the diffractive elements for the HMD system. These technologies are becoming well established however, the elements are still fairly expensive in small quantities. We have also determined that replication schemes using stable materials that meet military specifications exist; this is important for any subsequent production phase.

We have also performed a detailed investigation of the effects of diffraction efficiency on imaging performance. It was determined that the undiffracted light degrades the modulation transfer function by an amount proportional to the reduction in the integrated efficiency. With reference to the tolerated system in Section 3.0 (see also Appendix C), due to the relatively large zone spacing, it appears likely that the diffractive element can be fabricated in such a way as to maximize the integrated efficiency.

We are currently preparing a Federal SBIR Phase II proposal that describes a development effort to build on the success of the Phase I R&D. The initial goal of the Phase II effort is to produce a viable design of a color-corrected, off-axis HMD system that utilizes diffractive optics technology. Since the primary goal of Phase II is to generate hardware, we are assembling a strong team of engineers and subcontractors with experience in optical design for helmet-mounted displays, fabrication of visor/combiners, optical coatings, opto-mechanical engineering and surface-relief diffractive optics. Our goal is to continue through the SBIR program to generate flyable hardware in Phase III.

The technical advances to date regarding kinoform fabrication, replication and testing strongly suggest that diffractive optics technology can provide unique solutions in the development of several military and commercial applications both with bulk optics and waveguide optics. The Federal Government, and particularly the Department of Defense, considers diffractive optics technology *critical* to the United States. Currently RPC, in a collaborative effort with a larger company, is developing an internal capability to fabricate diffractive optics for military and commercial systems. It is our intention to use our internal research and development partnership to develop fabrication methods and to use the SBIR program to develop applications of diffractive optics. The marriage of the two programs will enhance significantly the commercial opportunities which is exactly in line with the charter of the SBIR program. We have already identified several commercial application

areas that include bioengineering, optical data storage, optical testing, and materials processing that will benefit from the research proposed herein. Our goal is to be a leader in the fabrication and testing of systems based on diffractive optics by way of our industrial partnerships and the SBIR program.

Appendix A

Appendix A contains the design information for system A. The design parameters for system A are : on-axis, all-diffractive, monochromatic, monocular FOV $50^{\circ}\text{H} \times 37.5^{\circ}\text{V}$, binocular FOV $80^{\circ}\text{H} \times 37.5^{\circ}\text{V}$, overlapped FOV 20° , EPD 19 mm, CRT size 19 mm, eye relief 125 mm. The units for all of the parameters used in the design information are mm.

*LENS DATA

On-Axis All Diffractive HMD (19mm CRT)

SRF	RADIUS	THICKNESS	APERTURE	GLASS	SPE	NOTES
1	--	--	9.50000 S	AIR		
2	--	125.00000	9.50000 A	AIR		Exit Pupil
3	-150.00000	-50.00000	67.78846 S	REFLECT		Visor
4	--	137.50000 S	45.91154 S	REFLECT		Beamsplitter
5	--	-8.51448	14.25000 S	AIR		Image of Eye Pupil
6	-112.18577	2.00000	15.81841 S	BK7 C		Substrate
7	-112.18577	47.79763	15.67217 S	AIR	*	Diffractive Element
8	212.02012	2.00000	31.93663 S	BK7 C		Substrate
9	212.02012	36.16034	32.40600 S	AIR	*	Diffractive Element
10	78.41380	--	9.50000	BK7 C		CRT Faceplate
11	78.41380	--	9.50000	AIR		

*SPECIAL AND ASPHERIC DATA

7	SPECIAL TYPE DFR	DOR	1.00000	S1	-0.00297	S2	9.0592E-07	
7	S3	2.6716E-08	S4	-2.3850E-10	S5	1.0621E-12	S6	-3.3565E-15
7	S7	2.4811E-17	S8	-1.3798E-19	S9	2.6136E-22		
9	SPECIAL TYPE DFR	DOR	1.00000	S1	-0.01530	S2	8.8270E-07	
9	S3	-2.5731E-09	S4	6.6798E-12	S5	-3.6745E-15	S6	-1.7762E-17
9	S7	4.0191E-20	S8	-3.3364E-23	S9	1.0108E-26		

*GENERAL DATA

OSLO 2.02 RPC1

EPR	OBV	THO	CVO	CCO	UNITS
9.50000	-4.6631E+19	1.0000E+20	--	--	1.00000
IMS	AST	RFS	AFO	AMO	DESIGNER
11	2	2	0	TRA	CTCE
					IDNBR
					4118

*SOLVES

4 PYC --

*PICKUPS (TYPE SN1 SN2 INCREMENT)

NO PICKUP DATA

*APERTURES

SRF	TYPE	APERTURE
1	CMP	9.50000
2	SPC	9.50000
3	CMP	67.78846
4	CMP	45.91154
5	CMP	14.25000
6	CMP	15.81841
7	CMP	15.67217
8	CMP	31.93663
9	CMP	32.40600
10	SPC	9.50000
11	SPC	9.50000

*WAVELENGTHS

CURRENT	WV1	WV2	WV3
1	0.54500	0.54400	0.54600

*REFRACTIVE INDICES

SRF	GLASS	RN1	RN2	RN3	VNBR

1	AIR	--	--	--	--
2	AIR	--	--	--	--
3	REFLECT	--	--	--	--
4	REFLECT	--	--	--	--
5	AIR	--	--	--	--
6	BK7	1.51878	1.51883	1.51873	5020.99414
7	AIR	--	--	--	--
8	BK7	1.51878	1.51883	1.51873	5020.99414
9	AIR	--	--	--	--
10	BK7	1.51878	1.51883	1.51873	5020.99414
11	AIR	--	--	--	--

*PARAXIAL CONSTANTS

EFL	FNB	GIH	PIV	PTZRAD	TMAG
-431.17782	-14.94200	-132.38383	-2.91677	73.34351	2.8390E-18

Appendix B

Appendix B contains the design information for system B. The design parameters for system B are : on-axis, all-diffractive, monochromatic, monocular FOV $50^{\circ}\text{H} \times 37.5^{\circ}\text{V}$, binocular FOV $80^{\circ}\text{H} \times 37.5^{\circ}\text{V}$, overlapped FOV 20° , EPD 19 mm, CRT size 23 mm, eye relief 125 mm. The units for all of the parameters used in the design information are mm.

*LENS DATA

On-Axis All Diffractive HMD (23mm CRT)

SRF	RADIUS	THICKNESS	APERTURE	GLASS	SPE	NOTES
1	--	--	9.50000 S	AIR		
2	--	125.00000	9.50000 A	AIR		Exit Pupil
3	-150.00000	-50.00000	67.78846 S	REFLECT		Visor
4	--	137.50000 S	45.91154 S	REFLECT		Beamsplitter
5	--	-12.29168	14.25000 S	AIR		Image of Eye Pupil
6	-388.80525	2.00000	16.51419 S	BK7 C		Substrate
7	-388.80525 P	51.94035	16.30064 S	AIR	*	Diffractive Element
8	455.43817	2.00000	32.14857 S	BK7 C		Substrate
9	455.43817 P	44.17650	32.67548 S	AIR	*	Diffractive Element
10	74.46129	--	11.50000	BK7 C		CRT Faceplate
11	74.46129 P	--	11.50000	AIR		

*SPECIAL AND ASPHERIC DATA

7	SPECIAL TYPE DFR	DOR	1.00000	S1	-0.00278	S2	2.1455E-06	
7	S3	-7.8892E-09	S4	3.7557E-11	S5	5.8754E-13	S6	-7.5120E-15
7	S7	3.1343E-17	S8	-4.4248E-20	S9	-4.6752E-24		
9	SPECIAL TYPE DFR	DOR	1.00000	S1	-0.01306	S2	6.5015E-07	
9	S3	-1.7167E-09	S4	4.3470E-12	S5	-1.6996E-16	S6	-2.0644E-17
9	S7	4.1519E-20	S8	-3.3824E-23	S9	1.0246E-26		

*GENERAL DATA

OSLO 2.02 RPC1

EPR	OBY	THO	CVO	CCO	UNITS
9.50000	-4.6631E+19	1.0000E+20	--	--	1.00000
IMS	AST	RFS	AFO	AMO	DESIGNER
11	2	2	0	TRA	CTCE
IDNBR	4724				

*SOLVES

4 PYC --

*PICKUPS (TYPE SN1 SN2 INCREMENT)

7	PKP CV	6
9	PKP CV	8
11	PKP CV	10

*APERTURES

SRF	TYPE	APERTURE
1	CMP	9.50000
2	SPC	9.50000
3	CMP	67.78846
4	CMP	45.91154
5	CMP	14.25000
6	CMP	16.51419
7	CMP	16.30064
8	CMP	32.14857
9	CMP	32.67548
10	SPC	11.50000
11	SPC	11.50000

*WAVELENGTHS

CURRENT	WV1	WV2	WV3
1	0.54500	0.54500	0.54500

*REFRACTIVE INDICES

SRF	GLASS	RN1	RN2	RN3	VNBR
1	AIR	--	--	--	--
2	AIR	--	--	--	--
3	REFLECT	--	--	--	--
4	REFLECT	--	--	--	--
5	AIR	--	--	--	--
6	BK7	1.51878	1.51878	1.51878	--
7	AIR	--	--	--	--
8	BK7	1.51878	1.51878	1.51878	--
9	AIR	--	--	--	--
10	BK7	1.51878	1.51878	1.51878	--
11	AIR	--	--	--	--

*PARAXIAL CONSTANTS

EFL	FNB	GIH	PIV	PTZRAD	TMAG
-295.43012	-10.23781	-90.70543	-2.91677	75.28255	1.9452E-18

Appendix C

Appendix C contains the design information for system C. The design parameters for system C are : on-axis, hybrid refractive/diffractive, color corrected, monocular FOV $50^{\circ}\text{H} \times 37.5^{\circ}\text{V}$, binocular FOV $80^{\circ}\text{H} \times 37.5^{\circ}\text{V}$, overlapped FOV 20° , EPD 19 mm, CRT size 19 mm, eye relief 125 mm. The units for all of the parameters used in the design information are mm.

*LENS DATA

On-Axis Aspheric Hybrid HMD (19mm CRT)

SRF	RADIUS	THICKNESS	APERTURE	GLASS	SPE	NOTES
1	--	--	9.50000 S	AIR		
2	--	125.00000	9.50000 A	AIR		Exit Pupil
3	-150.00000	-50.00000	67.78846 S	REFLECT		Visor
4	--	137.50000 S	45.91154 S	REFLECT		Beamsplitter
5	--	--	14.25000 S	AIR		Image of Eye Pupil
6	29.10543	9.50000	19.00000	SF56 C	*	Asphere
7	137.30331	19.13094	16.00000	AIR	*	Diffraction Element
8	19.53911	8.00000	16.00000	FK5 C		
9	-423.64345	11.37056	13.00000	AIR	*	Asphere
10	-31.81183	2.00000	11.00000	F2 C		Field Flatteners
11	--	--	10.00000	AIR		
12	--	--	9.50000	AIR		CRT Faceplate

*SPECIAL AND ASPHERIC DATA

6	CC	-0.60615	AD	9.2864E-07	AE	-7.1144E-09	AF	1.5729E-11
6	AG	-4.3414E-14						
7	SPECIAL TYPE	DFR	DOR	1.00000	S1	-0.00230	S2	4.9053E-06
7	S3	-5.7925E-08	S4	6.8330E-10	S5	-5.3210E-12	S6	2.3689E-14
7	S7	-5.6374E-17	S8	5.5333E-20				
9	AD	4.1152E-05	AE	-4.5152E-08	AF	2.4337E-10	AG	3.2535E-13

*GENERAL DATA

OSLO 2.02 RPC1

EPR	OBY	THO	CVO	CCO	UNITS
9.50000	-4.6631E+19	1.0000E+20	--	--	1.00000
IMS	AST	RFS	AMO	DESIGNER	IDNBR
12	2	2	0	CTCE	3647

*SOLVES

4 PYC --

*PICKUPS (TYPE SN1 SN2 INCREMENT)

NO PICKUP DATA

*APERTURES

SRF	TYPE	APERTURE
1	CMP	9.50000
2	CMP	9.50000
3	CMP	67.78846
4	CMP	45.91154
5	CMP	14.25000
6	SPC	19.00000
7	SPC	16.00000
8	SPC	16.00000
9	SPC	13.00000
10	SPC	11.00000
11	SPC	10.00000
12	SPC	9.50000

*WAVELENGTHS

CURRENT	WV1	WV2	WV3
1	0.54500	0.49000	0.59000

*REFRACTIVE INDICES

SRF	GLASS	RN1	RN2	RN3	VNBR
1	AIR	--	--	--	--
2	AIR	--	--	--	--
3	REFLECT	--	--	--	--
4	REFLECT	--	--	--	--
5	AIR	--	--	--	--
6	SF56	1.79201	1.80502	1.78434	38.29189
7	AIR	--	--	--	--
8	FK5	1.48919	1.49203	1.48740	105.62350
9	AIR	--	--	--	--
10	F2	1.62420	1.63146	1.61983	53.65859
11	AIR	--	--	--	--
12	AIR	--	--	--	--

*PARAXIAL CONSTANTS

EFL	FNB	GIH	PIV	PTZRAD	TMAG
-24.67913	-1.29890	-11.50807	-4.42992	-241.57239	2.4679E-19

Appendix D

Appendix D contains the design information for system D. The design parameters for system D are : on-axis, hybrid refractive/diffractive, color corrected, monocular FOV $50^{\circ}\text{H} \times 37.5^{\circ}\text{V}$, binocular FOV $80^{\circ}\text{H} \times 37.5^{\circ}\text{V}$, overlapped FOV 20° , EPD 19 mm, CRT size 23 mm, eye relief 125 mm. The units for all of the parameters used in the design information are mm.

*LENS DATA

On-Axis Aspheric Hybrid HMD (23mm CRT)

SRF	RADIUS	THICKNESS	APERTURE	GLASS	SPE	NOTES
1	--	--	9.50000 S	AIR		
2	--	125.00000	9.50000 A	AIR		Exit Pupil
3	-150.00000	-50.00000	67.78846 S	REFLECT		Visor
4	--	137.50000 S	45.91154 S	REFLECT		Beamsplitter
5	--	--	14.25000 S	AIR		Image of Eye Pupil
6	36.17719	9.50000	19.00000	SF56 C	*	Asphere
7	330.93777	27.14132	16.00000	AIR	*	Diffraction Element
8	20.10497	9.12667	18.00000	FK5 C		
9	143.06284	13.57283	16.50000	AIR	*	Asphere
10	-43.20979	2.00000	13.00000	F2 C		Field Flatteners
11	--	--	12.00000	AIR		
12	--	--	11.50000	AIR		CRT Faceplate

*SPECIAL AND ASPHERIC DATA

6	CC	-0.90814	AD	-1.7324E-07	AE	1.1096E-10	AF	-1.1147E-11
6	AG	2.0482E-14						
7	SPECIAL TYPE DFR		DOR	1.00000	S1	-0.00172	S2	1.8901E-06
7	S3	-4.1846E-08	S4	5.6207E-10	S5	-4.4078E-12	S6	1.9224E-14
7	S7	-4.3855E-17	S8	4.0978E-20				
9	AD	3.0802E-05	AE	-1.2985E-08	AF	1.6992E-11	AG	1.9795E-13

*GENERAL DATA

OSLO 2.02 RPC1

EPR	OBV	THO	CVO	CCO	UNITS
9.50000	-4.6631E+19	1.0000E+20	--	--	1.00000
IMS	AST	RFS	AMO	DESIGNER	IDNBR
12	2	2	0	CTCE	3700

*SOLVES

4 PYC --

*PICKUPS (TYPE SN1 SN2 INCREMENT)

NO PICKUP DATA

*APERTURES

SRF	TYPE	APERTURE
1	CMP	9.50000
2	CMP	9.50000
3	CMP	67.78846
4	CMP	45.91154
5	CMP	14.25000
6	SPC	19.00000
7	SPC	16.00000
8	SPC	18.00000
9	SPC	16.50000
10	SPC	13.00000
11	SPC	12.00000
12	SPC	11.50000

*WAVELENGTHS

CURRENT	WV1	WV2	WV3
1	0.54500	0.49000	0.59000

*REFRACTIVE INDICES

SRF	GLASS	RN1	RN2	RN3	VNBR
1	AIR	--	--	--	--
2	AIR	--	--	--	--
3	REFLECT	--	--	--	--
4	REFLECT	--	--	--	--
5	AIR	--	--	--	--
6	SF56	1.79201	1.80502	1.78434	38.29189
7	AIR	--	--	--	--
8	FK5	1.48919	1.49203	1.48740	105.62350
9	AIR	--	--	--	--
10	F2	1.62420	1.63146	1.61983	53.65859
11	AIR	--	--	--	--
12	AIR	--	--	--	--

*PARAXIAL CONSTANTS

EFL	FNB	GIH	PIV	PTZRAD	TMAG
-29.46545	-1.55081	-13.73997	-4.42992	-370.83718	2.9465E-19

Appendix E

Appendix E contains the design information for system E. The design parameters for system E are : off-axis, hybrid refractive/diffractive, color corrected, monocular FOV $30^{\circ}\text{H} \times 22.5^{\circ}\text{V}$, binocular FOV $30^{\circ}\text{H} \times 22.5^{\circ}\text{V}$, fully overlapped field, EPD 19 mm, CRT size 19 mm, eye relief 100 mm. The units for all of the parameters used in the design information are mm.

*LENS DATA

Off-Axis Hybrid HMD 30 deg FOV

SRF	RADIUS	THICKNESS	APERTURE	GLASS	SPE	NOTES
1	--	--	7.50000 S	AIR		
2	--	--	7.50000 A	AIR		Exit Pupil
3	--	-100.00000	7.50000 S	AIR	*	60 deg Bend Angle
4	150.00000	300.00000 S	250.00000	REFLECT	*	Off-Axis Ellipse
5	--	-19.41427	22.50000 S	AIR		Image of Eye Pupil
6	-2076.63808	3.00000	22.29259 S	F2 C	*	Cylinder Lens
7	--	1.00109	22.32470 S	AIR		
8	48.25631	8.00000	22.34210 S	SF57 C	*	Asphere
9	212.68953	23.79899	20.70956 S	AIR	*	Diffraction Element
10	129.28016	13.00000	25.00000	FK5 C	*	Asphere
11	-108.69695	25.00148	25.00000	AIR		
12	--	--	10.58367 S	AIR	*	
13	51.93009	10.00000	10.00000	BK10 C		Decentered, Tilted
14	--	--	8.51380 S	AIR	*	Field Flatteners
15	--	--	8.51380 S	AIR		CRT Faceplate

*SPECIAL AND ASPHERIC DATA

3	DT	1.00000	TLA	60.00000			
4	CC	-0.25000					
6	CVX	--					
8	CC	0.24053	AD	-3.5468E-07	AE	-1.4268E-11	AF -2.0158E-12
8	AG	3.0617E-15					
9	SPECIAL TYPE DFR	DOR	1.00000	S1	0.00141	S2	-2.2070E-06
9	S3	1.8387E-08	S4	-9.9193E-11	S5	2.2920E-13	S6 1.5880E-16
9	S7	-2.0236E-18	S8	3.9648E-21	S9	-2.5924E-24	
10	CC	-0.90072	AD	-4.3624E-06	AE	2.5070E-09	AF -1.2838E-11
10	AG	-3.3871E-15					
12	DT	1.00000	DCY	-27.97506	TLA	21.59682	
14	DT	1.00000	DCY	-0.02641	TLA	-30.66121	

*GENERAL DATA

OSLO 2.02 RPC1

EPR	OBJ	THO	CVO	CCO	UNITS
7.50000	-2.6795E+19	1.0000E+20	--	--	1.00000
IMS	AST	RFS	AMO	DESIGNER	IDNBR
15	2	2	0	CTCE	4181

*SOLVES

4 PYC --

*PICKUPS (TYPE SN1 SN2 INCREMENT)

NO PICKUP DATA

*APERTURES

SRF	TYPE	APERTURE
1	CMP	7.50000
2	CMP	7.50000
3	CMP	7.50000
4	SPC	250.00000
5	CMP	22.50000

6	CMP	22.29259
7	CMP	22.32470
8	CMP	22.34210
9	CMP	20.70956
10	SPC	25.00000
11	SPC	25.00000
12	CMP	10.58367
13	SPC	10.00000
14	CMP	8.51380
15	CMP	8.51380

*WAVELENGTHS

CURRENT	WV1	WV2	WV3
1	0.54500	0.49000	0.59000

*REFRACTIVE INDICES

SRF	GLASS	RN1	RN2	RN3	VNBR
1	AIR	--	--	--	--
2	AIR	--	--	--	--
3	AIR	--	--	--	--
4	REFLECT	--	--	--	--
5	AIR	--	--	--	--
6	F2	1.62420	1.63146	1.61983	-53.65859
7	AIR	--	--	--	--
8	SF57	1.85529	1.87071	1.84623	-34.94066
9	AIR	--	--	--	--
10	FK5	1.48919	1.49203	1.48740	-105.62350
11	AIR	--	--	--	--
12	AIR	--	--	--	--
13	BK10	1.49965	1.50270	1.49773	-100.40182
14	AIR	--	--	--	--
15	AIR	--	--	--	--

*PARAXIAL CONSTANTS

EFL	FNB	GIH	PIV	PTZRAD	TMAG
-21.04106	1.40274	5.63793	-2.00962	-171.05109	-2.1041E-19